

**Low Thrust Optimal Trajectories in the Circular Restricted  
Three-Body Problem**

by

**Grant Hevia**

B.S., Engineering Mechanics and Astronautics, University of Wisconsin -  
Madison, 2021

A thesis submitted to the  
Faculty of the Graduate School of the  
University of Colorado in partial fulfillment  
of the requirements for the degree of  
Master of Science  
Department of Aerospace Engineering Sciences  
2023

Committee Members:

Natasha Bosanac, Chair

Jay McMahon

Marcus Holzinger

Hevia, Grant (M.S., Aerospace Engineering Sciences)

Low Thrust Optimal Trajectories in the Circular Restricted Three-Body Problem

Thesis directed by Prof. Natasha Bosanac

The increasing interest in cislunar spaceflight is a motivating factor for trajectory analysts to investigate the motion of a spacecraft in Earth-Moon system. Due to the new capabilities that arise from the modern innovations in rocketry and small satellite technology, this thesis focuses on the computation of optimal low-thrust trajectories for smaller satellites equipped with electric propulsion systems. The circular restricted three-body problem (CR3BP) is used to describe motion in Earth-Moon system, and the corresponding equations of motion and natural structures are derived. The equations are augmented to include continuous thrust. Numerical methods such as multiple shooting and parameter continuation are discussed and used to generate results. Primer vector theory using hyperbolic smoothing is introduced and applied to the thrust enabled equations to generate fuel-optimal transfers in the Earth-Moon CR3BP. The approach for computing optimal transfers is leveraged to generate optimal spiral out transfers between low Earth/Moon orbits and Lyapunov orbits about the  $L_1$  equilibrium point. The resulting low-thrust transfers are analyzed to investigate the properties of optimal transfers in the CR3BP.

## **Dedication**

I'd like to dedicate this thesis to my Mom and Dad, who have selflessly supported me and encouraged my education for as long I can remember. I'd also like to dedicate this to my girlfriend, who listened to me ramble about optimization and spirals every day for a full academic year.

## Acknowledgements

First and foremost, I need to thank my family for being so amazing and caring. I know I can count on you guys, thank you for trusting me to pursue my passion. I also would like to thank my awesome girlfriend, whose been supportive every step of the way. I'd also like to thank all the great teachers and mentors I've had over the years, who have inspired me to pursue interesting and challenging subjects.

I would also like to thank the professors and academic institutions that have allowed me to pursue this particular study. Thank you Professor Bosanac for giving me encouragement and sage guidance throughout this process. Thank you to CU Boulder for creating an environment that cultivates incredible research into spaceflight, and allows wide-eyed students to coexist with true savants of astrodynamics.

## Contents

### Chapter

<b>1</b>	<b>Introduction</b>	<b>1</b>
1.1	Motivation . . . . .	1
1.2	Cislunar Space . . . . .	2
1.3	Optimal Trajectories . . . . .	3
1.4	Thesis Overview . . . . .	5
<b>2</b>	<b>Dynamical Model: The Circular Restricted Three-Body Problem</b>	<b>7</b>
2.1	Equations of Motion . . . . .	7
2.2	Constant of Motion . . . . .	13
2.3	Equilibrium Points . . . . .	14
2.4	State Transition Matrix . . . . .	17
2.5	Periodic Orbits . . . . .	20
2.6	Stability and Hyperbolic Invariant Manifolds . . . . .	23
2.7	Frame Transformations . . . . .	24
2.8	Eccentricity Relative to the Primary Bodies . . . . .	26
2.9	Augmenting the CR3BP with Continuous Thrust . . . . .	27
<b>3</b>	<b>Numerically Computing Trajectories</b>	<b>30</b>
3.1	Single Shooting Method . . . . .	30
3.2	Multiple Shooting Method . . . . .	34

3.3	Natural Parameter Continuation . . . . .	37
3.4	Poincaré Maps . . . . .	38
<b>4</b>	<b>Optimal Control Theory in the CR3BP</b>	<b>40</b>
4.1	General Form of Hamiltonian Optimal Control . . . . .	40
4.2	Primer Vector Theory . . . . .	42
4.3	Primer Vector Theory in the CR3BP . . . . .	45
4.4	Smoothing . . . . .	46
4.5	State Transition Matrix for Adjoints . . . . .	47
<b>5</b>	<b>Technical Approach</b>	<b>49</b>
5.1	Changing the Jacobi Constant Efficiently . . . . .	49
5.2	Trajectory Itinerary and Initial Guess Construction . . . . .	50
5.3	Initial Adjoint Guesses . . . . .	52
5.4	Patching Onto a Stable Manifold . . . . .	54
5.5	Constraints and Free Variables . . . . .	54
5.6	Methodology . . . . .	58
<b>6</b>	<b>Results</b>	<b>60</b>
6.1	Electric Propulsion Systems . . . . .	60
6.2	Optimal Transfer from Medium Earth Orbit to L1 Lyapunov Orbit . . . . .	61
6.3	Optimal Transfer from Medium Lunar Orbit to L1 Lyapunov Orbit . . . . .	69
6.4	Optimal Transfer from Low Lunar Orbit to L1 Lyapunov Orbit . . . . .	76
6.5	Interpretation of Results . . . . .	81
<b>7</b>	<b>Conclusion</b>	<b>82</b>
7.1	Summary . . . . .	82
7.2	Future Work . . . . .	83

**Bibliography****86**

## Tables

### **Table**

2.1	Characteristic quantities of the Earth-Moon system. . . . .	10
2.2	Nondimensional position coordinates of the Earth-Moon Lagrange points . . . . .	17
5.1	Characteristics Earth/Moon centered orbits. Each of these orbits are circular in the two-body problem . . . . .	51
5.2	Characteristics of segments of periodic orbit families in the Earth-Moon CR3BP . .	51
6.1	Parameters for different electric propulsion systems that could be used for small satellites. [6] . . . . .	61
6.2	Parameters used for the results in this thesis. . . . .	61
6.3	Resulting final mass and transfer time for each selected case from the continuation method employed to compute a desired MEO to L1 Lyapunov transfer . . . . .	62
6.4	Resulting final mass and transfer time for each selected case from the continuation method employed to compute a desired MLO to L1 Lyapunov transfer . . . . .	71

## Figures

### **Figure**

2.1	Three point masses in three dimensional space . . . . .	9
2.2	The rotating frame is defined relative to the motion of the primary and secondary bodies . . . . .	11
2.3	The Lagrange Points of the Earth-Moon CR3BP . . . . .	15
2.4	X coordinate of the Lagrange points for different mass ratios . . . . .	16
2.5	Defining a trajectory relative to a neighboring reference trajectory . . . . .	18
2.6	The Earth-Moon $L_1$ Lyapunov orbit family . . . . .	21
2.7	The Earth-Moon Southern $L_2$ halo orbit family, 3D view . . . . .	22
2.8	The Earth-Moon Southern $L_2$ halo orbit family, 2D views . . . . .	22
2.9	Stable and unstable manifold of a $L_1$ Lyapunov orbit . . . . .	25
2.10	A trajectory displayed in the rotating and inertial frame . . . . .	26
3.1	Single shooting representative diagram . . . . .	31
3.2	Single Shooting example: Lyapunov orbit . . . . .	33
3.3	Quadratic convergence is seen in the constraint vector size for each successive iteration	34
3.4	Multiple shooting representative diagram . . . . .	35
3.5	Poincaré map diagram . . . . .	39
4.1	Smoothing via the hyperbolic tangent function . . . . .	47
5.1	Poincaré map of 3 crossings of a stable manifold and options of initial guess spirals	55

5.2	The closest matching initial guess spiral and stable manifold trajectory for a GEO to L1 Lyapunov orbit spiral out transfer . . . . .	55
5.3	Continuation process for computation of low spirals . . . . .	59
6.1	Data from the continuation method for computation of a MEO transfer . . . . .	62
6.2	Selected cases from the continuation method employed to compute a desired MEO to L1 Lyapunov transfer . . . . .	63
6.3	Control smoothing in computation of a MEO to L1 Lyapunov orbit transfer . . . . .	64
6.4	Control smoothing in computation of a MEO to L1 Lyapunov orbit transfer, zoomed for clarity . . . . .	65
6.5	Mass and Jacobi constant measured over time for MEO transfers with a different value of $\epsilon$ . . . . .	65
6.6	Eccentricity and distance relative to Earth for an optimal MEO to L1 Lyapunov orbit transfer . . . . .	66
6.7	The angle between thrust and velocity for each thrust arc for an optimal MEO to L1 Lyapunov transfer . . . . .	67
6.8	An optimal transfer from medium Earth orbit to an L1 Lyapunov orbit in the Earth-Moon CR3BP, plotted in the rotating frame . . . . .	68
6.9	An optimal transfer from medium Earth orbit to an L1 Lyapunov orbit in the Earth-Moon CR3BP, plotted in the inertial frame . . . . .	68
6.10	Data from the continuation method for computation of a MLO transfer . . . . .	69
6.11	Selected cases from the continuation method employed to compute a desired MLO to L1 Lyapunov transfer . . . . .	70
6.12	Control smoothing in computation of a MLO to L1 Lyapunov orbit transfer . . . . .	71
6.13	Control smoothing in computation of a MLO to L1 Lyapunov orbit transfer, zoomed for clarity . . . . .	72

6.14 Mass and Jacobi constant measured over time for MLO transfers with a different value of $\epsilon$ . . . . .	73
6.15 Eccentricity and distance relative to the Moon for an optimal MLO to L1 Lyapunov orbit transfer . . . . .	73
6.16 The angle between thrust and velocity for each thrust arc for an optimal MLO to L1 Lyapunov transfer . . . . .	74
6.17 An optimal transfer from medium lunar orbit to an L1 Lyapunov orbit in the Earth-Moon CR3BP, plotted in the rotating frame . . . . .	75
6.18 An optimal transfer from medium lunar orbit to an L1 Lyapunov orbit in the Earth-Moon CR3BP, plotted in the inertial frame . . . . .	75
6.19 Further continuation for a MLO to L1 Lyapunov orbit transfer . . . . .	76
6.20 Eccentricity and distance relative to the Moon for an optimal LLO to L1 Lyapunov orbit transfer . . . . .	77
6.21 Eccentricity and distance relative to the Moon for an optimal LLO to L1 Lyapunov orbit transfer . . . . .	78
6.22 Mass and Jacobi constant measured over time for a transfer from LLO . . . . .	79
6.23 The angle between thrust and velocity for each thrust arc for an optimal LLO to L1 Lyapunov transfer . . . . .	79
6.24 An optimal transfer from low lunar orbit to an L1 Lyapunov orbit in the Earth-Moon CR3BP, plotted in the rotating frame . . . . .	80
6.25 An optimal transfer from low lunar orbit to an L1 Lyapunov orbit in the Earth-Moon CR3BP, plotted in the inertial frame . . . . .	80

# **Chapter 1**

## **Introduction**

### **1.1 Motivation**

On November 16th, 2022, the world watched the beginning of the Artemis I mission as the Space Launch System (SLS) rocket launched an uncrewed Orion spacecraft into a trajectory around the Moon. In the following 25 days the spacecraft successfully performed tests, sent back breathtaking photos, and capped off the mission with a successful reentry and splashdown. This marked the start of America's return to human lunar exploration, this time with the intention to stay. The purpose of Artemis I was to test the rocket and spacecraft components in a cislunar environment.[22] Artemis II will carry four astronauts around the Moon and conduct similar tests.[23] These will be the first humans to travel beyond low Earth orbit since 1972, over 50 years ago. Artemis III plans to land humans on the Moon, and subsequent missions planned for the late 2020's aim to establish a sustainable lunar presence.[24] NASA first reached the Moon in a heroic effort to get there as fast as possible to beat the Soviet competition. This time around, the goal is to take a measured and sustainable approach in a way that can set an example for generations to come about how to reach the first stepping stone of the final frontier.

NASA is not alone in its quest to the Moon and beyond. China's robotic Chang'e-5 mission returned Moonrock samples to Earth in 2020.[21] India's Chandrayan-2 mission features a lunar orbiter that is mapping the Moon's topography and studying its surface composition.[19] CAPSTONE, a mission contracted to a private company by NASA, is a microwave sized satellite that is verifying the orbit planned for the Lunar Gateway station.[32] The Lunar Gateway is a planned

space station that will be in orbit about the Moon, and will play a major role in the later Artemis missions.

This renewed interest in space exploration is occurring alongside a few major revolutions in the technology needed for space travel. In rocketry, private companies such as SpaceX have made leaps in innovation that has made space more affordable and accessible. Among these innovations is the ability to recover and reuse a Vertical Take-off, Vertical Landing (VTVL) rocket, which SpaceX now does on a weekly basis.[33] The other important development in space travel is the CubeSat revolution. Recent advances in technology allow all the necessary satellite hardware to become smaller and smaller. Smaller satellites can hitch a ride on a rocket with a larger and more expensive payload, which lowers the cost of launch. This revolution was amplified by the creation of CubeSats – a class of miniature satellites that has a standardized set of design dimensions.[18] NASA's CubeSat Launch Initiative provided opportunities for universities and nonprofit organizations to design and operate a CubeSat in Earth orbit.[18] These and other small satellites can be used for communication constellations, hardware tests, inspection of larger satellites, research, etc. This development intensified the research area of smaller satellites, and other innovations in solar arrays, battery efficiency, and data storage were utilized to maximize the capabilities of these satellites.

The reduced mass of smaller satellites means that low thrust propulsion systems can have more authority over the motion of the spacecraft. Many electric propulsion systems have been developed and tested specifically for smaller satellites.[6] While these propulsion systems provide a smaller amount of thrust compared to chemical propulsion systems, the thrust can be applied continuously for long periods of time to accomplish the desired maneuver. All of these factors motivate the analysis of optimal low thrust trajectories in the Earth-Moon system.

## 1.2 Cislunar Space

The cislunar environment is often modeled using the Circular Restricted Three-Body Problem (CR3BP). The three-body problem is a dynamical system involving three bodies under the influence of the gravity of one another; the restricted case of this problem models the motion of an object

due to the gravity of two bodies following circular orbits around their shared center of mass. Isaac Newton was the first to derive equations that described the motion of celestial bodies, and actually tried to solve the three-body problem in its early form.[25] Using Newtonian mechanics, both Leonhard Euler and Joseph-Louis Lagrange made important foundational contributions to the three-body problem, such as the discovery of equilibrium points.[9, 16] Yet these developments were primarily concerned with celestial mechanics, which is the description of motion of planets and moons. Important contributions for astrodynamics, such as the development of halo orbits, were made in the 1960s as NASA embarked on a journey to the Moon.[10] As part of the Artemis program, the Lunar Gateway will use a halo orbit to orbit in the vicinity of the Moon for an extended period of time.[20] The study of cislunar dynamics has continued to grow over the years, and the subject will only continue to develop as cislunar space travel gains steam.

### 1.3 Optimal Trajectories

Optimization is a fascinating and powerful subject that can be defined for any general set of dynamics, but is commonly applied to space travel. The mathematics behind optimization deals with a proof that solution is optimal. For a given solution to be optimal, it must fulfil the necessary conditions of optimality. Imagine being tasked with finding the lowest point in a hilly grassland. Without needing to measure altitude at each point, it can be reasoned that the low point will be flat; if it had a slope, one could travel downward until the low point of the valley is reached. However, just because a point on a hilly grassland is flat does not mean that it is the low point; it could be the high point or a midpoint on a hill that happens to have no slope at that point. If the point is a minimum, then the necessary conditions must be fulfilled, but if the necessary conditions are fulfilled, that does not conclusively prove that the point is a minimum. However, it is common to prove that a solution meets the necessary conditions of optimality and treat that solution as a candidate for the true optimal.

There are many different methods of trajectory optimization, generally grouped as direct and indirect methods as well as hybrid methods that combine the two. Direct methods use numerical

techniques to first discretize the trajectory and then compute via nonlinear programming a set of discrete controls that optimizes a measure of performance.[34] Direct approaches tend to be more robust than indirect methods and can be constructed for a general set of dynamics or constraints. This means that direct methods can be used in high fidelity models, which is one reason that direct methods are popular in trajectory optimization.

Indirect methods, on the other hand, apply optimal control theory to a cost function to construct a boundary value problem. These methods utilize adjoints, which are a set of dynamic Lagrange multipliers, to obtain a solution. Solving for the adjoints can be difficult because they do not have a physical meaning. Indirect methods can be useful because they mathematically guarantee that the necessary conditions of optimality are satisfied.[3] Indirect methods are commonly used in simplified dynamical models because the additional complexity can make it impractical for higher fidelity models. Another advantage of indirect methods is that they produce continuous control profiles. This thesis applies an indirect method known as primer vector theory to the dynamics of the Earth-Moon CR3BP.

Optimal control theory uses Hamiltonian dynamics to prove that a time dependent solution continuously satisfies the necessary conditions of optimality.[3] The application of optimal control theory to space trajectories was pioneered by D.F. Lawden in the 1960s, who coined the term “primer vector.”[17] It is common to minimize measures of performance, such as flight time or propellant usage. A minimal time trajectory usually uses propellant to get from point A to point B as fast as possible. A minimal propellant trajectory, on the other hand, takes advantage of the dynamics at hand to get from point A to point B as efficiently as possible. There is usually a trade off between time and efficiency - the minimum time solution uses a lot of propellant, but the minimum propellant trajectory takes a lot of time.

A common goal in optimization is to minimize propellant mass usage because it is a limiting factor in space travel. Burning propellant is the spacecraft’s primary way of governing its path in space. It is important to minimize the amount of propellant mass required for each transfer to maximize the capabilities of a space mission. Optimal transfers represent the lower bound of

propellant usage that can drive a mission design.

Real space missions have many considerations that complicate the problem significantly. Outside of time constraints (a real mission cannot take 100 years to complete), the vehicle has limitations to the thrust profile. For instance, there may be constraints on the thrust direction history and the actuation period for a propulsion system. This is simply an engineering limitation for engines and orientation control. That being said, a minimal solution that does not take those considerations into account can be used as a limiting minimum case. The true engineering constraints can be applied afterward to modify the solution.

#### **1.4 Thesis Overview**

The focus of this thesis is to compute optimal low-thrust trajectories from lunar orbit and Earth orbit to Lyapunov orbits about L1 in the circular restricted three-body problem. The thesis is organized as follows:

- Chapter 2: The dynamical model that will be used to describe the cislunar system, the circular restricted three-body problem, is mathematically defined. The equations of motion are investigated to derive constants of motion and transformations to other coordinate systems. The natural structures in this system, such as periodic orbits and manifolds, are explored.
- Chapter 3: The numerical methods that are used to compute desired trajectories are introduced. This includes shooting methods, which will be used to compute trajectories, and complimentary methods to achieve the desired form.
- Chapter 4: Optimal control theory is described and the generalized equations are presented. Primer vector theory, which applies optimal control theory to solve for the minimal fuel trajectory, is derived and applied to the dynamics of the circular restricted three-body problem. Smoothing techniques are outlined to make the approach more suitable for numerical methods.

- Chapter 5: To converge to minimal solution, a very good initial guess is need. This chapter will establish a method of constructing an initial guess based on principles of optimality and the optimal control laws.
- Chapter 6: The process of computing optimal transfers is applied to spiral out trajectories from low Earth/Moon orbits to periodic orbits about an equilibrium point. Optimal low-thrust transfers are presented and analyzed.
- Chapter 7: The thesis paper is summarized and future work is suggested.

## Chapter 2

### Dynamical Model: The Circular Restricted Three-Body Problem

To approximate the motion of a small body, such as a spacecraft, influenced by the gravity of the larger two bodies, the Circular Restricted Three-Body Problem (CR3BP) is often employed. This section will derive the corresponding equations of motion along with useful properties such as the constant of motion, equilibrium points, periodic orbits, and stable/unstable manifolds. These natural equations of motion will then be augmented by continuous thrust.

#### 2.1 Equations of Motion

The equations of motion can be derived from first principles using Newtonian mechanics. Consider three bodies in space with masses  $M_1$ ,  $M_2$ , and  $M_3$ , where  $M_1$  is the largest and  $M_3$  is the smallest. The positions of these masses in an arbitrary inertial reference frame are labeled correspondingly as  $\mathbf{R}_1$ ,  $\mathbf{R}_2$ , and  $\mathbf{R}_3$ . These masses are modeled as spherically symmetric. These masses and their position vectors are shown in Figure 2.1. Also depicted are the relative position vectors of  $M_3$ , where  $\mathbf{R}_{j3} = \mathbf{R}_3 - \mathbf{R}_j$ . Note that vectors will be denoted by bold font in text, but figures will display an arrow ( $\vec{\cdot}$ ) for clarity. Using Newton's second law as well as Newton's law of gravity, the inertial acceleration of  $M_3$  is written as:

$$\widetilde{M}_3 \widetilde{\mathbf{R}}_3'' = -\frac{\widetilde{G}\widetilde{M}_1\widetilde{M}_3}{\widetilde{R}_{13}^3} \widetilde{\mathbf{R}}_{13} - \frac{\widetilde{G}\widetilde{M}_2\widetilde{M}_3}{\widetilde{R}_{23}^3} \widetilde{\mathbf{R}}_{23} \quad (2.1)$$

where the tildes ( $\widetilde{\cdot}$ ) correspond to dimensional quantities, the primes ( $\cdot$ )' correspond to a derivative with respect to an inertial frame, and  $\widetilde{G}$  is the universal gravitational constant. Given a position

vector for  $M_j$  in an inertial reference frame  $\hat{X}\hat{Y}\hat{Z}$  that is expressed as  $\mathbf{R}_j = X_j\hat{\mathbf{X}} + Y_j\hat{\mathbf{Y}} + Z_j\hat{\mathbf{Z}}$ , the equations of motion of the three-body problem are equal to:

$$\begin{aligned}\tilde{X}_3'' &= -\frac{\tilde{G}\tilde{M}_1(\tilde{X}_3 - \tilde{X}_1)}{\tilde{R}_{13}^3} - \frac{\tilde{G}\tilde{M}_2(\tilde{X}_3 - \tilde{X}_2)}{\tilde{R}_{23}^3} \\ \tilde{Y}_3'' &= -\frac{\tilde{G}\tilde{M}_1(\tilde{Y}_3 - \tilde{Y}_1)}{\tilde{R}_{13}^3} - \frac{\tilde{G}\tilde{M}_2(\tilde{Y}_3 - \tilde{Y}_2)}{\tilde{R}_{23}^3} \\ \tilde{Z}_3'' &= -\frac{\tilde{G}\tilde{M}_1(\tilde{Z}_3 - \tilde{Z}_1)}{\tilde{R}_{13}^3} - \frac{\tilde{G}\tilde{M}_2(\tilde{Z}_3 - \tilde{Z}_2)}{\tilde{R}_{23}^3}\end{aligned}\quad (2.2)$$

These three second-order differential equations govern the general motion of  $M_3$  in an inertial frame. Equations for  $M_1$  or  $M_2$  can be derived in a similar fashion, for a total of 9 second-order differential equation governing the system. This can also be formulated as 18 first-order differential equations, which requires 18 constants of motion to solve. However, there are only ten constants of motion can be derived from classical physics: six from the conservation of linear momentum, three from the conservation of angular momentum, and one from the conservation of energy.[37] The problem can be reformulated to model the motion of one body relative to one of the other bodies, which would reduce the number of first order equations to 12, but this is still insufficient.[1] This discrepancy does not allow for an analytical solution, thus, Eq. 2.2 can only be solved numerically.

Simplifying approximations are used to gain further insight into the motion of  $M_3$ , which is commonly modeled as the spacecraft.[36] First, it is assumed that  $M_3 \ll M_2 < M_1$ ; this is a reasonable assumption because a spacecraft does not have significant mass in comparison to celestial bodies. Then, the equations of motion for bodies one and two can disregard the gravitational effect of the third body. This reduces the motion of the two larger bodies, referred to as the primary and secondary bodies, to the classical two-body problem in which the motion is described by conic sections.[37] In the two-body problem, the barycenter is an inertial point, so a new reference frame can be formed such that the origin is at the barycenter. This new reference frame is oriented such that the orbits of the primary and secondary stay on the XY plane.[36] The next assumption is that the primary bodies orbit their mutual center of mass in perfectly circular orbits. The Earth's true orbit around the Sun has an eccentricity of about 0.0167, while the Moon's orbit around the

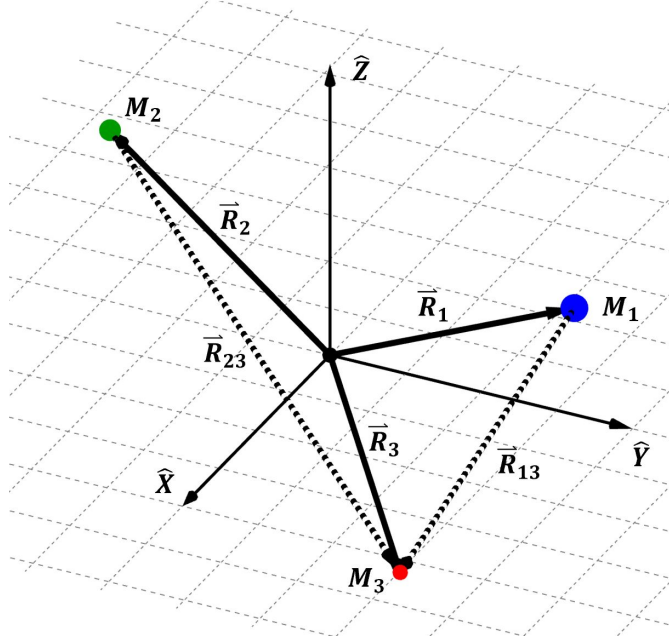


Figure 2.1: Three point masses in three dimensional space, shown with their corresponding position vectors relative to an arbitrary inertial frame.[12]

Earth has an eccentricity of about 0.055. These will be approximated as 0, but in higher fidelity models these eccentricities need to be accounted for.

Circular orbits have the property that certain quantities remain constant, such as the distance between bodies and the angular velocity. These can be used to define and characterize a system. The characteristic length  $l^*$  is defined as the distance between the primaries, and the characteristic time  $t^*$  is defined as the time required to traverse one radian. The characteristic mass  $m^*$  is defined as the total mass of the primary bodies. These are written below as

$$\tilde{m}^* = \tilde{M}_1 + \tilde{M}_2 \quad (2.3)$$

$$\tilde{l}^* = |\tilde{\mathbf{R}}_1| + |\tilde{\mathbf{R}}_2| \quad (2.4)$$

$$\tilde{t}^* = \sqrt{\frac{\tilde{l}^{*3}}{G\tilde{m}^*}} \quad (2.5)$$

A parameter  $\mu$  is defined as the ratio of  $M_2$  to  $M_1 + M_2$ . The relationships between the dimensional

and nondimensional quantities are shown below:

$$\mu = \frac{\tilde{M}_2}{\tilde{m}^*} \quad (2.6)$$

$$1 - \mu = \frac{\tilde{M}_1}{\tilde{m}^*} \quad (2.7)$$

where nondimensional quantities do not have a tilde and  $\mathbf{R}$  corresponds to  $\mathbf{R}_3$ , as the subscript is dropped for convenience. These characteristic quantities are used to nondimensionalize variables in the problem. These constants are defined below for the Earth-Moon system.

Table 2.1: Characteristic quantities of the Earth-Moon system.

System	$\tilde{l}^*$ (km)	$\tilde{m}^*$ (kg)	$\tilde{t}^*$ (s)	$\mu$ (-)	$1 - \mu$ (-)
Earth-Moon	$3.844 \times 10^5$	$6.0456 \times 10^{24}$	$3.7519 \times 10^5$	0.012151	0.987849

The description of motion can be nondimensionalized using the constants defined above to make the equations independent of the individual masses  $M_1$  and  $M_2$ , and instead dependent on the ratio of masses. The nondimensionalized positions and times are written as:

$$\mathbf{R} = \frac{\tilde{\mathbf{R}}}{\tilde{l}^*} \quad (2.8)$$

$$t = \frac{\tilde{t}}{\tilde{t}^*} \quad (2.9)$$

Nondimensionalizing the equations of motion by using the characteristic quantities results in:

$$\mathbf{R}'' = -\frac{(1 - \mu)}{{R_{13}}^3}(\mathbf{R} - \mathbf{R}_1) - \frac{\mu}{{R_{23}}^3}(\mathbf{R} - \mathbf{R}_2) \quad (2.10)$$

With the assumption that  $\mathbf{R}_1$  and  $\mathbf{R}_2$  move in circular orbits, their coordinates can be described by sinusoidal functions of time about the center of mass. The inertial reference frame has been defined such that motion is only in the XY plane, so  $Z_1(t) = Z_2(t) = 0$ . The following equations describe the motion of the primary and secondary, given that the bodies lie along the X axis at time  $t = 0$ :

$$\begin{aligned} X_1(t) &= -\mu \cos(t) & X_2(t) &= (1 - \mu) \cos(t) \\ Y_1(t) &= -\mu \sin(t) & Y_2(t) &= (1 - \mu) \sin(t) \end{aligned} \quad (2.11)$$

Note that  $R_1 = \mu$  and  $R_2 = 1 - \mu$  due to the definition of the center of mass and the fact that  $R_{12} = 1$  in the nondimensionalized problem. Inserting the above definitions into the equations of motion, the inertial equations of motion of the CR3BP are expressed as:

$$\begin{aligned} X'' &= -\frac{(1-\mu)(X + \mu \cos(t))}{R_{13}^3} - \frac{\mu(X - (1-\mu) \cos(t))}{R_{23}^3} \\ Y'' &= -\frac{(1-\mu)(Y + \mu \sin(t))}{R_{13}^3} - \frac{\mu(Y - (1-\mu) \sin(t))}{R_{23}^3} \\ Z'' &= -\frac{(1-\mu)Z}{R_{13}^3} - \frac{\mu Z}{R_{23}^3} \end{aligned} \quad (2.12)$$

which are time dependent to account for the phasing of the revolving primary and secondary bodies relative to the spacecraft.

A rotating reference frame is defined to write equations of motions that are independent of time. In this new frame with axes  $\hat{x}\hat{y}\hat{z}$ , denoted by lowercase letters, the  $x$ -axis rotates with the bodies and the  $z$ -axis is aligned with the orbital angular momentum vector of the primaries. Thus, both of the primary bodies are fixed on the  $x$ -axis, with  $x_1 = -\mu$  and  $x_2 = 1 - \mu$ . The relationship between the axes is depicted in Figure 2.2.

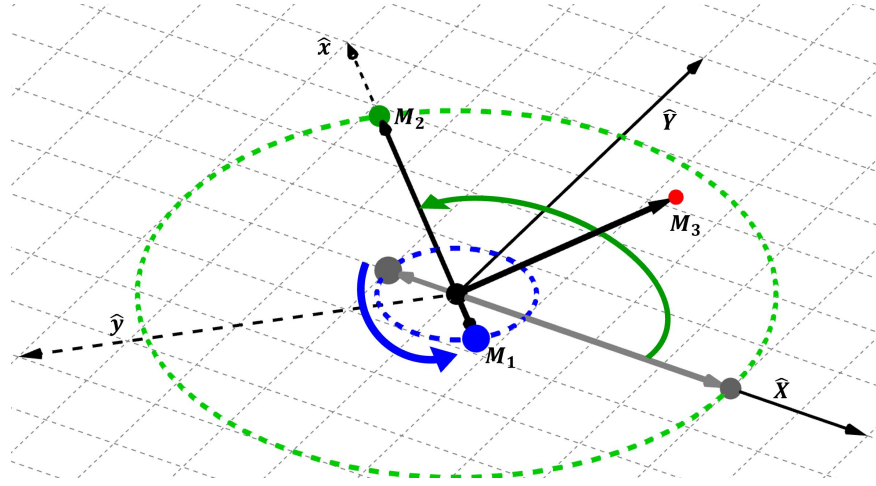


Figure 2.2: Three point masses and their corresponding position vector relative to frame that is centered at the barycenter and has an  $XY$  axis defined by the orbit plane of  $M_1$  and  $M_2$ . The rotating frame is defined such that the  $x$ -axis aligns with the two primary bodies

The description of motion in the inertial frame can be converted a description of motion

in the rotating frame. To transform position vectors between the coordinate systems, a rotation matrix is employed. The transformation from inertial coordinates to rotating coordinates is written as

$$\begin{bmatrix} x \\ y \\ z \end{bmatrix} = \begin{bmatrix} \cos(t) & \sin(t) & 0 \\ -\sin(t) & \cos(t) & 0 \\ 0 & 0 & 1 \end{bmatrix} \begin{bmatrix} X \\ Y \\ Z \end{bmatrix} \quad (2.13)$$

In this formulation, the angular velocity of the rotating frame is defined as  $\boldsymbol{\omega} = 1\hat{z}$ . This angular velocity can be used in the transport theorem to define the velocity in the rotating frame in relation to the velocity in the inertial frame:

$$\mathbf{r}' = (\dot{x} - y)\hat{x} + (\dot{y} + x)\hat{y} + \dot{z}\hat{z} \quad (2.14)$$

The transport theorem can be applied again to get a similar relationship for the acceleration:[29]

$$\mathbf{r}'' = (\ddot{x} - 2\dot{y} - x)\hat{x} + (\ddot{y} + 2\dot{x} - y)\hat{y} + \ddot{z}\hat{z} \quad (2.15)$$

where the dots ( $\cdot$ ) denote a derivative with respect to the rotating frame. Using the inertial acceleration from Eq 2.10, the equations of motion for the CR3BP in the rotating frame are written as:

$$\begin{aligned} \ddot{x} &= 2\dot{y} + x - \frac{(1 - \mu)(x + \mu)}{r_1^3} - \frac{\mu(x - 1 + \mu)}{r_2^3} \\ \ddot{y} &= -2\dot{x} + y - \frac{(1 - \mu)y}{r_1^3} - \frac{\mu y}{r_2^3} \\ \ddot{z} &= -\frac{(1 - \mu)z}{r_1^3} - \frac{\mu z}{r_2^3} \end{aligned} \quad (2.16)$$

where the relative distances are defined by

$$r_1 = \sqrt{(x + \mu)^2 + y^2 + z^2} \quad r_2 = \sqrt{(x - 1 + \mu)^2 + y^2 + z^2} \quad (2.17)$$

These time-invariant equations govern the motion of a spacecraft in the rotating frame in the CR3BP. Although there is no analytical solution to these equations, a constant of motion and fundamental solutions are used to gain insight into the motion of a spacecraft.

## 2.2 Constant of Motion

The Jacobi constant is the integral of motion of the CR3BP, which means that it is conserved for all time in a natural trajectory.[29] To derive the expression for this constant, the equations of motion are rewritten as derivatives of a pseudo-potential function  $U^*$ , defined as:

$$U^* = \frac{1}{2} (x^2 + y^2) + \frac{1 - \mu}{r_1} + \frac{\mu}{r_2} \quad (2.18)$$

Using this function, the equations of motion are rewritten as:

$$\begin{aligned} \ddot{x} - 2\dot{y} &= \frac{\partial U^*}{\partial x} \\ \ddot{y} + 2\dot{x} &= \frac{\partial U^*}{\partial y} \\ \ddot{z} &= \frac{\partial U^*}{\partial z} \end{aligned} \quad (2.19)$$

Taking the dot product of acceleration  $\ddot{\mathbf{r}}$  with velocity  $\dot{\mathbf{r}}$  produces the following equation:

$$\dot{x}\ddot{x} + \dot{y}\ddot{y} + \dot{z}\ddot{z} = \frac{\partial U^*}{\partial x}\dot{x} + \frac{\partial U^*}{\partial y}\dot{y} + \frac{\partial U^*}{\partial z}\dot{z} \quad (2.20)$$

Both sides of this equation can be integrated, producing

$$\frac{1}{2}v^2 = \int dU^* - \frac{dU^*}{dt} \quad (2.21)$$

where  $v^2 = \dot{x}^2 + \dot{y}^2 + \dot{z}^2$ . The pseudo-potential function  $U^*$  does not depend on time, so its derivative with respect to time is zero. The integration of  $U^*$  is carried out, and a constant of integration  $C$  is introduced as

$$v^2 = 2U^* - C \quad (2.22)$$

Rearranging this equation and inserting the definition of  $U^*$ , the Jacobi constant  $C$  is defined as

$$C = x^2 + y^2 + \frac{2(1 - \mu)}{r_1} + \frac{2\mu}{r_2} - v^2 \quad (2.23)$$

This is a constant of motion in the CR3BP, meaning any natural solution will have a constant value of  $C$  for all time. The Jacobi constant can be thought of as a negative energy-like quantity; decreasing the Jacobi constant corresponds to increasing the energy with respect to the three-body

system. Note that increasing  $v$ , the magnitude of the velocity, will lower the Jacobi constant. This will be an important consideration in following sections, as a thrust direction can be defined to produce a desired change in the Jacobi constant.

### 2.3 Equilibrium Points

While the CR3BP does not have a complete analytical solution, it does have fundamental solutions that can be used to gain understanding of the dynamics in the rotating frame. An important set of solutions are equilibrium points, also called Lagrange points or libration points. These are points at which both the velocity and the acceleration are zero. The positions of these points can be solved for by setting  $\ddot{x}$ ,  $\ddot{y}$ ,  $\ddot{z}$ ,  $\dot{x}$ ,  $\dot{y}$ , and  $\dot{z}$  equal to zero in Eq. 2.16. The resulting equations are written as:

$$0 = x - \frac{(1-\mu)(x+\mu)}{r_1^3} - \frac{\mu(x-1+\mu)}{r_2^3} = x \left( 1 - \frac{(1-\mu)}{r_1^3} - \frac{\mu}{r_2^3} \right) + \mu(1-\mu) \left( -\frac{1}{r_1^3} + \frac{1}{r_2^3} \right) \quad (2.24)$$

$$0 = y - \frac{(1-\mu)y}{r_1^3} - \frac{\mu y}{r_2^3} = y \left( 1 - \frac{(1-\mu)}{r_1^3} - \frac{\mu}{r_2^3} \right) \quad (2.25)$$

$$0 = -\frac{(1-\mu)z}{r_1^3} - \frac{\mu z}{r_2^3} = z \left( -\frac{(1-\mu)}{r_1^3} - \frac{\mu}{r_2^3} \right) \quad (2.26)$$

It is apparent by inspection that the  $z$  coordinate must be set to zero for all solutions, as that is the only way to satisfy Eq. 2.26 for all  $\mu$  values. There are two ways of satisfying the Eq. 2.25: setting  $y$  equal to zero, or setting  $(1 - \frac{(1-\mu)}{r_1^3} - \frac{\mu}{r_2^3})$  equal to zero.

First examine the case when  $y = 0$  to locate the collinear equilibrium points. Modifying the definition of  $r_1$  and  $r_2$  to account for the fact that  $z = y = 0$ , the Eq. 2.24 becomes

$$0 = x - \frac{(1-\mu)(x+\mu)}{|x+\mu|^3} - \frac{\mu(x-1+\mu)}{|x-1+\mu|^3} \quad (2.27)$$

This equation is singular at the location of the primaries, meaning that the solutions could lie between the primaries or on either side of them on the  $x$ -axis. This equation must be solved numerically to find the exact solutions, using a different initial guess for a solution between the primaries and on either side. The solutions for equilibrium points to the Hill three-body problem, which can be analytically derived, can be used as an initial guess.[30] One of the approximations in

the Hill three-body problem is that  $\mu \ll 1$ , so these initial guesses are best suited to systems with very small  $\mu$  values. The three initial guesses for the  $x$  coordinate of the three collinear equilibrium points are

$$\begin{aligned} x_1 &= 1 - \left(\frac{\mu}{3}\right)^{(1/3)} \\ x_2 &= 1 + \left(\frac{\mu}{3}\right)^{(1/3)} \\ x_3 &= -1 \end{aligned} \quad (2.28)$$

where  $x_1$  corresponds to the solution between the primaries,  $x_2$  corresponds to the solution greater than  $1 - \mu$ , and  $x_3$  corresponds to the solution less than  $-\mu$ . This is the convention used for Lagrange points as well, labeled respectively  $L_1$ ,  $L_2$ , and  $L_3$ . These are known as the collinear Lagrange points. The three solutions to Eq. 2.27 are shown over the full range of  $\mu$  values in Figure 2.4. The Lagrange points are shown for the Earth-Moon system in Figure 2.3.

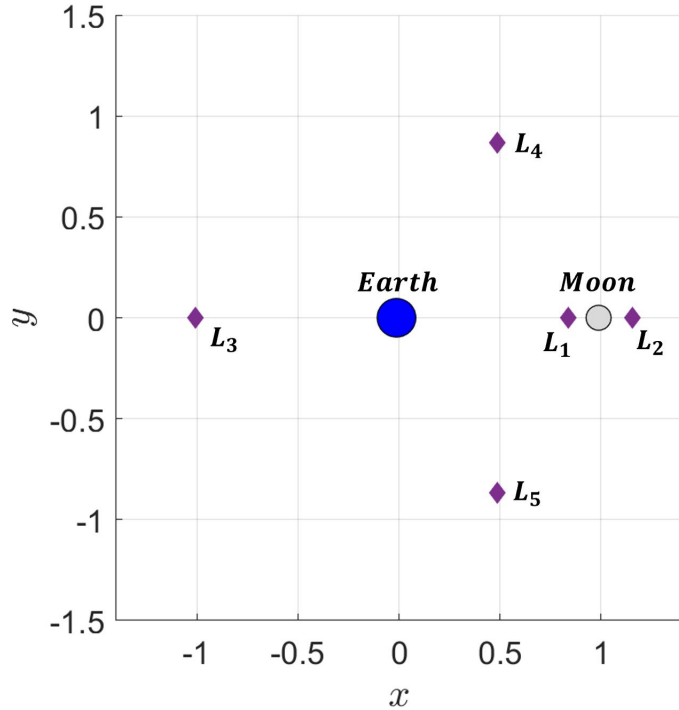


Figure 2.3: The Lagrange points of the Earth-Moon Circular Restricted Three-Body Problem.  $L_1$ ,  $L_2$ , and  $L_3$  are the collinear Lagrange points, while  $L_4$  and  $L_5$  are the equilateral Lagrange points.

The other way of satisfying Eq. 2.25 is to set  $(1 - \frac{(1-\mu)}{r_1^3} - \frac{\mu}{r_2^3})$  equal to zero, producing the two triangular equilibrium points. To satisfy Eq. 2.24 as well,  $(-\frac{1}{r_1^3} + \frac{1}{r_2^3})$  must also be set to zero. This means that  $r_1$  must equal  $r_2$ , so  $(1 - \frac{(1-\mu)}{r_1^3} - \frac{\mu}{r_2^3})$  becomes  $(1 - \frac{1}{r_1^3})$ . The root of this expression is  $r_1 = r_2 = 1$ , which means that the points where  $r_1 = r_2 = 1$  are equilibrium points. Considering the  $z$  coordinate is set to zero, there are two of these points, located at  $x = 1/2 - \mu$  and  $y = \pm\sqrt{3}/2$ . The point with a positive  $y$  value is labeled  $L_4$ , and the point with a negative  $y$  value is labeled  $L_5$ . These form equilateral triangles with the primary and secondary body, and are appropriately known as equilateral or triangular Lagrange points.[36]

The  $x$  coordinate of the Lagrange points depends on the value of  $\mu$  for the system; this dependency is shown in Figure 2.4, and this thesis will only use the  $\mu$  value from the Earth-Moon CR3BP. The coordinates of the Lagrange points for the Earth-Moon system are written in the table below. At each point, the velocity and the acceleration are zero. The truncated value of the Jacobi constant is also computed for each point and shown in the table below. All five of the Lagrange points for the Earth-Moon system are shown in Figure 2.3.

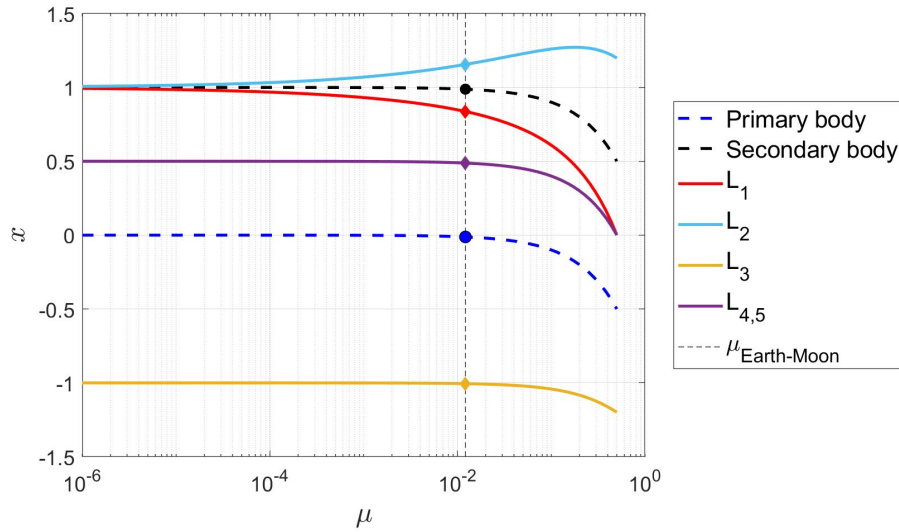


Figure 2.4: The  $x$  coordinate of the Lagrange points is dependent on the mass ratio. All of the Lagrange points are on the xy plane ( $z = 0$ ), the collinear Lagrange points are on the x axis ( $y = 0$ ), and the equilateral Lagrange points have a  $y$  value of  $\pm\sqrt{3}/2$ .

Table 2.2: Nondimensional position coordinates of the Earth-Moon Lagrange points

Lagrange Point	$x$	$y$	$z$	$C$
<b>L1</b>	0.8369	0	0	3.188
<b>L2</b>	1.1557	0	0	3.172
<b>L3</b>	-1.0051	0	0	3.012
<b>L4</b>	0.4879	0.8660	0	2.988
<b>L5</b>	0.4879	-0.8660	0	2.988

A spacecraft located perfectly at a Lagrange point can stay there indefinitely with no maneuvers needed for corrections. With that in mind, it is not reasonable to expect a spacecraft to be perfectly located at a point in space. It is possible for a spacecraft to orbit about a Lagrange point, which is a more feasible goal for a spacecraft. Common types of fundamental solutions near the equilibrium points include periodic orbits, stable manifolds, and unstable manifolds.

## 2.4 State Transition Matrix

Given a reference trajectory, the behavior of neighboring trajectories is often approximated using a first-order analyses. Consider a state variation  $\delta\mathbf{x}(t)$  measured relative to a reference state  $\mathbf{x}_r(t)$ . The absolute state corresponding to this variation equals

$$\mathbf{x}(t) = \mathbf{x}_r(t) + \delta\mathbf{x}(t) \quad (2.29)$$

This variation changes over time as the reference state and neighboring state are propagated to produce unique paths. A variation value at time  $t_0$  may be different from the value at time  $t_1$ . This is shown in Figure 2.5. The purpose of this analyses is to gain a better understanding of how the variation propagates.

To investigate the motion of neighboring trajectories, the equation of motion is linearized about the reference trajectory. The generalized differential equation for this motion can be expressed as:

$$\dot{\mathbf{x}} = \dot{\mathbf{x}}_r + \delta\dot{\mathbf{x}} = \mathbf{f}(\mathbf{x}_r + \delta\mathbf{x}) \quad (2.30)$$

where  $\mathbf{f}(\mathbf{x})$  reflects the equations of motion in Eq. 2.16. The value of  $\mathbf{f}(\mathbf{x})$  can be approximated

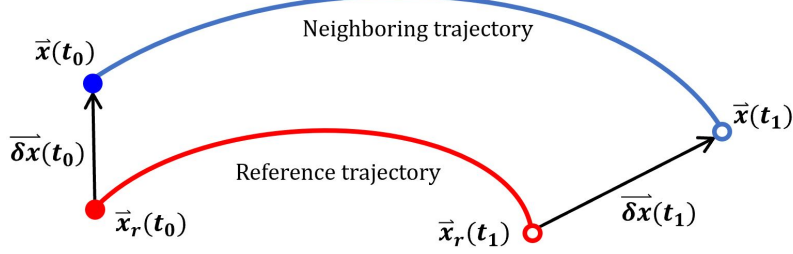


Figure 2.5: Defining a trajectory in terms of the difference relative to a neighboring reference trajectory

using a first order Taylor series expansion about  $\mathbf{x}_r$ . The first order terms will be the dominant terms if  $\delta\mathbf{x}(t)$  is sufficiently small, because if  $1 \gg \delta x$  then  $\delta x \gg (\delta x)^2$ . The first order Taylor expansion is:

$$\dot{\mathbf{x}} = \dot{\mathbf{x}}_r + \delta\dot{\mathbf{x}} \approx \mathbf{f}(\mathbf{x}_r, t) + \left. \frac{\partial \mathbf{f}}{\partial \mathbf{x}} \right|_r \delta\mathbf{x} \quad (2.31)$$

The terms  $\dot{\mathbf{x}}_r$  and  $\mathbf{f}(\mathbf{x}_r, t)$  are equal to each other, so this equation simplifies to:

$$\dot{\delta\mathbf{x}} \approx \left. \frac{\partial \mathbf{f}}{\partial \mathbf{x}} \right|_r \delta\mathbf{x} \quad (2.32)$$

A solution to this differential equation between times  $t_0$  and  $t_1$  is

$$\delta\mathbf{x}(t) = \Phi(t, t_0) \delta\mathbf{x}(t_0) \quad (2.33)$$

where  $\Phi(t, t_0)$  is the state transition matrix (STM).[27] The STM is a linear mapping from a state deviation at  $t_0$  to a state deviation at  $t_1$ . If  $t_0 = t_1$ , the STM  $\Phi(t_0, t_0)$  is equal to the identity matrix. Starting from this initial condition, the STM can be propagated along with the reference state to map to any small deviation. The differential equation for the STM is derived by substituting Eq. 2.33 into Eq. 2.32, and equals

$$\dot{\Phi}(t, t_0) = [\mathbf{A}] \Phi(t, t_0) \quad (2.34)$$

where the matrix  $[\mathbf{A}]$  is defined as  $\left. \frac{\partial \mathbf{f}}{\partial \mathbf{x}} \right|_r$ . For a state defined as  $\mathbf{x} = [x, y, z, \dot{x}, \dot{y}, \dot{z}]^T$ , the STM is

equivalent to:

$$\Phi(t, t_0) = \frac{\partial \mathbf{x}(t)}{\partial \mathbf{x}(t_0)} = \begin{bmatrix} \frac{\partial x(t)}{\partial x(t_0)} & \frac{\partial x(t)}{\partial y(t_0)} & \frac{\partial x(t)}{\partial z(t_0)} & \frac{\partial x(t)}{\partial \dot{x}(t_0)} & \frac{\partial x(t)}{\partial \dot{y}(t_0)} & \frac{\partial x(t)}{\partial \dot{z}(t_0)} \\ \frac{\partial y(t)}{\partial x(t_0)} & \frac{\partial y(t)}{\partial y(t_0)} & \frac{\partial y(t)}{\partial z(t_0)} & \frac{\partial y(t)}{\partial \dot{x}(t_0)} & \frac{\partial y(t)}{\partial \dot{y}(t_0)} & \frac{\partial y(t)}{\partial \dot{z}(t_0)} \\ \frac{\partial z(t)}{\partial x(t_0)} & \frac{\partial z(t)}{\partial y(t_0)} & \frac{\partial z(t)}{\partial z(t_0)} & \frac{\partial z(t)}{\partial \dot{x}(t_0)} & \frac{\partial z(t)}{\partial \dot{y}(t_0)} & \frac{\partial z(t)}{\partial \dot{z}(t_0)} \\ \frac{\partial \dot{x}(t)}{\partial x(t_0)} & \frac{\partial \dot{x}(t)}{\partial y(t_0)} & \frac{\partial \dot{x}(t)}{\partial z(t_0)} & \frac{\partial \dot{x}(t)}{\partial \dot{x}(t_0)} & \frac{\partial \dot{x}(t)}{\partial \dot{y}(t_0)} & \frac{\partial \dot{x}(t)}{\partial \dot{z}(t_0)} \\ \frac{\partial \dot{y}(t)}{\partial x(t_0)} & \frac{\partial \dot{y}(t)}{\partial y(t_0)} & \frac{\partial \dot{y}(t)}{\partial z(t_0)} & \frac{\partial \dot{y}(t)}{\partial \dot{x}(t_0)} & \frac{\partial \dot{y}(t)}{\partial \dot{y}(t_0)} & \frac{\partial \dot{y}(t)}{\partial \dot{z}(t_0)} \\ \frac{\partial \dot{z}(t)}{\partial x(t_0)} & \frac{\partial \dot{z}(t)}{\partial y(t_0)} & \frac{\partial \dot{z}(t)}{\partial z(t_0)} & \frac{\partial \dot{z}(t)}{\partial \dot{x}(t_0)} & \frac{\partial \dot{z}(t)}{\partial \dot{y}(t_0)} & \frac{\partial \dot{z}(t)}{\partial \dot{z}(t_0)} \end{bmatrix} \quad (2.35)$$

This matrix is useful to understand how a state deviation at an initial time will influence a state deviation at another time.

Following the dynamics described by Eq. 2.34, the STM is typically propagated along with the state itself. The  $[\mathbf{A}]$  matrix is defined  $\left. \frac{\partial \mathbf{f}}{\partial \mathbf{x}} \right|_r$ , which can be derived by hand. The dynamics of the CR3BP can be rewritten as:

$$\mathbf{f}(\mathbf{r}, \mathbf{v}) = \mathbf{g}(\mathbf{r}) + \mathbf{h}(\mathbf{v}) \quad (2.36)$$

where  $\mathbf{g}(\mathbf{r})$  represents the position dependent part of Eq 2.16 and  $\mathbf{h}(\mathbf{v})$  represents the velocity dependent part of Eq 2.16. The  $[\mathbf{A}]$  matrix can therefore be rewritten as:

$$\mathbf{A} = \begin{bmatrix} \mathbf{0}_{3 \times 3} & \mathbf{I}_{3 \times 3} \\ \mathbf{G}(\mathbf{r}) & \mathbf{H}(\mathbf{v}) \end{bmatrix} \quad (2.37)$$

where  $\mathbf{I}_{3 \times 3}$  is the identity matrix,  $\mathbf{G}(\mathbf{r}) = \frac{\partial \mathbf{g}}{\partial \mathbf{r}}$  and  $\mathbf{H}(\mathbf{v}) = \frac{\partial \mathbf{h}}{\partial \mathbf{v}}$ . The  $\mathbf{G}$  and  $\mathbf{H}$  matrices are defined as:

$$\mathbf{G}(\mathbf{r}) = \begin{bmatrix} U_{xx}^* & U_{xy}^* & U_{xz}^* \\ U_{yx}^* & U_{yy}^* & U_{yz}^* \\ U_{zx}^* & U_{zy}^* & U_{zz}^* \end{bmatrix} \quad \mathbf{H}(\mathbf{v}) = \begin{bmatrix} 0 & 2 & 0 \\ -2 & 0 & 0 \\ 0 & 0 & 0 \end{bmatrix} \quad (2.38)$$

where  $U_{ij}^* = \frac{\partial U^*}{\partial i \partial j}$ . These derivatives are equal to the following analytical expressions:

$$\begin{aligned}
 U_{xx}^* &= 1 - \frac{1-\mu}{r_1^3} - \frac{\mu}{r_2^3} + \frac{3(1-\mu)(x+\mu)^2}{r_1^5} + \frac{3\mu(x-1+\mu)^2}{r_2^5} \\
 U_{yy}^* &= 1 - \frac{1-\mu}{r_1^3} - \frac{\mu}{r_2^3} + \frac{3y^2(1-\mu)}{r_1^5} + \frac{3\mu y^2}{r_2^5} \\
 U_{zz}^* &= -\frac{1-\mu}{r_1^3} + \frac{3z^2(1-\mu)}{r_1^5} - \frac{\mu}{r_2^3} + \frac{3\mu z^2}{r_2^5} \\
 U_{xy}^* = U_{yx}^* &= \frac{3y(1-\mu)(x+\mu)}{r_1^5} + \frac{3\mu y(x-1+\mu)}{r_2^5} \\
 U_{xz}^* = U_{zx}^* &= \frac{3z(1-\mu)(x+\mu)}{r_1^5} + \frac{3\mu z(x-1+\mu)}{r_2^5} \\
 U_{yz}^* = U_{zy}^* &= \frac{3yz(1-\mu)}{r_1^5} + \frac{3\mu yz}{r_2^5}
 \end{aligned} \tag{2.39}$$

These equations are used to propagate the STM, which must be done simultaneously with the reference trajectory itself.

## 2.5 Periodic Orbits

Although the CR3BP does not admit Keplerian orbits like the two-body problem does, periodic orbits do exist. These trajectories repeat in the rotating frame and exist in continuous families. Typically, these orbits are computed numerically from an initial guess. Smaller orbits can be derived from oscillatory eigenmodes of the  $[A]$  matrix evaluated about a Lagrange point, but larger orbits deviate from the linearized motion. These orbits can have a variety of shapes.

One family of periodic orbits is the  $L_1$  Lyapunov orbit family. These are planar orbits about the  $L_1$  point. Small Lyapunov orbits can be derived by analyses of the eigenmodes of  $[A]$  evaluated at the  $L_1$  point, and these will closely resemble the sinusoidal motion from the linearized system. At larger amplitudes the shape of the orbits become more skewed. Selected orbits from the  $L_1$  Lyapunov family in the Earth-Moon CR3BP are shown in Figure 2.6. These orbits can have many different uses for a real space mission. The Earth-Moon  $L_1$  point is between the primary and secondary bodies, so a spacecraft could utilize an  $L_1$  orbit to relay data, provide coverage of the Moon's surface, dock with another spacecraft, idle for systems confirmation and station-keeping, or any other reason relevant to space missions.

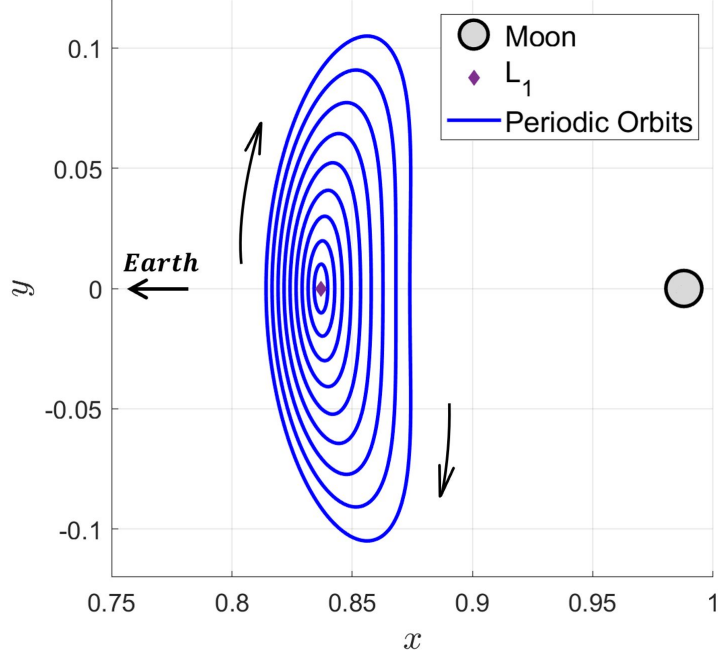


Figure 2.6: Selected orbits from the Earth-Moon  $L_1$  Lyapunov orbit family

Periodic orbits do not have to be planar, and often out-of-plane components can be desirable. One example of an orbit family with out-of-plane components is the  $L_2$  halo orbit family. This family is grouped into northern orbits, in which most of the time along the orbit is spent above the  $xy$  plane, and southern orbits, in which most of the time along the orbit is spent below the  $xy$  plane. These orbits are more well known because NASA announced that the Lunar Gateway would use an orbit in the southern  $L_2$  halo family. This particular orbit is known as a near rectilinear halo orbit (NRHO) and has very close approaches to the Moon.[20] Selected orbits from the southern  $L_2$  halo orbit family are shown in the Figures 2.7 and 2.8. These orbits have favorable stability qualities, and the out-of-plane component can ensure access to Earth communications while having the ability to observe the Moon at different latitudes.

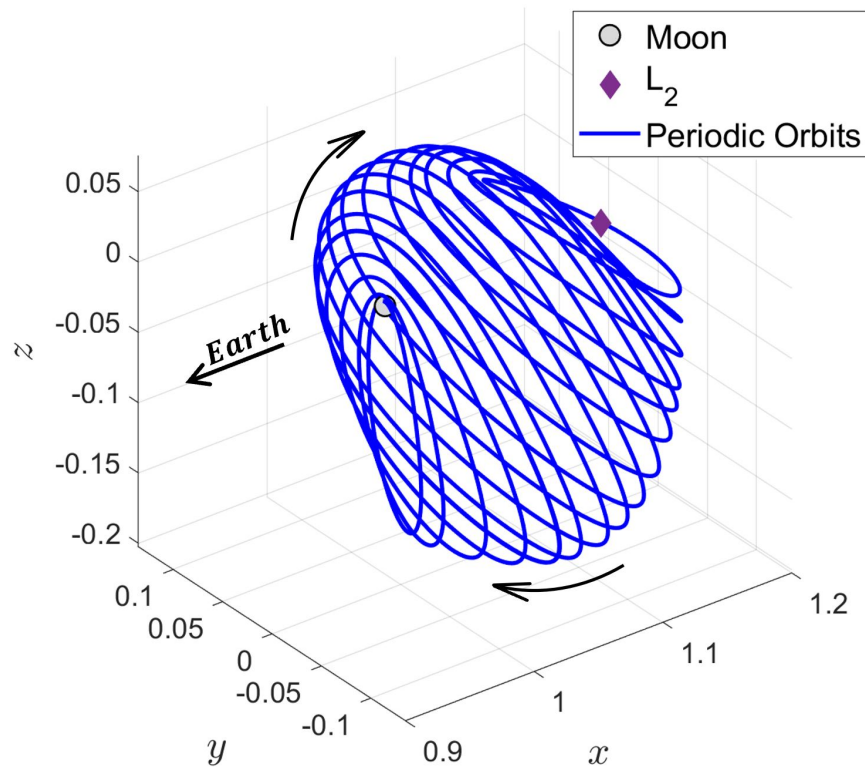


Figure 2.7: Selected orbits from the Earth-Moon Southern  $L_2$  halo orbit family.

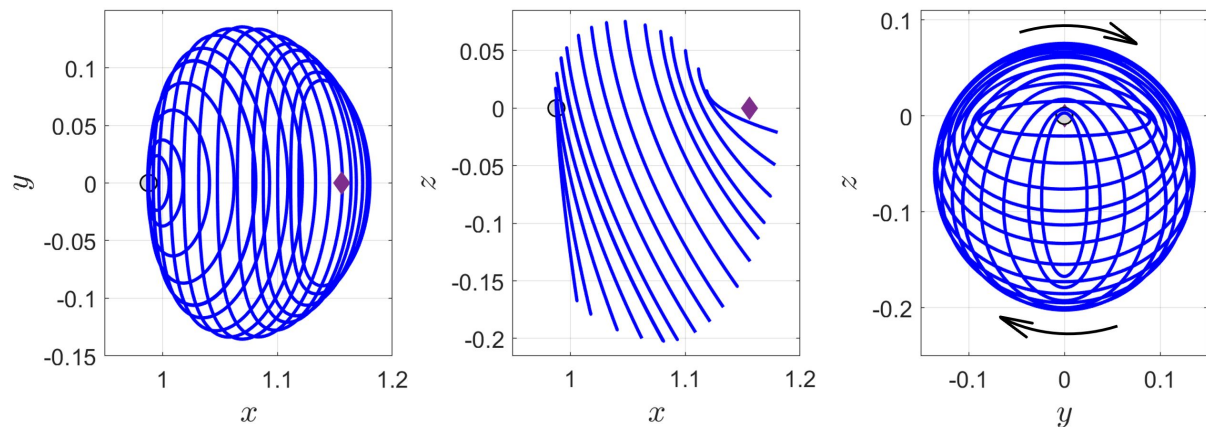


Figure 2.8: Selected orbits from the Earth-Moon Southern  $L_2$  halo orbit family, viewed from their 2D projection from three directions

## 2.6 Stability and Hyperbolic Invariant Manifolds

The stability of an equilibrium point is typically assessed by examining eigenvalues and eigenvectors of the  $[A]$  matrix. A six by six matrix will have six eigenvalues, each with a corresponding eigenvector. For a matrix  $[M]$ , the eigenvalues  $\lambda$  and eigenvectors  $v$  have the relationship:

$$[M]v = \lambda v \quad (2.40)$$

Substituting this equation into the linearized system in Eq. 2.32 produces the relationship

$$[A]\delta x_v = \lambda \delta x_v = \delta \dot{x} \quad (2.41)$$

where  $\delta x_v$  is a state deviation aligned with an eigenvector. By inspection, a negative real eigenvalue will cause  $\delta x_v$  to have a derivative in its opposing direction,  $\delta \dot{x} = -|\lambda| \delta x_v$ , causing the state deviation to shrink in magnitude and approach the equilibrium point. This deviation is associated with a stable mode. A real eigenvalue that is positive will have the opposite effect: a given deviation will grow arbitrarily, meaning it is associated with an unstable mode. A small deviation in a stable or unstable eigenvector direction can be propagated to find the stable or unstable manifolds of the equilibrium point. A stable manifold, which must be propagated backwards in time from a reference point, is a set of states that will approach the reference point in forward time as time tends to infinity. An unstable manifold is the opposite; a state on the unstable manifold will diverge from the reference point.

A similar approach is used to assess the stability of periodic orbits. The monodromy matrix is defined as the STM propagated along the periodic orbit for one orbit period  $\tau$ .[27] This monodromy matrix possesses eigenvalues that define the stability of the periodic orbit. The relationship between the monodromy matrix and its eigenvector and eigenvalue is written as

$$\lambda \delta x_v(t_0 + \tau) = \Phi(t_0 + \tau, t_0) \delta x_v(t_0) \quad (2.42)$$

If an eigenvector is associated with a real eigenvalue with a magnitude greater than 1, then a small deviation in that eigenvector's direction will increase in magnitude after one period. This

growth will compound over multiple periods, and the trajectory will eventually diverge from the orbit, corresponding to an unstable mode. Similarly, if an eigenvector has real eigenvalue with a magnitude less than 1, a small deviation in that direction will shrink over one period. Over multiple periods, the deviation will get arbitrarily small and the trajectory will asymptotically approach the orbit, corresponding to a stable mode.

To generate stable and unstable manifolds, the eigenvalues of the monodromy matrix at each state along the orbit are used. By evaluating the stable eigenvectors at each state in an orbit and imparting a small deviation in that direction, a set of initial states that asymptotically approach the periodic orbit in forward time can be generated. Propagating these states backwards in time creates a set of trajectories that asymptotically approach the periodic orbit. This set of trajectories produces a stable manifold. The inverse can be done for the unstable manifold. Propagating the states with a deviation in the direction of the unstable eigenvectors at many points in the orbit creates a set of trajectories that naturally diverge from the periodic orbits. Both manifolds are shown in Figure 2.9 for a Lyapunov orbit about  $L_1$  in the Earth-Moon CR3BP with a period of 2.72 nondimensional time units. The stable manifold, shown in blue, naturally flows into the periodic orbit as time tends towards infinity. The unstable manifold, shown in red, naturally flows out of the periodic orbit as time tends towards infinity.

These natural manifolds are very useful to mission designers. If it is desirable for a spacecraft to be in a periodic orbit, the spacecraft can target a state on a stable manifold and use the natural dynamics of the system to approach the desired orbit without using maneuvers. If the spacecraft is stationed on a periodic orbit and needs to transfer to another desired destination, it can utilize an unstable manifold to leave the orbit with small maneuver requirements.

## 2.7 Frame Transformations

It is often useful to convert between states expressed in the inertial and rotating frame. Rotation matrices enable the transformation between any position vector expressed in the rotating frame (denoted by lowercase  $\mathbf{r}$ ) and the corresponding position vector in the inertial frame (denoted

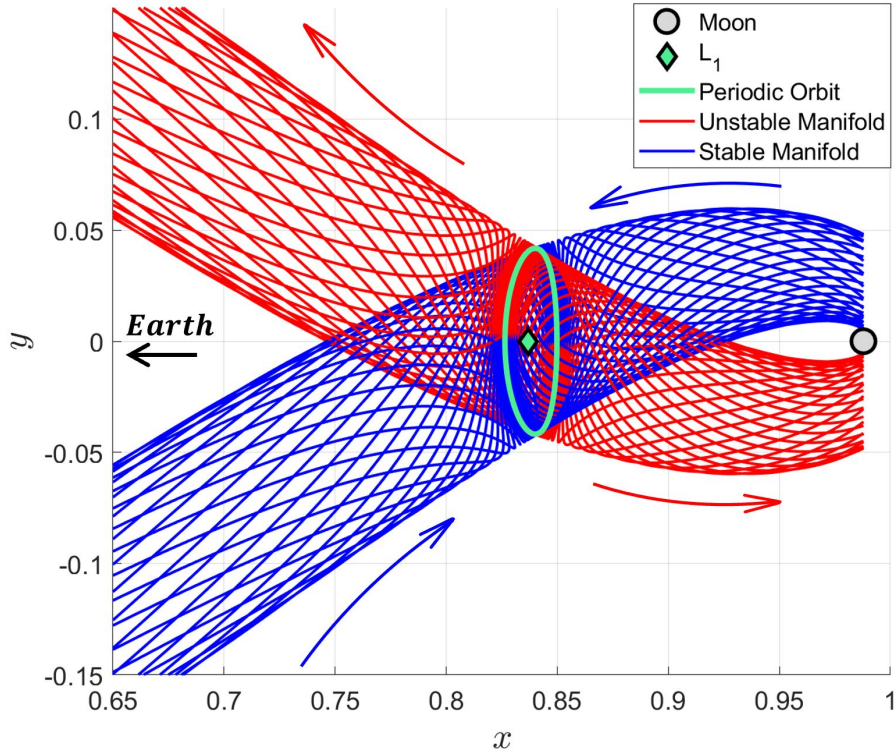


Figure 2.9: Sets of trajectories on the stable and unstable half manifolds of a  $L_1$  Lyapunov orbit. The stable manifold asymptotically approaches the orbit, while the unstable manifold asymptotically diverges from the orbit

by uppercase  $\mathbf{R}$ ). The rotation matrices use the nondimensional value of time  $t$  that is zero or a multiple of  $2\pi$  when  $\mathbf{r} = \mathbf{R}$ .

$$\mathbf{r} = \begin{bmatrix} \cos(t) & \sin(t) & 0 \\ -\sin(t) & \cos(t) & 0 \\ 0 & 0 & 1 \end{bmatrix} \mathbf{R} \quad \mathbf{R} = \begin{bmatrix} \cos(t) & -\sin(t) & 0 \\ \sin(t) & \cos(t) & 0 \\ 0 & 0 & 1 \end{bmatrix} \mathbf{r} \quad (2.43)$$

Most trajectories in this thesis are computed in the rotating frame, but many trajectories are more intuitive in the inertial frame. This can be seen in the figure below for an arbitrary trajectory propagated in the Earth-Moon CR3BP. Viewing the trajectory in the inertial frame, the spacecraft follows a nearly elliptical orbit about Earth and the motion is perturbed by the Moon.

The relative position between the spacecraft (denoted  $\mathbf{r}_3$ ) and an arbitrary point (denoted  $\mathbf{r}_P$ ) is simply  $\mathbf{r}_{P3} = \mathbf{r}_3 - \mathbf{r}_P$ . In the case that the point is one of the primary bodies, this can be

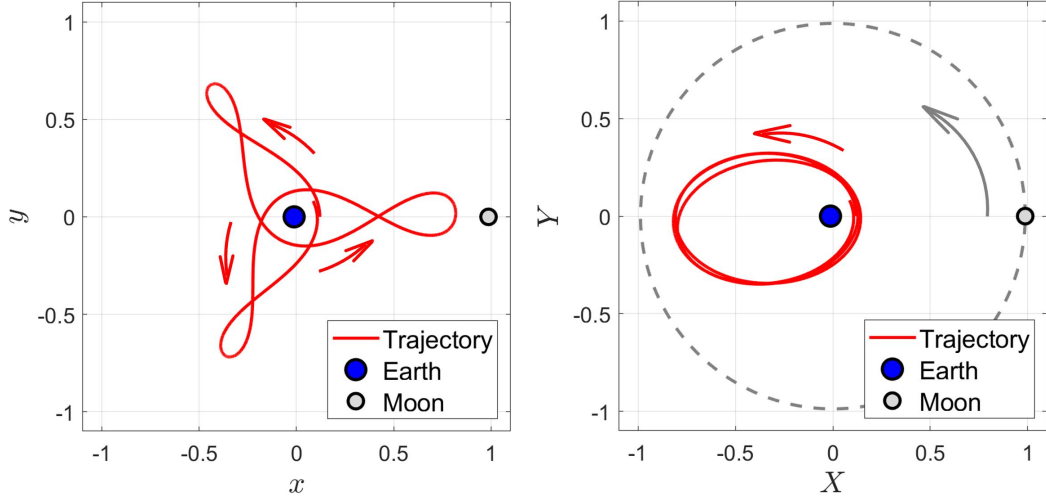


Figure 2.10: The lefthand plot shows a trajectory propagated in the CR3BP rotating frame. The righthand plot shows the same trajectory after a conversion to the inertial frame. Note that the Earth and Moon do not move in the lefthand rotating frame, but revolve around the origin in the righthand inertial frame.

applied to derive  $\mathbf{r}_{13} = \mathbf{r}_3 - \mathbf{r}_1$  and  $\mathbf{r}_{23} = \mathbf{r}_3 - \mathbf{r}_2$ . This holds true for inertial vectors as well. Once the relative position is computed in one frame, a rotation matrix defined above can be applied to put the relative position in the desired frame.

## 2.8 Eccentricity Relative to the Primary Bodies

The magnitude of the eccentricity is an orbital element in the classical two-body problem that can be used to measure how close an orbit is to a circle. An eccentricity of zero corresponds to a circle. Many practical problems involve orbits that are measured as circular and exist close to a primary body. It is useful to have an expression for eccentricity relative to each body. If all three components of the eccentricity vector are zero, then the state corresponds to a circular orbit in the two-body problem.

The classical eccentricity vector takes the form below:[37]

$$\mathbf{e} = \frac{\tilde{\mathbf{V}} \cdot \tilde{\mathbf{V}}}{\tilde{GM}} \tilde{\mathbf{R}} - \frac{\tilde{\mathbf{R}} \cdot \tilde{\mathbf{V}}}{\tilde{GM}} \tilde{\mathbf{V}} - \frac{\tilde{\mathbf{R}}}{\tilde{R}} \quad (2.44)$$

where  $\tilde{\mathbf{R}}$  and  $\tilde{\mathbf{V}}$  are dimensional position and velocity vectors relative to a body, with the velocity

taken relative to the inertial frame. Nondimensionalizing results in the following equations for the eccentricity relative to bodies 1 and 2.

$$\mathbf{e}_1 = \frac{\mathbf{v}_1 \cdot \mathbf{v}_1}{1 - \mu} \mathbf{r}_1 - \frac{\mathbf{r}_1 \cdot \mathbf{v}_1}{1 - \mu} \mathbf{v}_1 - \frac{\mathbf{r}_1}{r_1} \quad (2.45)$$

$$\mathbf{e}_2 = \frac{\mathbf{v}_2 \cdot \mathbf{v}_2}{\mu} \mathbf{r}_2 - \frac{\mathbf{r}_2 \cdot \mathbf{v}_2}{\mu} \mathbf{v}_2 - \frac{\mathbf{r}_2}{r_2} \quad (2.46)$$

where the 1 subscript denotes variables with respect to the primary body and the 2 subscript denotes variables with respect to the secondary body. Recall from the previous sections that the relative position vectors can be expressed in the rotating frame as follows:

$$\mathbf{r}_1 = \mathbf{r} + \mu \hat{\mathbf{x}} \quad \mathbf{r}_2 = \mathbf{r} - (1 - \mu) \hat{\mathbf{x}} \quad (2.47)$$

To calculate the relative velocity vectors taken in the inertial frame (but expressed in the rotating frame), Eq. 2.14 must be applied to the relative position. This is shown below.

$$\mathbf{r}'_{P3} = \mathbf{r}'_3 - \mathbf{r}'_P = ((\dot{x} - \dot{x}_P) - (y - y_P)) \hat{\mathbf{x}} + ((\dot{y} - \dot{y}_P) + (x - x_P)) \hat{\mathbf{y}} + (\dot{z} - \dot{z}_P) \hat{\mathbf{z}}. \quad (2.48)$$

This can be useful to convert a state on a computed trajectory in the CR3BP to the inertial frame relative to a primary body. The inertial frame is relative to the barycenter, but in cases where the trajectory is close to a primary body, it is desirable to get state information relative to the body itself. To derive the equations for this conversion, the values for  $\dot{x}_P$ ,  $\dot{y}_P$ , and  $\dot{y}_P$  are set to zero because the bodies are on the x axis and have no velocity in the rotating frame. The  $x$  value of each body is then input to arrive at the following equations.

$$\begin{aligned} \mathbf{r}'_{23} &= (\dot{x} - y) \hat{\mathbf{x}} + (\dot{y} + x - 1 + \mu) \hat{\mathbf{y}} + \dot{z} \hat{\mathbf{z}} \\ \mathbf{r}'_{13} &= (\dot{x} - y) \hat{\mathbf{x}} + (\dot{y} + x + \mu) \hat{\mathbf{y}} + \dot{z} \hat{\mathbf{z}} \end{aligned} \quad (2.49)$$

## 2.9 Augmenting the CR3BP with Continuous Thrust

To add continuous thrust into the equations of motion, the original formulation must be revisited. Starting with Eq. 2.1, a thrust force is added. This thrust has a maximum value  $T_{max}$  and is applied in a direction  $\hat{\mathbf{u}}$ . The throttle vector  $\mathbf{u}$ , defined such that  $|\mathbf{u}| \leq 1$ , determines the

magnitude and direction of the thrust. This means that the propulsion is modeled with variable thrust. The addition of thrust is reflected in the equation below:

$$\widetilde{M}_3 \widetilde{\mathbf{R}}_3'' = -\frac{\widetilde{G}\widetilde{M}_1\widetilde{M}_3}{\widetilde{R}_{13}^3} \widetilde{\mathbf{R}}_{13} - \frac{\widetilde{G}\widetilde{M}_2\widetilde{M}_3}{\widetilde{R}_{23}^3} \widetilde{\mathbf{R}}_{23} + \widetilde{T}_{max} \mathbf{u} \quad (2.50)$$

Applying thrust will change the mass of the spacecraft as propellant mass is expelled. This means that while the masses of the primaries stay constant, the mass of the spacecraft will change. The rate of change in mass is a property of the propulsion system, which can be written as [8]

$$\dot{\widetilde{M}}_3 = \frac{-\widetilde{T}_{max}|\mathbf{u}|}{\widetilde{I}_{sp}\widetilde{g}_0} \quad (2.51)$$

These equations can be nondimensionalized using the characteristic parameters. The mass change rate is nondimensionalized by  $\tilde{t}^*$  and the initial mass of the spacecraft  $\tilde{m}_0$ , where  $m = \widetilde{M}_3/\tilde{m}_0$ . The nondimensional mass rate, as well as the nondimensional equations of motion comparable to Eq. 2.10 are shown below.

$$\mathbf{R}'' = -\frac{(1-\mu)}{{R_{13}}^3}(\mathbf{R} - \mathbf{R}_1) - \frac{\mu}{{R_{23}}^3}(\mathbf{R} - \mathbf{R}_2) + \frac{T^*}{m} \mathbf{u} \quad (2.52)$$

$$\dot{m} = -b^*|\mathbf{u}| \quad (2.53)$$

where the nondimensional parameters  $T^*$  and  $b^*$  are defined below.

$$T^* = \frac{\widetilde{T}_{max}(\tilde{t}^*)^2}{\tilde{l}^*\tilde{m}_0} \quad b^* = \frac{\widetilde{T}_{max}\tilde{t}^*}{\widetilde{I}_{sp}\widetilde{g}_0\tilde{m}_0} \quad (2.54)$$

After accounting for the rotational frame, the equations of motion for the CR3BP with continuous thrust are

$$\begin{aligned} \ddot{x} &= 2\dot{y} + x - \frac{(1-\mu)(x+\mu)}{r_1^3} - \frac{\mu(x-1+\mu)}{r_2^3} + \frac{T^*}{m} u_x \\ \ddot{y} &= -2\dot{x} + y - \frac{(1-\mu)y}{r_1^3} - \frac{\mu y}{r_2^3} + \frac{T^*}{m} u_y \\ \ddot{z} &= -\frac{(1-\mu)z}{r_1^3} - \frac{\mu z}{r_2^3} + \frac{T^*}{m} u_z \end{aligned} \quad (2.55)$$

where  $u_x$ ,  $u_y$ , and  $u_z$  are components of the thrust throttle direction vector in axes of the rotating frame. These equations can be propagated for any given propulsion system, and the direction and throttle of the thrust can be adjusted over time to impart desired motion. It is important to note

that the direction and magnitude of the thrust can be changed continuously. If desired, the thrust can be in the velocity direction and change continuously with the velocity.

## Chapter 3

### Numerically Computing Trajectories

Unlike the two-body problem, which can be solved in closed form, the computation of desired solutions in the CR3BP requires numerical methods. Shooting methods are commonly used to compute a trajectory between known end points. Single shooting attempts to correct the transfer by iteratively updating the state of a trajectory, while multiple shooting splits the trajectory into segments and then iteratively updates the segments simultaneously. Multiple shooting is used to compute transfers in this thesis. Other methods such as natural parameter continuation and Poincaré maps are introduced in this chapter as well, which are both utilized to generate results in Chapter 6.

#### 3.1 Single Shooting Method

Shooting methods are commonly used to solve boundary value problems, which involve computing a trajectory between two known boundary points using the given differential equations of motion. The shooting method approach to solving a boundary value problem has been developed for any general differential equations. In the single shooting method, a single state is propagated from the initial time to the final time. An initial guess must be used as the first trial, and then the result of the propagation of that initial guess is compared to the desired end point. An updated guess is constructed based on the difference between the initial guess result and the desired result. A second trial is conducted by using this updated guess to produce a trajectory, and the results again determine the guess for the next trial. This continues until the boundary conditions are met

to a specified tolerance. A representation of this approach is shown in Figure 3.1, where  $\vec{x}_{d,0}$  and  $\vec{x}_{d,f}$  represent the initial and final desired states, respectively. The state at the end of a trajectory at iteration  $i$  is represented by  $\vec{x}_{i,f}$ .

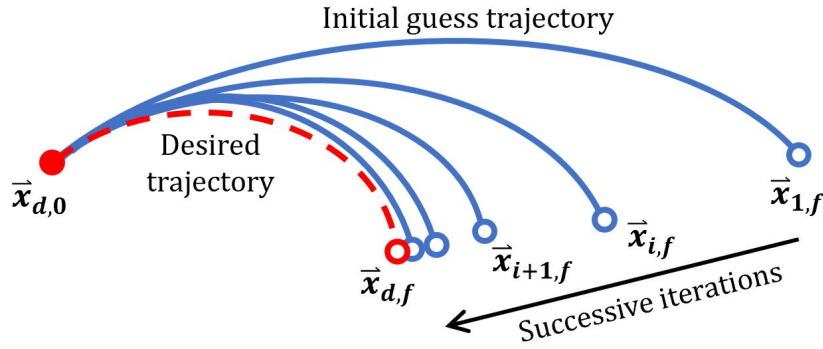


Figure 3.1: The iterative updates of the single shooting method.

The updates and constraints must be described mathematically. This definition involves two vectors: a free variable vector  $\mathbf{V}$  that is composed of all parameters than can be updated, and a constraint vector  $\mathbf{F}$  that is composed of all the constraint equations, where  $\mathbf{F} = \mathbf{0}$  indicates that the constraints are satisfied. It is assumed that the initial guess  $\mathbf{V}_0$  is close to the desired solution  $\mathbf{V}^*$ , where  $\mathbf{F}(\mathbf{V}^*) = \mathbf{0}$ . The initial guess must be close enough for the numerical corrector to converge on the solution. Generating a solution that is “close enough” can be very challenging and will be the topic of Chapter 5. Linearizing about the initial guess by using a first-order Taylor series expansion produces

$$\mathbf{F}(\mathbf{V}^*) = \mathbf{0} = \mathbf{F}(\mathbf{V}_0) + \left. \frac{\partial \mathbf{F}}{\partial \mathbf{V}} \right|_{\mathbf{V}_0} \delta \mathbf{V} \quad (3.1)$$

which can be rearranged:

$$\mathbf{F}(\mathbf{V}_0) = - \left. \frac{\partial \mathbf{F}}{\partial \mathbf{V}} \right|_{\mathbf{V}_0} \delta \mathbf{V} \quad (3.2)$$

The correction  $\delta \mathbf{V}$  can be solved for by inverting the Jacobian  $\frac{\partial \mathbf{F}}{\partial \mathbf{V}}$ , but only if it is invertible. Only square matrices can be inverted, and the Jacobian will only be square if the number of constraints is equal to the number of free variables. This is often not the case in boundary value problems. In those cases, the minimum norm solution will be used instead, which results in the following update

equation:[2]

$$\delta \mathbf{V} = - \left[ \frac{\partial \mathbf{F}}{\partial \mathbf{V}} \right]^T \left[ \left[ \frac{\partial \mathbf{F}}{\partial \mathbf{V}} \right] \left[ \frac{\partial \mathbf{F}}{\partial \mathbf{V}} \right]^T \right]^{-1} \mathbf{F}(\mathbf{V}_0) \quad (3.3)$$

Adding this difference to the previous guess will update the free variables for the next iteration.

The update equation at iteration  $i$  is equal to

$$\mathbf{V}^{i+1} = \mathbf{V}^i - (\mathbf{DF})^T [(\mathbf{DF})(\mathbf{DF})^T]^{-1} \mathbf{F} \quad (3.4)$$

where the  $i$  superscript represents the  $i$ th iteration and  $\mathbf{DF}$  is the Jacobian  $\left[ \frac{\partial \mathbf{F}}{\partial \mathbf{V}} \right]$ . The Jacobian can be derived either numerically or analytically, but in this research it is derived analytically.

The computation of a Lyapunov orbit will be used as an example. The initial guess for this orbit can be generated from investigation of eigenmodes as mentioned in Chapter 2. The initial guess can be constructed using the leftmost point of the orbit that intersects the  $x$  axis; at this point,  $y = 0$ ,  $\dot{x} = 0$ , and  $\dot{y} > 0$ . The mirror theorem can be used to generate constraints. The mirror theorem states that a trajectory flipped over the  $xz$  plane is valid if it's direction of motion is reversed. [28] In other words, if  $y$  is set to  $-y$  and  $t$  is set to  $-t$ , the dynamics in Eq. 2.16 do not change. This means that only half of the Lyapunov orbit needs to be computed as the other half will be symmetric if  $\dot{x} = 0$  at the  $x$  axis. So a trajectory that is propagated in the positive  $y$  region until it crosses the  $x$  axis will create an orbit if  $y = 0$  and  $\dot{x} = 0$ . A free variable vector and constraint vector can then be defined as:

$$\mathbf{V} = \begin{bmatrix} \dot{y}_0 & t_f & \beta \end{bmatrix}^T \quad (3.5)$$

$$\mathbf{F} = \begin{bmatrix} y(t_f) & \dot{x}(t_f) & (t_f - \beta^2) \end{bmatrix}^T \quad (3.6)$$

where  $\beta$  is a slack variable ensuring that  $t_f > 0$ . The initial state  $\mathbf{x}_0$  is set to  $[x_0, 0, 0, 0, \dot{y}_0, 0]^T$ , where  $x_0$  is predetermined and  $\dot{y}_0$  updates for each guess. Note that  $t_f$  also updates each iteration, so the propagation time of the desired trajectory must be determined as well.

To construct the  $\mathbf{DF}$  matrix, the partial derivatives of each of the constraints with respect to each of the free variables are computed. Recall from Eq. 2.35 that the STM  $\Phi(t, t_0)$  is defined

as the partial derivative of a final state with respect to an initial state,  $\frac{\partial \mathbf{x}(t)}{\partial \mathbf{x}(t_0)}$ . The  $\mathbf{DF}$  matrix for the Lyapunov orbit boundary value problem is shown below.

$$\mathbf{D}\tilde{\mathbf{F}} = \begin{bmatrix} \Phi_{2,5} & \dot{y}_f & 0 \\ \Phi_{4,5} & \ddot{x}_f & 0 \\ 0 & 1 & -2\beta \end{bmatrix} \quad (3.7)$$

where the subscripts on  $\Phi$  indicate the respective row and column of the STM. This matrix can be used in the update equation to compute the top half of a Lyapunov orbit given an initial guess for free variable vector. An example of this computation for an  $L_1$  Lyapunov orbit is displayed in Figure 3.2. It can be seen that the initial guess does not result in a periodic orbit, but iterative corrections result in convergence to the desired orbit. A tolerance of  $10^{-10}$  was used for this example.

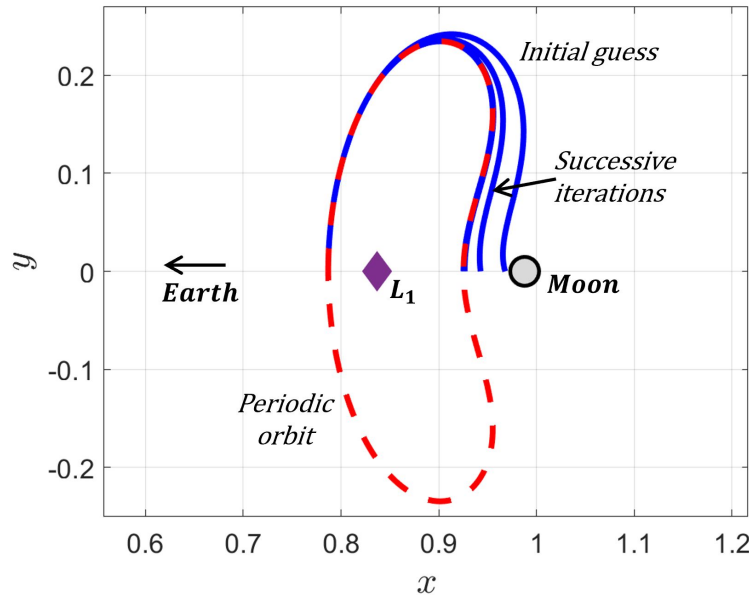


Figure 3.2: An example of a single shooting method used to compute an  $L_1$  Lyapunov orbit.

For a program that correctly implements a single shooting method for a sufficiently close initial guess, there should be quadratic convergence. Quadratic convergence means that the plot of the constraint vector magnitude for each successive iteration should appear to be a quadratic function. This type of convergence is associated with Newton's method, and the update equation

(Eq. 3.4) is the matrix version of Newton's method. The geometric norm of the constraint vector for each iteration is shown in Figure 3.3 for the example  $L_1$  Lyapunov orbit computation. The size of the constraint vector gets arbitrarily small, but can never reach zero because of machine precision and the computational difficulties of handling very small numbers.

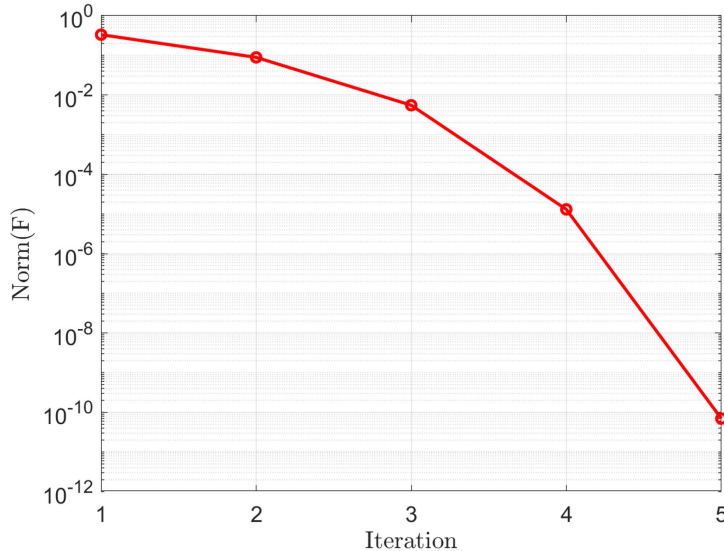


Figure 3.3: The geometric norm of each successive iteration for the example Lyapunov orbit computation shows quadratic convergence

The single shooting method can be insufficient for longer trajectories. The updates can be very sensitive if just one start point is used, and a large update on an inadequate initial guess can prevent the solution from converging.

### 3.2 Multiple Shooting Method

A more robust approach to corrections is to split a trajectory into multiple segments and iteratively update all of these segments simultaneously. This is appropriately known as multiple shooting. Along with the boundary conditions, the continuity of the trajectory between segments needs to be enforced via constraints. This means that the difference between the final state of one segment and the beginning state of the following segment must be zero.

For  $n$  trajectory segments,  $n$  free variable subvectors are defined to describe each segment. There are  $n+1$  constraint subvectors, and constraints are enforced at all intermediate points as well as the boundaries. The interior constraints, which will have the same form for each intermediate segment, enforce continuity. Boundary constraints on the beginning of the first segment and the end of the last segment enforce the desired boundary conditions. The intermediate and boundary constraint subvectors are stacked into a single column vector to form a full constraint vector, and the same applies for the free variable vector. These general free variable and constraint vectors are then defined as

$$\mathbf{V} = \left[ \mathbf{V}_1^T, \mathbf{V}_2^T, \dots, \mathbf{V}_i^T, \dots, \mathbf{V}_n^T \right]^T \quad (3.8)$$

$$\mathbf{F} = \left[ \mathbf{F}_{D,0}^T, \mathbf{F}_1^T, \mathbf{F}_2^T, \dots, \mathbf{F}_i^T, \dots, \mathbf{F}_{n-1}^T, \mathbf{F}_{D,f}^T \right]^T \quad (3.9)$$

Finally, the  $\mathbf{DF}$  matrix needs to be defined, utilizing the STM for each segment. This will be used in the update equation to correct an trajectory. A diagram of a multiple shooting problem is shown in Figure 3.4.

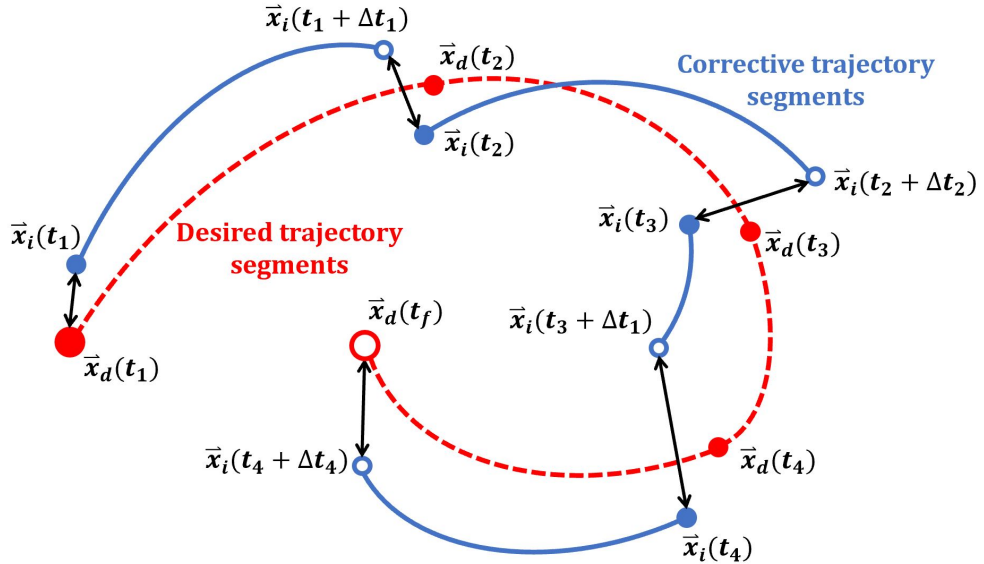


Figure 3.4: Schematic diagram of the elements of multiple shooting

The computation of a periodic orbit will be used as an example of multiple shooting. In this example case, imagine that a single position along an orbit has been given, and the trajectory of the orbit is to be found. The boundaries conditions are that the initial state is at the given position, and that the final state matches the initial state. Intermediate constraints are also needed to enforce continuity and make sure each segment is propagated in forward time. For the  $i$ th segment of the trajectory, the free variables and constraints are written as

$$\mathbf{V}_i = \left[ \mathbf{x}_{i,0}^T, \Delta t_i, \beta_i \right]^T \quad (3.10)$$

$$\mathbf{F}_i = \left[ (\mathbf{x}_{i,f} - \mathbf{x}_{i+1,0})^T, \Delta t_i - \beta_i^2 \right]^T \quad (3.11)$$

$$\mathbf{F}_{D,f} = \left[ (\mathbf{x}_{n,f} - \mathbf{x}_{1,0})^T, \Delta t_n - \beta_n^2 \right]^T \quad (3.12)$$

$$\mathbf{F}_{D,0} = \left[ \mathbf{r}_{1,0} - \mathbf{r}_{D,0} \right] \quad (3.13)$$

These vectors are used to construct the full free variable and constraint vector as shown in Eqs. 3.9 and 3.8. The  $\mathbf{DF}$  matrix can be constructed in blocks, and is equal to

$$\mathbf{DF}(\mathbf{V}) = \left[ \frac{\partial \mathbf{F}}{\partial \mathbf{V}} \right] = \begin{bmatrix} \frac{\partial \mathbf{F}_{D,0}}{\partial \mathbf{V}_1} & 0 & \dots & \dots & \dots & \dots & \dots & 0 \\ \frac{\partial \mathbf{F}_1}{\partial \mathbf{V}_1} & \frac{\partial \mathbf{F}_1}{\partial \mathbf{V}_2} & \ddots & & & & & \vdots \\ 0 & \frac{\partial \mathbf{F}_2}{\partial \mathbf{V}_2} & \frac{\partial \mathbf{F}_2}{\partial \mathbf{V}_3} & \ddots & & & & \vdots \\ \vdots & \ddots & \ddots & \ddots & \ddots & & & \vdots \\ \vdots & & \ddots & \frac{\partial \mathbf{F}_i}{\partial \mathbf{V}_i} & \frac{\partial \mathbf{F}_i}{\partial \mathbf{V}_{i+1}} & \ddots & & \vdots \\ \vdots & & & \ddots & \ddots & \ddots & \ddots & \vdots \\ \vdots & & & & \ddots & \frac{\partial \mathbf{F}_{n-2}}{\partial \mathbf{V}_{n-2}} & \frac{\partial \mathbf{F}_{n-2}}{\partial \mathbf{V}_{n-1}} & 0 \\ 0 & & & & & \ddots & \frac{\partial \mathbf{F}_{N-1}}{\partial \mathbf{V}_{N-1}} & \frac{\partial \mathbf{F}_{N-1}}{\partial \mathbf{V}_N} \\ \frac{\partial \mathbf{F}_{D,f}}{\partial \mathbf{V}_1} & 0 & \dots & \dots & \dots & \dots & 0 & \frac{\partial \mathbf{F}_{D,f}}{\partial \mathbf{V}_n} \end{bmatrix} \quad (3.14)$$

where each block partial derivative is defined below.

$$\frac{\partial \mathbf{F}_i}{\partial \mathbf{V}_i} = \begin{bmatrix} \Phi_{i,6 \times 6} & \dot{\mathbf{x}}_{i,f} & 0_{6 \times 1} \\ 0_{1 \times 6} & 1 & -2\beta_i \end{bmatrix}_{7 \times 8} \quad (3.15)$$

$$\frac{\partial \mathbf{F}_i}{\partial \mathbf{V}_{i+1}} = \begin{bmatrix} -I_{6 \times 6} & 0_{6 \times 1} & 0_{6 \times 1} \\ 0_{1 \times 6} & 0 & 0 \end{bmatrix}_{7 \times 8} \quad (3.16)$$

$$\frac{\partial \mathbf{F}_{D,0}}{\partial \mathbf{V}_1} = \begin{bmatrix} I_{3 \times 3} & 0_{3 \times 5} \end{bmatrix}_{3 \times 8} \quad (3.17)$$

$$\frac{\partial \mathbf{F}_{D,f}}{\partial \mathbf{V}_1} = \begin{bmatrix} -I_{6 \times 6} & 0_{6 \times 2} \\ 0_{1 \times 6} & 0_{1 \times 2} \end{bmatrix}_{7 \times 8} \quad (3.18)$$

$$\frac{\partial \mathbf{F}_{D,f}}{\partial \mathbf{V}_n} = \begin{bmatrix} \Phi_{n,6 \times 6} & \dot{\mathbf{x}}_{n,f} & 0_{6 \times 1} \\ 0_{1 \times 6} & 1 & -2\beta_N \end{bmatrix}_{7 \times 8} \quad (3.19)$$

The free variable, constraint, and  $\mathbf{DF}$  matrix defined above can be used in the update equation to compute any periodic orbit. An algorithm using this method is used to generate the halo orbits displayed in Figures 2.7 and 2.8.

### 3.3 Natural Parameter Continuation

Continuation is a strategy commonly used to find trajectories that are very close to a known solution. By taking a known trajectory and enforcing a constraint that it must be slightly different, a new nearby trajectory can be computed efficiently. A slight parameter change, whether it be to the initial state or another parameter of interest, can be enforced and the original trajectory can be used as a very good initial guess for a nearby trajectory. This method is employed successfully in Chapter 6.

For example, when computing a family of periodic orbits, one periodic orbit can be used as the initial guess for computation of another one. Imagine an orbit is given with a Jacobi constant of  $C_0$ . A different orbit can be computed by enforcing a constraint that the new orbit is to have

$C = C_0 + \delta C$ , and the original orbit can be used as an initial guess. Assuming the  $\delta C$  was sufficiently small and a solution exists, a numerical correction scheme may compute the desired trajectory quickly because the solutions are very close. Continuation can also be applied to a thrust-enabled transfer to compute solutions while gradually varying the magnitude of the thrust, or the mass, or the shape of the transfer. The theoretical concept that trajectories with continuously differing parameters lie near each other can be utilized effectively in numerical computation. A first solution that was generated by a manually constructed initial guess may not be the desired solution, but continuation can be applied to iteratively change the solution until the desired parameters are reached.

### 3.4 Poincaré Maps

A common difficulty is determining patterns in a trajectory or set of trajectories. Simply plotting the trajectories can sometimes be helpful for visualization, but Poincaré maps offer a format to synthesize trajectory information into a more digestible and analyzable format.[26] To create a Poincaré map, a surface of section must first be defined. A surface of section is a plane that a trajectory can pass through. An instance of a trajectory crossing this surface can be recorded and plotted on the Poincaré map. After many crossings, a pattern may emerge that was not clear beforehand or a set of trajectories can be visualized more straightforwardly. A periodic orbit will appear as a point on a suitably-defined, one-sided Poincaré map because it will traverse the same exact trajectory each revolution, while a quasi-periodic orbit will trace the outline of a closed curve on a Poincaré map.

A Poincaré map can be especially useful for analysis of planar trajectories in the CR3BP. Consider a surface of section defined as the  $xz$  plane, which includes the  $y$  axis line. Each crossing of this line will have a set of four state elements;  $x$ ,  $y$ ,  $\dot{x}$ , and  $\dot{y}$ . Yet the trajectory must have a conserved Jacobi constant, and the definition of the surface of section can provide an equation for the states (in this case,  $x = 0$ ), so that makes two equations for four unknowns. Two of the recorded state elements can be plotted to completely define the state. This means that simply by

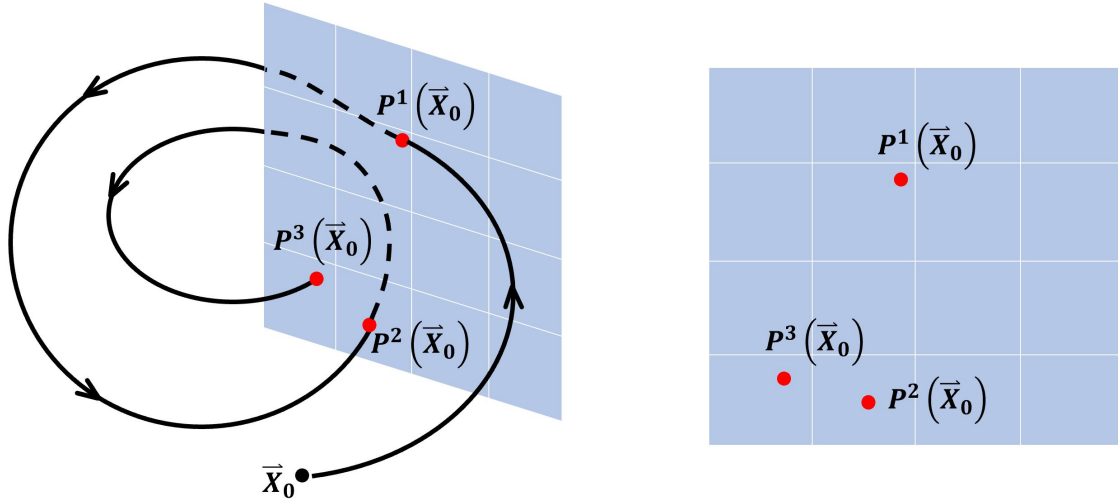


Figure 3.5: A Poincaré map records the intersections of a trajectory with a surface of section and displays the crossings in two dimensions

looking at a point on Poincaré map, the entire state of a point can be determined.

A Poincaré map is also useful for designing an initial guess. Points that appear very close on a Poincaré map are good candidates for patching the trajectory together at that point. A transfer from one structure to another, such as an unstable manifold to a stable manifold, can be designed based on where the structures come closest to intersecting on the Poincaré map. This method will be used in following sections of this research to patch a spiral out trajectory onto a stable manifold.

## Chapter 4

### Optimal Control Theory in the CR3BP

#### 4.1 General Form of Hamiltonian Optimal Control

Optimal control theory is very powerful because it can analytically optimize any cost function using any set of dynamics for any desired constraints. In this thesis, it will be applied to the thrust enabled CR3BP to minimize propellant usage. Before applying optimal control theory to the CR3BP, the form of the theory will be laid out in general terms. The proof that this method produces an optimal result will not be provided here, but the procedure for practical purposes will be discussed.[4] For an  $n$ -dimensional state  $\mathbf{x}(t)$  and an  $m$ -dimensional control vector  $\mathbf{u}$ , suppose the system's differential equations of motion are in the form

$$\dot{\mathbf{x}} = \mathbf{f}(\mathbf{x}, \mathbf{u}, t) \quad (4.1)$$

and suppose the problem also has some terminal constraints specified. These could be any constraint equations that use the initial state, initial time, final state, or final time. They are written in a form to be set to zero, with the initial time being  $t_0$  and the final time being  $t_f$  such that

$$\Psi(\mathbf{x}(t_0), t_0, \mathbf{x}(t_f), t_f) = \mathbf{0} \quad (4.2)$$

Then a scalar cost function,  $J$ , is specified. The goal of this analysis is to minimize this cost function. The cost function can be a function of the initial or final states, or a continuous sum of some form that is integrated along the path of the state, generally defined as

$$J = K(\mathbf{x}(t_0), t_0, \mathbf{x}(t_f), t_f) + \int_{t_0}^{t_f} L(\mathbf{x}, \mathbf{u}, t) d\tau \quad (4.3)$$

The first step in computing an optimal solution is to define a system Hamiltonian  $H$ , defined by

$$H(\mathbf{x}, \mathbf{p}, \mathbf{u}, t) = \mathbf{p}(t) \cdot \mathbf{f}(\mathbf{x}, \mathbf{u}, t) + L(\mathbf{x}, \mathbf{u}, t) \quad (4.4)$$

where  $\mathbf{p}(t)$  is a vector of co-states or adjoints. These can be thought of as dynamic Lagrange multipliers that aid in finding an optimal solution, but have no physical representation.[3] These adjoints will change over time.

The goal of optimal control theory is to find the control vector  $\mathbf{u}$  that minimizes the Hamiltonian. The optimal control vector is denoted  $\mathbf{u}^*$ . Pontryagin's minimum principle states that applying  $\mathbf{u}^*$  to the dynamics will satisfy the necessary conditions of optimality.[3] Once an optimal control law is found, it can be input back into the Hamiltonian to create the optimal Hamiltonian  $H^*$ , shown below.

$$H^*(\mathbf{x}, \mathbf{p}, t) = \mathbf{p}(t) \cdot \mathbf{f}(\mathbf{x}, \mathbf{u}^*(\mathbf{x}, \mathbf{p}, t), t) + L(\mathbf{x}, \mathbf{u}^*(\mathbf{x}, \mathbf{p}, t), t) \quad (4.5)$$

The dynamics of the state and adjoints are then defined by the following differential equations: [4]

$$\dot{\mathbf{p}} = - \left( \frac{\partial H^*}{\partial \mathbf{x}} \right)^T \quad \dot{\mathbf{x}} = \left( \frac{\partial H^*}{\partial \mathbf{p}} \right)^T \quad (4.6)$$

The terminal constraints of the Hamiltonian and adjoints are determined by the constant part of the cost function and the constraint vector. These are known as the transversality conditions:

$$\mathbf{p}(t_0) = - \frac{\partial K}{\partial \mathbf{x}_0} - \boldsymbol{\lambda} \cdot \frac{\partial \Psi}{\partial \mathbf{x}_0} \quad (4.7a)$$

$$\mathbf{p}(t_f) = \frac{\partial K}{\partial \mathbf{x}_f} + \boldsymbol{\lambda} \cdot \frac{\partial \Psi}{\partial \mathbf{x}_f} \quad (4.7b)$$

$$H(t_0) = \frac{\partial K}{\partial t_0} + \boldsymbol{\lambda} \cdot \frac{\partial \Psi}{\partial t_0} \quad (4.7c)$$

$$H(t_f) = - \frac{\partial K}{\partial t_f} - \boldsymbol{\lambda} \cdot \frac{\partial \Psi}{\partial t_f} \quad (4.7d)$$

If adjoints exist that satisfy the dynamics and transversality conditions, then the resulting dynamics and control satisfy the necessary conditions of optimality. That means that the resulting path between the endpoints is a candidate for a solution to minimize the cost function. This formulation is very powerful because it can fit to any set of dynamics. In the following sections it will be applied to the dynamics of gravity with the cost function being the total thrust applied.

## 4.2 Primer Vector Theory

Primer vector theory is the application of Hamiltonian optimization to a spacecraft trajectory under the influence of gravity and potentially thrust.[4] This is commonly applied to the two-body problem. There are a few different forms of this derivation and definition, but most follow the same general steps. The state vector is written as

$$\mathbf{x} = \begin{bmatrix} \mathbf{r}^T & \mathbf{v}^T & m \end{bmatrix}^T \quad (4.8)$$

where  $\mathbf{r}$  is the position vector,  $\mathbf{v}$  is the velocity vector, and  $m$  is the mass. The state is governed by a dynamical system that incorporates gravity, which is a function of only the position vector. The spacecraft is also applying thrust, which imparts an acceleration and also lowers the mass. The dynamics in the two-body problem are described by the following equation:

$$\dot{\mathbf{x}} = \mathbf{f}(\mathbf{x}, \mathbf{u}, t) = \begin{bmatrix} \mathbf{v} \\ \mathbf{g}(\mathbf{r}) + \frac{\Gamma}{m}\mathbf{u} \\ -b|\mathbf{u}| \end{bmatrix} \quad (4.9)$$

where  $\Gamma$  is the thrust force magnitude,  $\mathbf{g}(\mathbf{r})$  is the gravitational acceleration,  $b$  is the mass flow rate at maximum thrust, and  $\mathbf{u}$  is the control throttle direction vector such that  $|\mathbf{u}| \leq 1$ . These are the dynamics that will be used in the optimal control formulation.

Constraints also need to be specified mathematically. Before optimality is introduced, it is essential to specify the constraints that would make this trajectory admissible. If the boundary points are known states, then these constraints specify that boundary values must have a specified position and velocity. The mass at the initial state is also known. These are written as

$$\Psi = [(\mathbf{r}(t_0) - \mathbf{r}_0)^T, (\mathbf{v}(t_0) - \mathbf{v}_0)^T, (\mathbf{r}(t_f) - \mathbf{r}_f)^T, (\mathbf{v}(t_f) - \mathbf{v}_f)^T, m(t_0) - m_0] = \mathbf{0} \quad (4.10)$$

where  $\mathbf{r}_0$ ,  $\mathbf{v}_0$ ,  $\mathbf{r}_f$ ,  $\mathbf{v}_f$ , and  $m_0$  are the input desired boundary values. In this formulation, the final time is unconstrained. It is also possible to specify the times, which would be the time fixed case.

The objective of this problem is to find a trajectory from one location to another that minimizes total thrust, which is equivalent to maximizing final mass. The objective function to be

minimized is defined as:

$$J = \int_{t_0}^{t_f} b|\mathbf{u}|d\tau \quad (4.11)$$

Note that this is an application of Eq. 4.3 that defines  $K$  as zero and  $L$  as  $b|\mathbf{u}|$ . The Hamiltonian can then be written as

$$H = \mathbf{p}_r \cdot \mathbf{v} + \mathbf{p}_v \cdot \left( \mathbf{g}(\mathbf{r}) + \frac{\Gamma}{m} \mathbf{u} \right) - p_m b |\mathbf{u}| + b |\mathbf{u}| \quad (4.12)$$

where adjoint vector  $\mathbf{p}$  has been defined as a column vector with components corresponding to the state vector and mass as

$$\mathbf{p} = \begin{bmatrix} \mathbf{p}_r^T & \mathbf{p}_v^T & p_m \end{bmatrix}^T \quad (4.13)$$

Pontryagin's minimum principle is used to minimize the Hamiltonian, rewritten as

$$H = \mathbf{p}_r \cdot \mathbf{v} + \mathbf{p}_v \cdot \mathbf{g}(\mathbf{r}) + b |\mathbf{u}| (1 - p_m) + \frac{\Gamma}{m} \mathbf{p}_v \cdot \mathbf{u} \quad (4.14)$$

Notice that only the rightmost term is dependent on the direction of the control vector. The optimal control law for the direction can be derived using just this term. To minimize that term, the dot product between  $\mathbf{p}_v$  and  $\mathbf{u}$  must be minimized. This can be accomplished by enforcing that the control must be in the opposite direction of  $\mathbf{p}_v$ , which will cause the most negative dot product between the vectors. This optimal control law is shown as

$$\hat{\mathbf{u}}^* = -\frac{\mathbf{p}_v}{p_v} \quad (4.15)$$

The adjoint for velocity,  $\mathbf{p}_v$ , is referred to as the primer vector because of its importance in this problem.[17]

The direction of the control can be determined, but the magnitude must be determined as well to have a complete optimal control law. Inserting Eq. 4.15 back into the Hamiltonian, it can be rewritten as:

$$H = \mathbf{p}_r \cdot \mathbf{v} + \mathbf{p}_v \cdot \mathbf{g}(\mathbf{r}) + b |\mathbf{u}| \left( 1 - p_m - \frac{\Gamma p_v}{bm} \right) \quad (4.16)$$

The optimal size of the control vector is dependent on the coefficient it is multiplied by. If the coefficient is negative, the control should be at its maximum magnitude to amplify its negative

effect and minimize the Hamiltonian. If the coefficient is positive, the magnitude should be zero to negate the effect of the term. The coefficient is defined as the switching function because of this switch in optimal control modes. The switching function is defined as

$$S(m, p_v, p_m) = \left(1 - p_m - \frac{\Gamma p_v}{bm}\right) \quad (4.17)$$

The optimal control law can then be written as:

$$\left. \begin{aligned} |\mathbf{u}^*| &= |\mathbf{u}|_{max} = 1, & \text{if } S < 0 \\ |\mathbf{u}^*| &= |\mathbf{u}|_{min} = 0, & \text{if } S > 0 \end{aligned} \right\} |\mathbf{u}^*| = \frac{1}{2}(1 - \text{sign}(S)) \quad (4.18)$$

which specifies the magnitude of the throttle depending on the sign of the switching function.

The final step is to find the boundary conditions and adjoint dynamics. Applying Eqs. 4.7a and 4.7b produces the boundary condition:

$$p_m(t_f) = 0 \quad (4.19)$$

If the time is fixed, then this is the only constraint. A trajectory that satisfies only this condition will be a local optimal for the specific transfer time. If time is considered free, then Eqs. 4.7c and 4.7d can be used to generate the following two additional constraints:

$$H(t_0) = 0 \quad H(t_f) = 0 \quad (4.20)$$

Trajectories that satisfy all of the above constraints are local optimal for any transfer time. Note that the result of the transversality conditions also includes many relationships between  $p_i$  and  $\lambda_i$ , but these are neglected because  $\lambda_i$  is unknown. The adjoints abide by dynamics as per Eq. 4.6, written as [4]

$$\dot{\mathbf{p}}_r = -\frac{\partial H}{\partial \mathbf{r}} = -\frac{\partial}{\partial \mathbf{r}}(\mathbf{p}_v \cdot \mathbf{g}(\mathbf{r})) = -[\mathbf{G}(\mathbf{r})]^T \mathbf{p}_v \quad (4.21)$$

$$\dot{\mathbf{p}}_v = -\frac{\partial H}{\partial \mathbf{v}} = -\frac{\partial}{\partial \mathbf{v}}(\mathbf{p}_r \cdot \mathbf{v}) = -\mathbf{p}_r \quad (4.22)$$

$$\dot{\mathbf{p}}_m = -\frac{\partial H}{\partial m} = -|\mathbf{u}| \frac{\Gamma p_v}{bm^2} \quad (4.23)$$

where  $[\mathbf{G}(\mathbf{r})] = \left(\frac{\partial \mathbf{g}}{\partial \mathbf{r}}\right)$  as defined by Eq. 2.38. If a path is found such that adjoints exist that satisfy the above dynamics and constraints, then the path satisfies the necessary conditions for optimality.

Computing this path requires solving a boundary value problem, which must be done numerically in this case.

### 4.3 Primer Vector Theory in the CR3BP

Primer vector theory can also be used in the CR3BP.[38] The same state is considered, but the dynamics are now that of the CR3BP in the rotating frame. This not only accounts for the gravity of both bodies, but also captures the formulation in the rotating frame. In the CR3BP, the dynamics are written as:

$$\dot{\mathbf{x}} = \mathbf{f}(\mathbf{x}, \mathbf{u}, t) = \begin{bmatrix} \mathbf{v} \\ \mathbf{g}(\mathbf{r}) + \mathbf{h}(\mathbf{v}) + \frac{T^*}{m}\mathbf{u} \\ -b^*|\mathbf{u}| \end{bmatrix} \quad (4.24)$$

where  $T^*$  and  $b^*$  replace the general  $\Gamma$  and  $b$ , and are defined as in Eq. 2.54. The functions  $\mathbf{g}(\mathbf{r})$  and  $\mathbf{h}(\mathbf{v})$  account for the components dependent on position and velocity, respectively, in Eq. 2.55, and are equal to

$$\mathbf{g}(\mathbf{r}) = \begin{bmatrix} x - \frac{(1-\mu)(x+\mu)}{r_1^3} - \frac{\mu(x-1+\mu)}{r_2^3} \\ y - \frac{y(1-\mu)}{r_1^3} - \frac{y\mu}{r_2^3} \\ -z(1-\mu) - \frac{z\mu}{r_2^3} \end{bmatrix} \quad \mathbf{h}(\mathbf{v}) = \begin{bmatrix} 2\dot{y} \\ -2\dot{x} \\ 0 \end{bmatrix} \quad (4.25)$$

From this point, the same steps as in primer vector theory can be followed and control laws can be derived. The only difference is the addition of a velocity dependent acceleration in the Hamiltonian. This modified Hamiltonian is:

$$H = \mathbf{p}_r \cdot \mathbf{v} + \mathbf{p}_v \cdot (\mathbf{g}(\mathbf{r}) + \mathbf{h}(\mathbf{v})) + b|\mathbf{u}|S(m, p_v, p_m) \quad (4.26)$$

where the switching function is defined by:

$$S(m, p_v, p_m) = \left(1 - p_m - \frac{T^* p_v}{b^* m}\right) \quad (4.27)$$

The optimal control laws are the same as that of primer vector theory for this modified Hamiltonian:

$$\hat{\mathbf{u}}^* = -\frac{\mathbf{p}_v}{p_v} \quad |\mathbf{u}^*| = \frac{1}{2}(1 - \text{sign}(S)) \quad (4.28)$$

The transversality boundary conditions also hold as defined in Eqs. 4.19 and 4.20. The addition of a velocity dependent acceleration term has an effect on the Hamiltonian and thus the adjoint equations of motion. The modified adjoint dynamics are then equal to.

$$\dot{\mathbf{p}}_r = -\left(\frac{\partial H}{\partial \mathbf{r}}\right)^T = -\frac{\partial}{\partial \mathbf{r}}(\mathbf{p}_v \cdot \mathbf{g}(\mathbf{r})) = -[\mathbf{G}(\mathbf{r})]^T \mathbf{p}_v \quad (4.29)$$

$$\dot{\mathbf{p}}_v = -\left(\frac{\partial H}{\partial \mathbf{v}}\right)^T = -\frac{\partial}{\partial \mathbf{v}}(\mathbf{p}_r \cdot \mathbf{v} + \mathbf{p}_v \cdot \mathbf{h}(\mathbf{v})) = -\mathbf{p}_r - [\mathbf{H}(\mathbf{v})]^T \mathbf{p}_v \quad (4.30)$$

$$\dot{\mathbf{p}}_m = -\frac{\partial H}{\partial m} = -|\mathbf{u}| \frac{\Gamma p_v}{bm^2} \quad (4.31)$$

where  $[\mathbf{H}(\mathbf{v})] = \left(\frac{\partial \mathbf{h}}{\partial \mathbf{v}}\right)$  as defined by Eq. 2.38. The above equations create a set of dynamics and boundary conditions that can be solved as a boundary value problem.

#### 4.4 Smoothing

It may be noted that the control law in Eq. 4.15 creates a “bang-bang” control due to the sign function. This means that  $|\mathbf{u}|$  is either set to one or zero; the thrust is either at a maximal value or off completely. This discontinuous behavior creates challenges during numerical corrections. To account for this, a smoothing function is introduced to approximate the sign function. The technique used will be hyperbolic smoothing, as it has been shown to be preferable over homotopic smoothing.[31] This will use a hyperbolic tangent function to approximate the sign function, and incorporates a smoothing factor that can be lowered to approach bang-bang control. The comparison between the hyperbolic tangent function and the sign function is shown in Figure 4.1.

Substituting the hyperbolic tangent in for the sign function, the optimal control law becomes:

$$|\mathbf{u}^*| = \frac{1}{2} \left( 1 - \tanh\left(\frac{S}{\epsilon}\right) \right) \quad (4.32)$$

A solution will first be found by setting the smoothing parameter  $\epsilon$  to 1, and then natural parameter continuation will be used to successively lower it to a near zero value. At arbitrarily small values of  $\epsilon$ , the function is very close to the bang-bang optimal control, but is a continuous function. This is easier for a numerical corrector to handle.

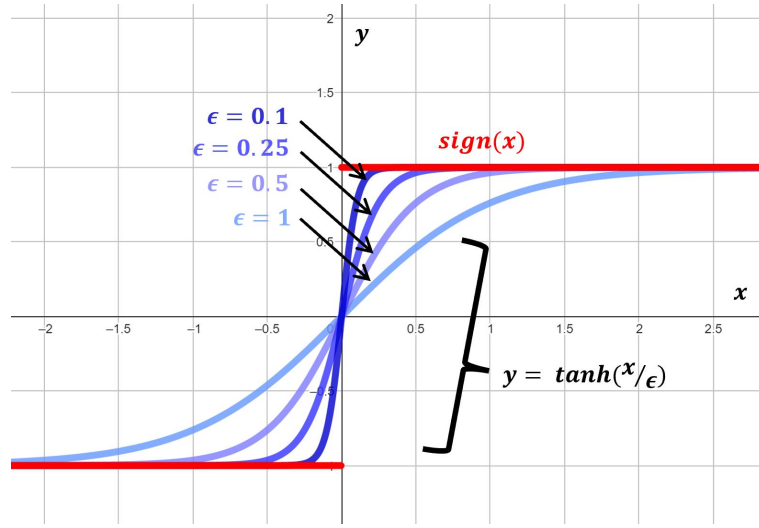


Figure 4.1: The sign function can be smoothed using the hyperbolic tangent. The smoothing factor  $\epsilon$  can be decreased to approach the sign function.

## 4.5 State Transition Matrix for Adjoints

To support the dynamics of both the state variables and adjoint variables, a new state transition matrix can be derived. First, consider an augmented state vector

$$\mathbf{y} = [\mathbf{r}^T, \mathbf{v}^T, m, \mathbf{p}_r^T, \mathbf{p}_v^T, p_m]^T \quad (4.33)$$

The new STM, still denoted  $\Phi$ , is defined by the differential equation in Eq. 2.34, however the  $[\mathbf{A}]$  matrix needs an updated definition. This is shown below.

$$[\mathbf{A}] = \frac{\partial \dot{\mathbf{y}}}{\partial \mathbf{y}} = \begin{bmatrix} \mathbf{0}_{3 \times 3} & \mathbf{I}_{3 \times 3} & \mathbf{0}_{3 \times 1} & \mathbf{0}_{3 \times 3} & \mathbf{0}_{3 \times 3} & \mathbf{0}_{3 \times 1} \\ \mathbf{G}_{3 \times 3} & \mathbf{H}_{3 \times 3} & \Omega_{3 \times 1}^{(1)} & \mathbf{0}_{3 \times 3} & \Omega_{3 \times 3}^{(2)} & \Omega_{3 \times 1}^{(3)} \\ \mathbf{0}_{1 \times 3} & \mathbf{0}_{1 \times 3} & \Omega_{1 \times 1}^{(4)} & \mathbf{0}_{1 \times 3} & \Omega_{1 \times 3}^{(5)} & \Omega_{3 \times 1}^{(6)} \\ \gamma_{3 \times 3} & \mathbf{0}_{3 \times 3} & \mathbf{0}_{3 \times 1} & \mathbf{0}_{3 \times 3} & -\mathbf{G}_{3 \times 3}^T & \mathbf{0}_{3 \times 1} \\ \mathbf{0}_{3 \times 3} & \mathbf{0}_{3 \times 3} & \mathbf{0}_{3 \times 1} & -\mathbf{I}_{3 \times 3} & -\mathbf{H}_{3 \times 3}^T & \mathbf{0}_{3 \times 1} \\ \mathbf{0}_{1 \times 3} & \mathbf{0}_{1 \times 3} & \Omega_{1 \times 1}^{(7)} & \mathbf{0}_{1 \times 3} & \Omega_{1 \times 3}^{(8)} & \Omega_{1 \times 1}^{(9)} \end{bmatrix} \quad (4.34)$$

where the  $\mathbf{G}$  and  $\mathbf{H}$  matrices are defined by Eq. 2.38,  $\gamma$  is  $\frac{\partial(-[\mathbf{G}(\mathbf{r})]\mathbf{p}_v)}{\partial \mathbf{r}}$ , and the variables denoted by  $\Omega^{(i)}$  depend on the control.

The magnitude of the control vector is given by Eq. 4.32 and is dependent on the switching function given by Eq. 4.27. The derivatives of the control vector magnitude can be taken by using the dependencies of the switching function, and are equal to

$$\frac{\partial u}{\partial m} = \frac{-T^* p_v}{2\epsilon b m^2} \left( 1 - \tanh \left( \frac{S}{\epsilon} \right)^2 \right) \quad (4.35a)$$

$$\frac{\partial u}{\partial p_m} = \frac{1}{2\epsilon} \left( 1 - \tanh \left( \frac{S}{\epsilon} \right)^2 \right) \quad (4.35b)$$

$$\frac{\partial u}{\partial \mathbf{p}_v} = \frac{T^*}{2\epsilon b m p_v} \left( 1 - \tanh \left( \frac{S}{\epsilon} \right)^2 \right) \mathbf{p}_v^T \quad (4.35c)$$

Using Eq. 4.35c above and the direction of the control outlined in Eq. 4.15, the following equation can be derived:

$$\frac{\partial \mathbf{u}}{\partial \mathbf{p}_v} = \frac{-T^*}{2\epsilon b m p_v^2} \left( 1 - \tanh \left( \frac{S}{\epsilon} \right)^2 \right) \mathbf{p}_v \mathbf{p}_v^T - \left( \mathbf{I}_{3 \times 3} - \frac{\mathbf{p}_v \mathbf{p}_v^T}{p_v^2} \right) \frac{u}{p_v} \quad (4.36)$$

The equations above can be used to define the  $\Omega^{(i)}$  variables. These definitions are written as

$$\begin{aligned} \Omega^{(1)} &= \frac{-T^* \mathbf{p}_v}{m p_v} \left( \frac{\partial u}{\partial m} \right) - \frac{T^* \mathbf{u}}{m^2} & \Omega^{(2)} &= \frac{T^*}{m} \left( \frac{\partial \mathbf{u}}{\partial \mathbf{p}_v} \right) & \Omega^{(3)} &= \frac{-T^* \mathbf{p}_v}{m p_v} \left( \frac{\partial u}{\partial p_m} \right) \\ \Omega^{(4)} &= -b \left( \frac{\partial u}{\partial m} \right) & \Omega^{(5)} &= -b \left( \frac{\partial u}{\partial \mathbf{p}_v} \right) & \Omega^{(6)} &= -b \left( \frac{\partial u}{\partial p_m} \right) \\ \Omega^{(7)} &= \frac{-T^* p_v}{m^2} \left( \frac{\partial u}{\partial m} \right) + \frac{2T^* p_v u}{m^3} & \Omega^{(8)} &= \frac{-T^* p_v}{m^2} \left( \frac{\partial u}{\partial \mathbf{p}_v} \right) - \frac{T^* u \mathbf{p}_v^T}{p_v m^2} & \Omega^{(9)} &= \frac{-T^* p_v}{m p_v} \left( \frac{\partial u}{\partial p_m} \right) \end{aligned} \quad (4.37)$$

The equations input into Eq. 4.34 can be used in an integrator to propagate the state with position, velocity, mass, the corresponding adjoints, and the STM. This STM is useful for numerical corrections purposes.

## Chapter 5

### Technical Approach

When correcting a trajectory in the CR3BP via multiple shooting, a reasonably close initial guess is required for success. This is a challenging venture because of the complexities of the dynamics and the optimization method. The term “good enough” depends on the problem, but this certain problem can be very sensitive because of the chaotic nature of the CR3BP and adjoint dynamics. This chapter covers the necessary information to create an adequate guess. Once a transfer has been computed from that initial guess, continuation is used to modify the transfer to have the desired parameters. The technical approach used in this thesis is suited to the complexities of computing transfers using primer vector theory in the CR3BP.

#### 5.1      Changing the Jacobi Constant Efficiently

The Jacobi constant is useful in the CR3BP because it is conserved under the natural dynamics. Transfers are often desired between orbits of different Jacobi constants, which means thrust must be applied. To investigate the effect of continuous thrust, the derivative of the Jacobi constant is taken. This is written as

$$\dot{C} = 2x\dot{x} + 2y\dot{y} - \frac{2(1-\mu)}{r_1^2}\dot{r}_1 - \frac{2\mu}{r_2^2}\dot{r}_2 - 2\mathbf{v} \cdot \dot{\mathbf{v}} \quad (5.1)$$

Note that  $\dot{\mathbf{v}} = \ddot{\mathbf{r}}$ . The thrust enabled equations of motion, shown in Eq. 2.55, are inserted into equation 5.1 to produce

$$\begin{aligned}\dot{C} = & 2x\dot{x} + 2y\dot{y} - \frac{2(1-\mu)}{r_1^2}\dot{r}_1 - \frac{2\mu}{r_2^2}\dot{r}_2 - 2\dot{x}\left(2\dot{y} + x - \frac{(1-\mu)(x+\mu)}{r_1^3} - \frac{\mu(x-1+\mu)}{r_2^3} + \frac{T^*}{m}u_x\right) \\ & - 2\dot{y}\left(-2\dot{x} + y - \frac{(1-\mu)y}{r_1^3} - \frac{\mu y}{r_2^3} + \frac{T^*}{m}u_y\right) - 2\dot{z}\left(-\frac{(1-\mu)z}{r_1^3} - \frac{\mu z}{r_2^3} + \frac{T^*}{m}u_z\right)\end{aligned}\quad (5.2)$$

Using the definition of  $r_1$  and  $r_2$  from Eq. 2.17, the derivatives can be taken as

$$\dot{r}_1 = \frac{\dot{x}(x+\mu) + \dot{y}y + \dot{z}z}{r_1} \quad \dot{r}_2 = \frac{\dot{x}(x-1+\mu) + \dot{y}y + \dot{z}z}{r_2} \quad (5.3)$$

Inserting these definitions into Eq. 5.1 causes many terms to cancel, resulting in

$$\dot{C} = \frac{-2T^*}{m}\mathbf{v} \cdot \mathbf{u} = \frac{-2T^*}{m}|\mathbf{v}||\mathbf{u}|\cos\alpha \quad (5.4)$$

where  $\alpha$  is the angle between the thrust direction and the velocity direction. By inspection of the above equation, the control vector  $\mathbf{u}$  can be applied strategically to maximize the size of  $\dot{C}$ , the change in Jacobi constant. These principles to efficiently change the Jacobi constant are as follows:

- The values of the angle  $\alpha$  that maximize the magnitude of  $\cos(\alpha)$  are  $0^\circ$  and  $180^\circ$ . This means that the optimal thrust direction is in the velocity or anti-velocity direction
- The thrust should be applied at the maximal  $|\mathbf{v}|$ , which occurs at periapsis or closest approach

This is very important, as the primary objective of many transfers is to alter the Jacobi constant of the motion. Optimal transfers will use thrust efficiently to accomplish this objective. These principles are used to construct an initial guess.

## 5.2 Trajectory Itinerary and Initial Guess Construction

Certain transfers resemble spirals because thrust is applied continuously to change the energy level, but the thrust is low enough that the energy transfer happens over multiple revolutions. If high thrust impulsive maneuvers were used, an energy change could be accomplished in a few impulses

and the trajectory would not require multiple revolutions. This is not the case for continuous low thrust engines, which are the subject of this study. “Spiral in” trajectories occur when a transfer continuously lowers the radius and energy over multiple revolutions. This would be the case for a transfer from GEO to LEO. “Spiral out” trajectories are the opposite; continuously raising the radius and energy. The case of a transfer from low lunar orbit or low Earth orbit to a periodic orbit in the CR3BP incorporates a spiral out transfer. Recall that the Jacobi constant is a negative energy-like quantity; low energies correspond to high Jacobi constants and vice versa. So in the CR3BP, a spiral out trajectory is continuously lowering the Jacobi constant. Tables 5.1 and 5.2 provide the Jacobi constant and other relevant data for selected low Earth and low lunar orbits, as well as periodic orbits in the Earth-Moon CR3BP.[14, 15] Orbits about Earth include low Earth orbit (LEO), medium Earth orbit (MEO), and geostationary equatorial orbit (GEO). Orbits about the Moon include low lunar orbit (LLO) and medium lunar orbit (MLO).

Table 5.1: Characteristics Earth/Moon centered orbits. Each of these orbits are circular in the two-body problem

Orbit	Central Body	Altitude (km)	Radius (km)	Radius (ndim)	$C$
<b>LEO</b>	Earth	< 2000	< 8378	< 0.02157	> 45.48
<b>GEO</b>	Earth	35786	42164	0.10856	9.60
<b>MEO</b>	Earth	2000 – 35786	8378 – 42164	0.0216 – 0.1086	45.48 – 9.60
<b>LLO</b>	Moon	< 100	< 1837	< 0.00473	> 5.49
<b>MLO</b>	Moon	100 – 4000	1837 – 5737	0.00473 – 0.01477	5.49 – 3.74

Table 5.2: Characteristics of segments of periodic orbit families in the Earth-Moon CR3BP

Orbit Family	Period (days)	$C$
<b>L1 Halo</b>	7.995 – 13.845	0.195 – 3.174
<b>L2 Halo</b>	3.187 – 15.140	3.015 – 3.158
<b>L1 Lyapunov</b>	11.931 – 33.005	2.742 – 3.188
<b>L2 Lyapunov</b>	14.952 – 36.409	2.873 – 3.172

To construct a guess for an optimal spiral trajectory, the principles from Eq. 5.4 are used. The guess trajectories are propagated with the thrust in the velocity direction and the magnitude

of the thrust is increased near periapsis. To determine what qualifies as “near periapsis,” orbital elements in the classical two-body problem are used. The semilatus rectum is defined as

$$\tilde{p} = \frac{(\tilde{\mathbf{R}} \times \tilde{\mathbf{V}}) \cdot (\tilde{\mathbf{R}} \times \tilde{\mathbf{V}})}{\tilde{GM}} \quad (5.5)$$

where  $\tilde{\mathbf{R}}$  and  $\tilde{\mathbf{V}}$  refer to the dimensional position and velocity relative to the body that the desired spiral is around.[37] If  $\tilde{p}$  is greater than  $\tilde{R}$ , then the magnitude of the true anomaly is less than  $90^\circ$  and the trajectory is considered close to periapsis; in this case, the throttle is set to a higher value. If  $\tilde{p}$  is less than  $\tilde{R}$ , then the magnitude of the true anomaly is greater than  $90^\circ$ ; in this case, the throttle is set to a lower value. The thrust would either be on or off if this were an initial guess for a bang-bang transfer, but this is a guess for a smoothed trajectory. The control magnitude for the initial guess is set to 0.6 if the magnitude of the true anomaly is less than  $90^\circ$  and 0.4 if the magnitude of the true anomaly is greater than  $90^\circ$ .

### 5.3 Initial Adjoint Guesses

The position, velocity, and mass are all governed by the dynamics in Eqs. 2.55 and 2.53 applied to the initial guess method described above. The initial conditions for these values are prescribed as a spacecraft in an orbit with a mass corresponding to a full fuel tank. The adjoints, however, do not have prescribed initial conditions. The relations from the optimal control law and the principles derived from Eq 5.4 are used to construct initial guess for the form of the adjoints.

The optimal control law dictates that the control vector is in the opposite direction of the primer vector. The principles of efficiently changing the Jacobi constant postulate that the control vector is in the direction of the velocity. Both of these relationships to the control vector can be combined as

$$\hat{\mathbf{u}}^* = \frac{\mathbf{v}}{v} = -\frac{\mathbf{p}_v}{p_v} \quad (5.6)$$

which leads to a relationship between the primer vector and the velocity vector, written as

$$\mathbf{p}_v = -\gamma \mathbf{v} \quad (5.7)$$

where  $\gamma$  is a positive scaling factor. This expression can be inserted into the adjoint vector dynamics in Eq. 4.6 as

$$\dot{\mathbf{p}}_v = -\gamma \dot{\mathbf{v}} = -\mathbf{p}_r - [\mathbf{H}]^T \mathbf{p}_v \quad (5.8)$$

This equation can be rearranged to solve for  $\mathbf{p}_r$  as

$$\mathbf{p}_r = \gamma \dot{\mathbf{v}} - [\mathbf{H}]^T \mathbf{p}_v \quad (5.9)$$

The above equations can be used to construct initial guesses for  $\mathbf{p}_r$  and  $\mathbf{p}_v$ . The scalar  $\gamma$  is treated as a tuning parameter, which can be changed until the corrections process is successful. The value of  $\gamma$  that worked in this study tended to be around 0.1, but that could be affected by the thrust values used and the specific problem at hand.

The last state variable to solve for is  $p_m$ . The differential equation for  $p_m$  can be utilized, noting that the magnitude of the primer vector appears, so Eq. 5.7 can be used. Other assumptions will be made to simplify the expression just for construction of an initial guess; the throttle magnitude and the mass of the spacecraft are assumed to be constant for the entire trajectory. The mass will decrease over time as fuel is used, but this decrease will be limited, so the nondimensional spacecraft mass is assumed to be 1 for the entire trajectory. The throttle will also change over the trajectory; the optimal control law dictates that the throttle change between 0 and 1 instantaneously. However, this initial guess is for computation of the smoothed case, so the throttle can be approximated as constant. These assumptions are written in equation form as

$$\dot{p}_m = -\frac{T^* u p_v}{m^2} \approx -T^* \gamma u_{avg} v(t) \quad (5.10)$$

A final piece of information to use is that the value of  $p_m(t_f)$  is constrained to be zero. The end point and derivative are known, so an expression for  $p_m(t)$  can be formed as

$$p_m(t) = T^* \gamma u_{avg} v(t) (t_f - t) \quad (5.11)$$

## 5.4 Patching Onto a Stable Manifold

The transfers computed in this thesis start on a desired low Earth/Moon orbit, and end on a desired periodic orbit. There are infinite options on both ends for which precise initial and final state to choose. To choose these points, a Poincaré map is used.

From a chosen number of points along the target periodic orbit, a stable manifold is created using the technique described in Chapter 2. This manifold is propagated only until it crosses the surface of section, which is defined as the  $x$  value of the desired primary. For a Moon-centered transfer this would be  $x = 1 - \mu$ , and for an Earth centered transfer it would be  $x = -\mu$ . At this crossing, the value of  $y$  and  $\dot{y}$  are recorded. The manifold can be propagated for more crossings, and at each crossing the state is recorded for a Poincaré map. This can be seen in Figure 5.1, where the blue dots represent trajectories from the stable manifold of an  $L_1$  Lyapunov orbit. The red dots represent trajectories from initial guesses, generated by applying the method described in the sections above for a chosen number of points along the initial low orbit. The thrust portion of these transfers is propagated until the Jacobi constant matches that of the desired orbit, at which point the state is propagated until it crosses the surface of section. These crossings are compared to the stable manifold crossings to identify the points with the smallest difference in state, or the “closest match.” These two trajectories are chosen to patch together. This is shown in Figure 5.2 for an example transfer from GEO to an  $L_1$  orbit, where the highlighted red and blue trajectories are chosen because they were the closest match. The state of the chosen arc along the stable manifold at the surface of section is used as the target end state for the corrections process. The transfer is considered complete if this state is reached; then, the trajectory is dictated by the natural motion of the CR3BP and the adjoints are no longer considered.

## 5.5 Constraints and Free Variables

A multiple shooting method is used to compute an optimal transfer from a low Earth/Moon orbit to a  $L_1$  Lyapunov orbit. As described in Chapter 3, the method enforces boundary conditions

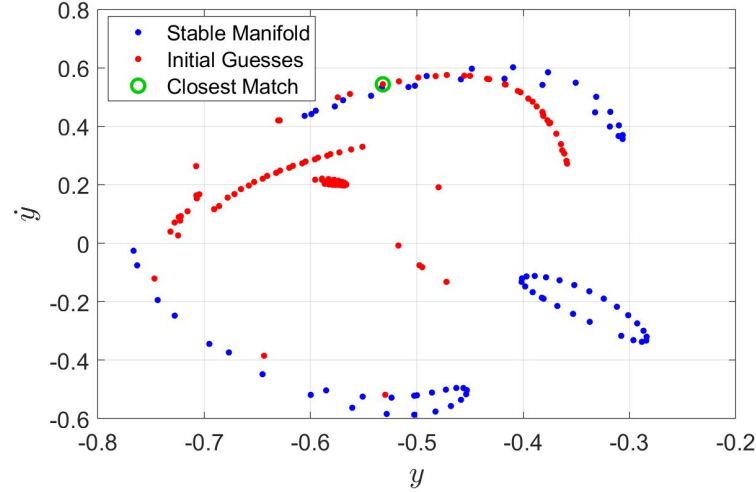


Figure 5.1: Poimcaré map showing 3 crossings of a stable manifold compared to crossings of multiple options of initial guess spirals. All of these trajectory points have a Jacobi constant of 3.013

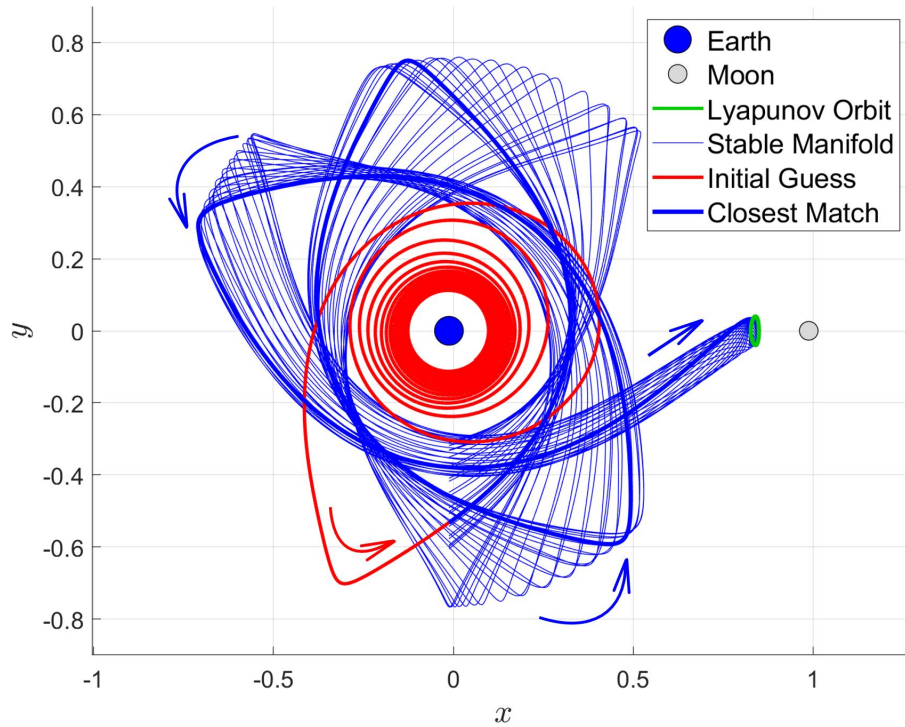


Figure 5.2: The closest matching initial guess spiral and stable manifold trajectory for a GEO to L1 Lyapunov orbit out transfer

on the endpoints and continuity constraints on the interior points. The free variables are the states

and adjoints at the start of each segment as well as a slack variable to enforce a positive propagation time. The trajectory is divided into segments such that each spiral has an equal number of segments. The interior subvectors for the free and constraint vector are written as

$$\mathbf{V}_i = \left[ \mathbf{y}_{i,0}^T, \Delta t_i, \beta_i \right]_{16 \times 1}^T \quad (5.12)$$

$$\mathbf{F}_i = \left[ (\mathbf{y}_{i,f} - \mathbf{y}_{i+1,0})^T, \Delta t_i - \beta_i^2 \right]_{15 \times 1}^T \quad (5.13)$$

where  $\mathbf{y} = [\mathbf{r}, \mathbf{v}, m, \mathbf{p}_r, \mathbf{p}_v, p_m]$ . The endpoint constraints must enforce the boundary conditions of the optimal transfer. These conditions are listed below:

- The nondimensional mass of the spacecraft must be 1 at the initial time ( $m(t_i) = 1$ )
- The initial state must correspond to a circular orbit about the primary or secondary ( $\mathbf{e}_i = \mathbf{0}$ )
- The initial state must correspond to a specified Jacobi constant ( $C(\mathbf{x}(t_i)) = C_d$ )
- The final state must be equal to a state on the stable manifold of the desired periodic orbit ( $(\mathbf{x}(t_f) = \mathbf{x}_d)$ )
- The final value of  $p_m$  must be zero ( $p_m(t_f) = 0$ )

These are enforced via the initial and final constraints:

$$\mathbf{F}_{D,f} = \left[ (\mathbf{x}_{n,f} - \mathbf{x}_d)^T, \Delta t_n - \beta_n^2 \right]_{7 \times 1}^T \quad (5.14)$$

$$\mathbf{F}_{D,0} = \left[ \mathbf{e}^T, m - 1, (C(\mathbf{x}_{i,0}) - C_d) \right]_{5 \times 1}^T \quad (5.15)$$

These definitions are input into Eqs. 3.8 and 3.9 to construct the full free variable vector and constraint vector.

The  $\mathbf{DF}$  matrix can be built using a block formation, written as

$$\mathbf{DF}(\mathbf{V}) = \begin{bmatrix} \frac{\partial \mathbf{F}_{D,0}}{\partial \mathbf{V}_1} & 0 & \dots & \dots & \dots & \dots & \dots & 0 \\ \frac{\partial \mathbf{F}_1}{\partial \mathbf{V}_1} & \frac{\partial \mathbf{F}_1}{\partial \mathbf{V}_2} & \ddots & & & & & \vdots \\ 0 & \frac{\partial \mathbf{F}_2}{\partial \mathbf{V}_2} & \frac{\partial \mathbf{F}_2}{\partial \mathbf{V}_3} & \ddots & & & & \vdots \\ \vdots & \ddots & \ddots & \ddots & \ddots & & & \vdots \\ \vdots & & \ddots & \frac{\partial \mathbf{F}_i}{\partial \mathbf{V}_i} & \frac{\partial \mathbf{F}_i}{\partial \mathbf{V}_{i+1}} & \ddots & & \vdots \\ \vdots & & & \ddots & \ddots & \ddots & \ddots & \vdots \\ \vdots & & & & \ddots & \frac{\partial \mathbf{F}_{n-2}}{\partial \mathbf{V}_{n-2}} & \frac{\partial \mathbf{F}_{n-2}}{\partial \mathbf{V}_{n-1}} & 0 \\ \vdots & & & & & \ddots & \frac{\partial \mathbf{F}_{N-1}}{\partial \mathbf{V}_{N-1}} & \frac{\partial \mathbf{F}_{N-1}}{\partial \mathbf{V}_N} \\ 0 & \dots & \dots & \dots & \dots & \dots & 0 & \frac{\partial \mathbf{F}_{D,f}}{\partial \mathbf{V}_n} \end{bmatrix} \quad (5.16)$$

The intermediate blocks, which will compose a majority of the total  $\mathbf{DF}$  matrix, are derived below.

$$\frac{\partial \mathbf{F}_i}{\partial \mathbf{V}_i} = \begin{bmatrix} \Phi_{i,14 \times 14} & \dot{\mathbf{y}}_{i,f} & \mathbf{0}_{14 \times 1} \\ \mathbf{0}_{1 \times 14} & 1 & -2\beta_i \end{bmatrix}_{15 \times 16} \quad (5.17)$$

$$\frac{\partial \mathbf{F}_i}{\partial \mathbf{V}_{i+1}} = \begin{bmatrix} -I_{14 \times 14} & \mathbf{0}_{14 \times 1} & \mathbf{0}_{14 \times 1} \\ \mathbf{0}_{1 \times 14} & 0 & 0 \end{bmatrix}_{15 \times 16} \quad (5.18)$$

where the STM is defined in Section 4.5. The initial and final blocks can be defined similarly, written as

$$\frac{\partial \mathbf{F}_{D,0}}{\partial \mathbf{V}_1} = \begin{bmatrix} \frac{\partial \mathbf{e}}{\partial \mathbf{r}} & \frac{\partial \mathbf{e}}{\partial \mathbf{v}} & \mathbf{0}_{3 \times 1} \\ \frac{\partial C}{\partial \mathbf{r}} & \frac{\partial C}{\partial \mathbf{v}} & 0 \\ \mathbf{0}_{1 \times 3} & \mathbf{0}_{1 \times 3} & 0 \end{bmatrix}_{5 \times 7} \quad (5.19)$$

$$\frac{\partial \mathbf{F}_{D,f}}{\partial \mathbf{V}_n} = \begin{bmatrix} \Phi_n(1 : 6, 1 : 14) & \dot{\mathbf{x}}_{n,f}(1 : 6) & \mathbf{0}_{6 \times 1} \\ \mathbf{0}_{1 \times 14} & 1 & -2\beta_N \\ \Phi_n(14, 1 : 14) & \dot{\mathbf{x}}_{n,f}(14) & 0 \end{bmatrix}_{8 \times 16} \quad (5.20)$$

where  $\mathbf{e}$  and  $C$  are defined in Chapter 2. These free variables, constraints, and partial derivative relationships are used to create a multiple shooting scheme. This is described in Chapter 3.

## 5.6 Methodology

Optimal trajectories from a low Earth/Moon orbit to an  $L_1$  Lyapunov orbit in the CR3BP are computed by leveraging the contents of all previous chapters. The optimal trajectories are computed in the Earth-Moon CR3BP via multiple shooting. Each transfer uses primer vector theory and is expected to use a control profile that approaches bang-bang. This introduces several challenges:

- Bang-bang control is difficult to recover numerically using the multiple shooting implementation. Typically, the initial guess must be very close to the true solution in order to iterate to the precise switch times.
- The solution space is very sensitive near the primaries in the chaotic CR3BP. Note that Eq. 2.55 has terms divided by  $r_1^3$  and  $r_2^3$ , and Eq. 4.6 has terms divided by  $r_1^5$  and  $r_2^5$ . For very small values nondimensional values of  $r_1$  and  $r_2$ , which can be seen in Table 5.1, this division can create very large accelerations. Without regularization, this can produce ill-conditioning between parameters close to and far from the primaries
- The STM approximates the deviation from a trajectory in a linearized system; this approximation breaks down near the primaries. The STM propagation defined in Section 4.5 involves terms divided by  $r_1^5$ ,  $r_2^5$ ,  $r_1^7$ , and  $r_2^7$ . The free variable vector, which updates using the STM of different segments, is therefore very sensitive near the primaries.

Because of these challenges, this thesis uses continuation methods in order to close in on a desired solution. First, initial transfers are computed using a smoothed optimal control law with a smoothing parameter  $\epsilon$  of 1. The transfer is initially computed for an initial orbit that is larger than the desired orbit. Continuation will then be used to lower the radius of the initial orbit to the desired value. The continuation will also be used to gradually lower the smoothing parameter. This approach is conceptually depicted in Figure 5.3 for a case where the transfer is to begin at a Jacobi constant  $C_2$ . In practice the continuation method is applied using steps that change the

parameter of interest. The step size of this continuation process is variable; the step size is lower near sensitive regions, and the step size is reduced if the correction method fails to converge.

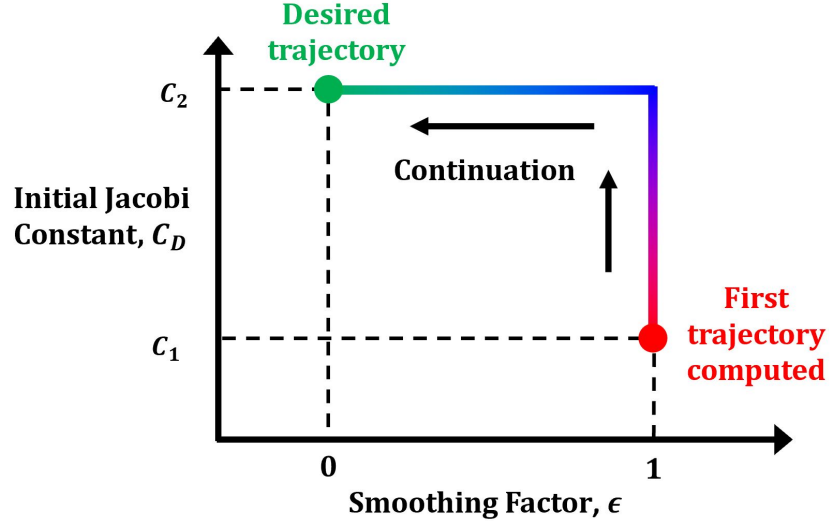


Figure 5.3: The continuation method employed for computation of low spirals. A continuation method is first used to raise the initial Jacobi constant, and then another continuation method is used to lower the smoothing factor to get bang-bang control

## Chapter 6

### Results

#### 6.1 Electric Propulsion Systems

The purpose of this study is to compute optimal low thrust trajectories, but the parameters that define the propulsion system must be specified first. Chemical propulsion systems are commonly used to provide large amounts of thrust in short periods of time. Chemical propulsion utilizes chemical reactions to release energy and generate thrust. Electric propulsion, on the other hand, provides a smaller amount of thrust and can be sustained for a longer time. Electric propulsion systems use either magnetic fields or electric heating to accelerate the exhaust mass, which increases the generated momentum. Alternatively, electrical power can be used to ionize the propellant before it is accelerated via electrodes. Electric propulsion can be very efficient, but the small size of the thrust sacrifices the amount of time it takes to complete a transfer.

Recall from Eqs. 2.53 and 2.54 that the thrust and mass flow rate used in the dynamics are dependent on the parameters  $I_{sp}$  and  $T_{max}$ , which are the specific impulse and maximum thrust of the propulsion system, respectively. Specific impulse is the ratio of the output thrust to the mass flow rate of the propellant, and essentially measures of the efficiency of the propulsion system. The values of  $I_{sp}$  and  $T_{max}$  are shown below for different electric propulsion systems.

The propulsion system can also be a driving force into the size of a spacecraft. CubeSats, for example, have a standardized dimension of  $10\text{ cm} \times 10\text{ cm} \times 10\text{ cm}$ , which cannot accommodate larger engines. Certain types of engines require larger machinery to handle to run properly, so this must be taken into account as well. Electric propulsion systems also require a certain amount of

Table 6.1: Parameters for different electric propulsion systems that could be used for small satellites.  
[6]

Name	System Type	Thruster Type	$I_{sp}$ (s)	$T_{max}$ (N)	Power (W)
<b>MR-512</b>	Electrothermal	Arcjet	502	0.254	1800
<b>MR-502</b>	Electrothermal	Resistojet	304	0.5	840
<b>ATOS</b>	Electrothermal	Arcjet	400	0.1	750
<b>NSTAR Ion</b>	Electrostatic	GIT	3100	0.092	2300
<b>PPS-1350 G</b>	Electrostatic	Hall	1660	0.09	1500

power, which can be a driving factor for the size of the spacecraft batteries and solar panels.

To generate results using the formulation in this research, parameter values must be determined for the specific impulse  $I_{sp}$ , the maximum thrust  $T_{max}$ , and the initial wet mass  $\tilde{m}_0$  of the spacecraft. These are chosen to correspond to a spacecraft using the ATOS thruster, shown in Table 6.1. The wet mass of this propulsion system is approximately 50 kg.[7] For electric propulsion systems, the propulsion system typically compromises approximately one third of the total spacecraft mass.[11] This results in a total spacecraft initial wet mass of about 150 kg. The parameters used to generate results in this section are recorded in Table 6.2.

Table 6.2: Parameters used for the results in this thesis.

$I_{sp}$ (s)	$T_{max}$ (N)	$\tilde{m}_0$ (kg)
400	0.1	150

## 6.2 Optimal Transfer from Medium Earth Orbit to L1 Lyapunov Orbit

To compute an optimal trajectory beginning from medium Earth orbit, an initial trajectory is computed beginning from GEO with a smooth control profile. This initial trajectory is computed using the initial guess construction method from Chapter 5. Then, continuation methods are applied until the desired transfer is computed from a circular orbit with a radius of 21,140 km and a Jacobi constant of 18.45. This process is shown conceptually in Figure 5.3. The data from this method implemented for a MEO transfer is shown in Figure 6.1. Each circle in Figure 6.1

represents a computed transfer and Cases 1-6 are called out and plotted separately in Figure 6.2, where the color of the line represents the size of the control throttle magnitude; blue represents zero thrust, red represents maximum thrust. More information on the results from these cases is shown in Table 6.3. The patch point, or the point on the arc along the stable manifold that the transfer is targeting, is at  $x = -\mu$ ,  $y = -0.65$ , and is visible on the plot for Cases 1-3 as the point at which the trajectory turns from purple to blue. This point is the same for all cases.

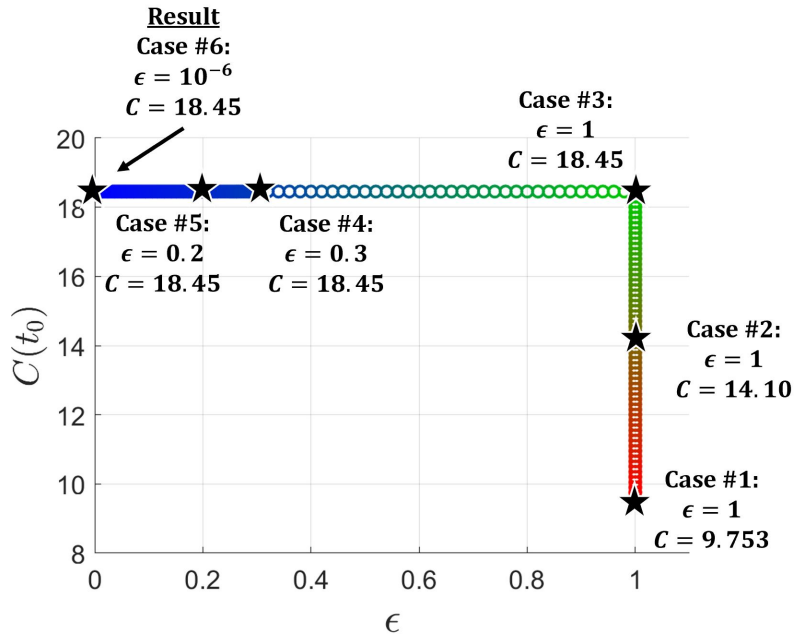


Figure 6.1: Trajectory data from the continuation method for computation of a MEO transfer

Table 6.3: Resulting final mass and transfer time for each selected case from the continuation method employed to compute a desired MEO to L1 Lyapunov transfer

Case	$\epsilon$	$C(t_0)$	$t_f$ (days)	$m(t_f)$
1	1	9.753	53.4	0.648
2	1	14.10	79.2	0.543
3	1	18.45	106.1	0.464
4	0.3	18.45	115.0	0.480
5	0.2	18.45	113.7	0.503
6	0.000001	18.45	115.2	0.540

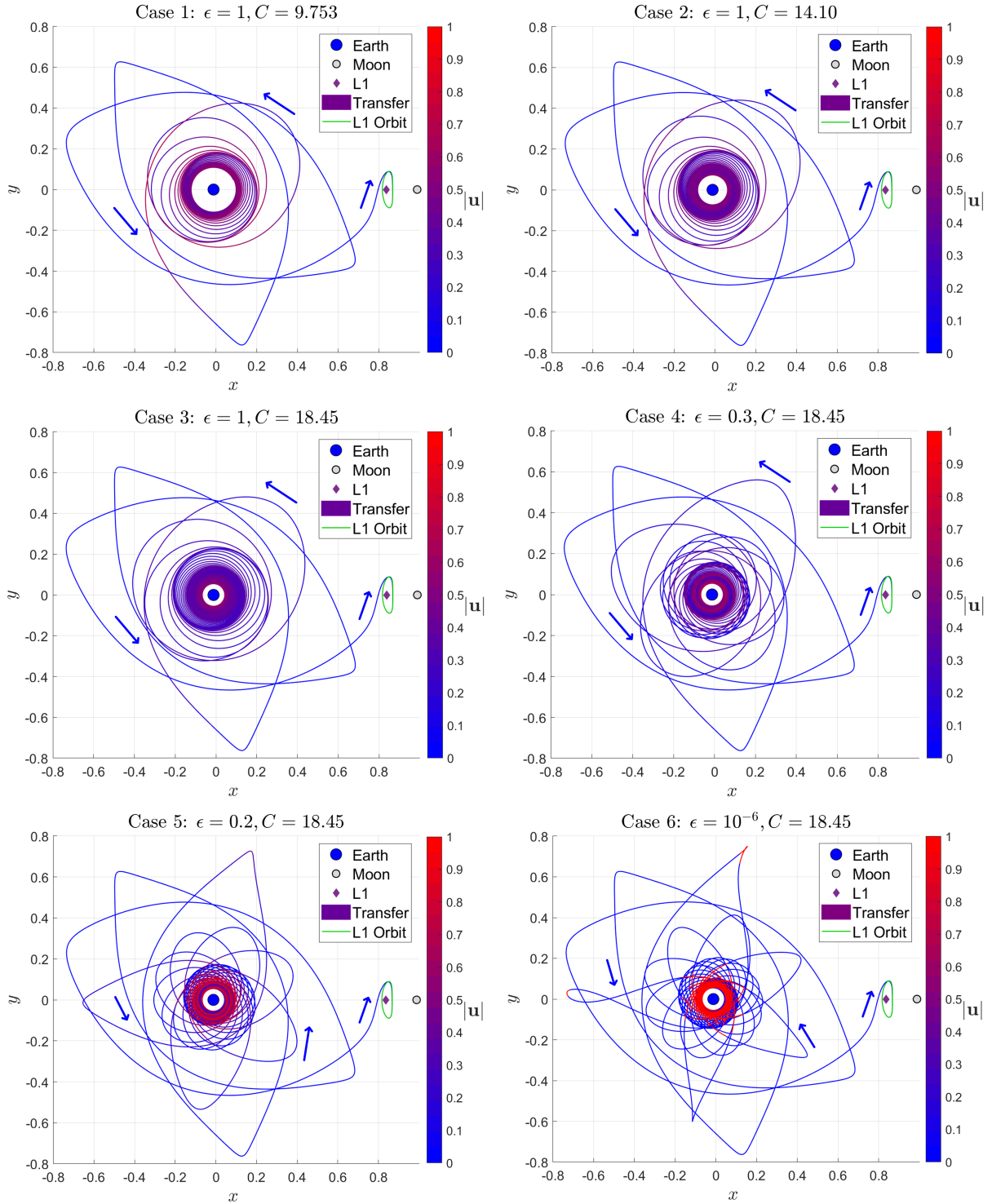


Figure 6.2: Selected cases (labeled in Figure 6.1) from the continuation methods employed to compute a desired MEO to L1 Lyapunov transfer

The smoothing affects the control magnitude, which can be compared as the smoothing factor  $\epsilon$  is lowered. The magnitude of the control vector and the switching function are shown in Figure 6.3 for the intermediate transfers computed during the continuation process of lowering  $\epsilon$  for  $C(t_0) = 18.45$ . Figure 6.4 shows the same control zoomed for just the first 1.5 time units for clarity. The control profile starts smooth at  $\epsilon = 1$ , but approaches a bang-bang control as the smoothing factor is lowered. The relationship between the control and the switching function is working as intended; the throttle is on when the switching function is below zero and off when the switching function is above zero, but the smoothing function makes this control law less rigid. Towards the end of the transfer, the switching function stays in the vicinity of zero for extended amounts of time, making control with small  $\epsilon$  values smooth. Yet for the final value, chosen as  $10^{-6}$ , the control is either in “on” or “off” mode; this is approximately the optimal bang-bang control.

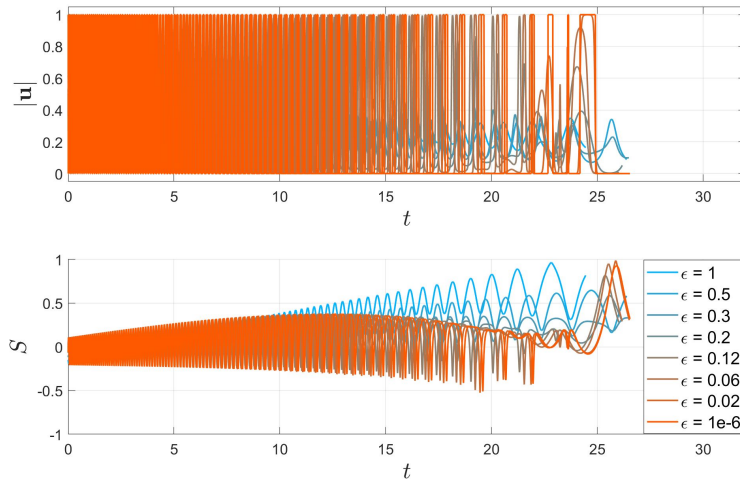


Figure 6.3: Control smoothing in computation of a MEO to L1 Lyapunov orbit transfer

The final transfer is a local optimal (minimal fuel) transfer that uses maneuvers to lower the Jacobi constant and inject into the  $L_1$  Lyapunov orbit. The mass and Jacobi control are shown over time in Figure 6.5 below for each of the smoothed cases. This figure shows that the smoothed cases use more propellant, and the bang-bang case resulted in the greatest final mass. The mass appears to get lower in increments, and these burns cause the Jacobi constant to get lower accordingly.

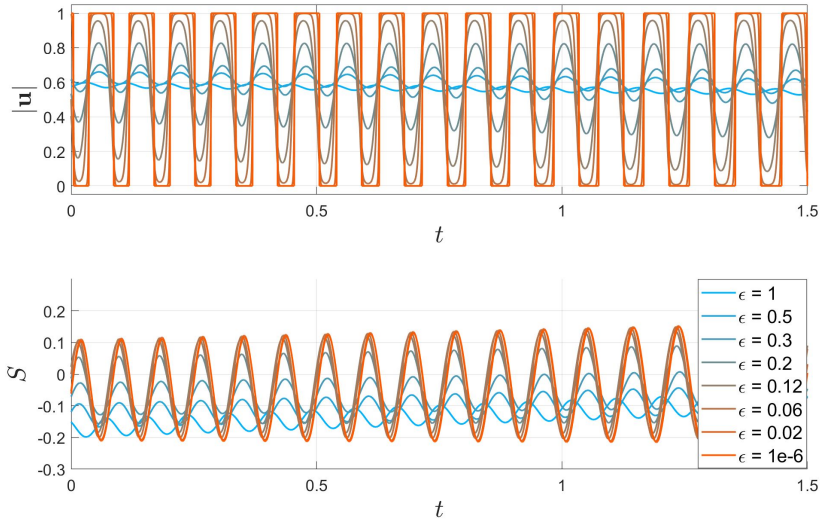


Figure 6.4: Control smoothing in computation of a MEO to L1 Lyapunov orbit transfer, zoomed to show the first 1.5 time units

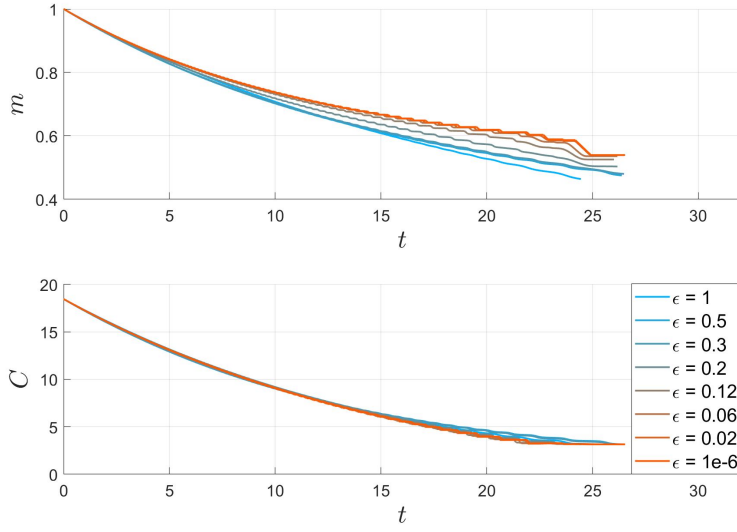


Figure 6.5: Mass and Jacobi constant measured over time for MEO transfers with a different value of  $\epsilon$

This shows that the burns are being applied strategically to reach the target Jacobi constant.

The final control has a pattern of cyclical “on” and “off” modes for the majority of the transfer. To investigate this phenomenon, the eccentricity and distance relative to Earth is calculated over the entire transfer. This is plotted in Figure 6.6, which shows that close to Earth, thrust is

centered around periapsis to raise the apoapsis of each spiral arc. This coincides with the principle of optimal trajectories from Eq. 5.4; the Jacobi constant is most effectively changed near periapsis. Yet the control deviates from this pattern towards the end of the transfer with two thrust segments occurring near apoapsis. This occurs at about  $t = 24$ . Notice from Figure 6.5 that this coincides with a large drop in final mass, but no noticeable change in Jacobi constant. There is, however, a large change in eccentricity for these burns. The spacecraft had an eccentricity of about 0.8 before the anomalous burns, but the target state required an eccentricity of about 0.4; these final thrust segments are needed to match the target value. This shows that these particular thrust segments do not have the purpose of changing the Jacobi constant, but rather correcting to the desired target state in the given time frame at the right phase. The transfer essentially has two phases: the first phase to lower the Jacobi constant, and the second phase to correct onto the stable manifold of the desired L1 orbit.

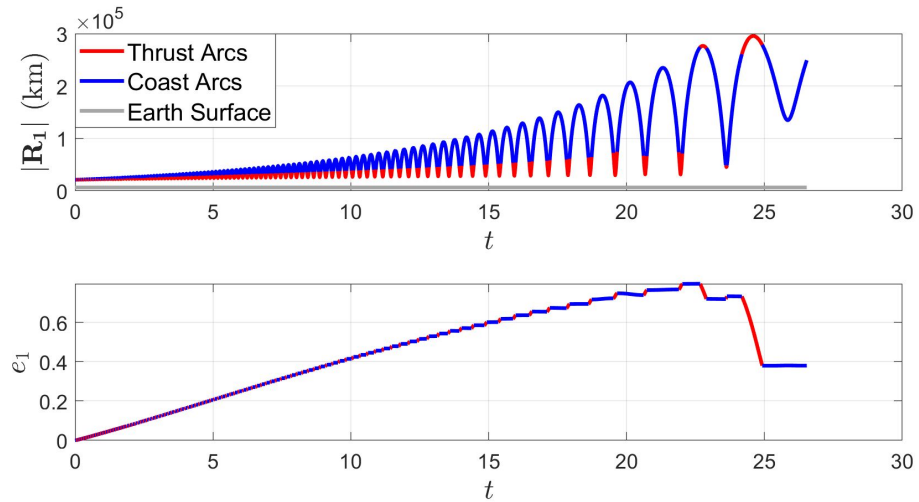


Figure 6.6: Eccentricity and distance relative to Earth for an optimal MEO to L1 Lyapunov orbit transfer. This transfer takes approximately four months

Another principle from Chapter 5 states that the thrust is most effective if it is applied in the velocity direction. This is also used to construct the initial guess. The angle  $\alpha$  is defined as the angle between the thrust and the velocity, so this angle was calculated for each thrust segment of

the final MEO transfer and plotted in Figure 6.7 to investigate this principle. Notice that for the majority of the thrust segments, the value of  $\alpha$  is near zero. This means that the thrust is applied almost exactly in the velocity direction. The result of primer vector theory matched the results of investigating Eq. 5.4. Also recall that the optimal control law dictated that the direction of the thrust is in the opposite direction of the primer vector. Figure 6.7 shows that the primer vector is almost in the opposite direction of the velocity for each thrust segment. Two thrust segments near the end of the transfer extend beyond axis limits. For these segments,  $\alpha$  actually grows to be more than  $180^\circ$ . These thrust arcs are part of the aforementioned second thrusting phase in which the trajectory is near the target Jacobi constant and must correct to the L1 orbit.

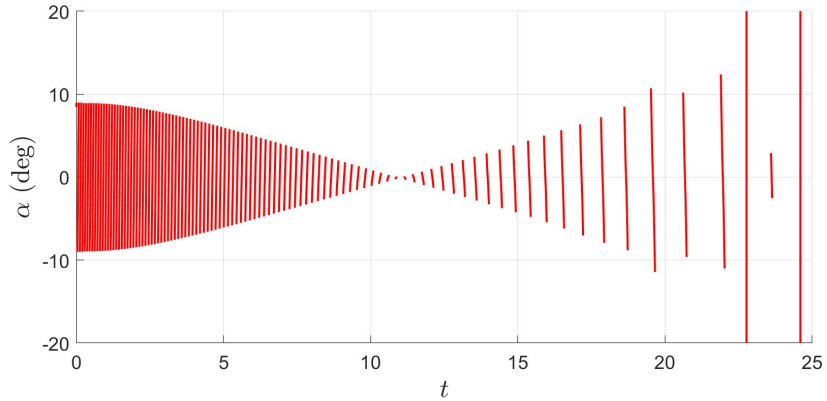


Figure 6.7: The angle between thrust and velocity for each thrust arc in an optimal MEO to L1 Lyapunov transfer

The final optimal transfer from a circular Earth orbit with a radius of 21,140 km to an L1 Lyapunov orbit is displayed in Figures 6.8 and 6.9, plotted respectively in the rotating and inertial frame. This trajectory could be used for a small spacecraft that is dropped into a circular Earth orbit with a radius of 21,140 km and must use an electric propulsion system to transfer into an  $L_1$  Lyapunov orbit. If there are mission constraints, such as limitations on the attitude control to change the thrust direction, this trajectory could be used as a first guess to compute the feasible transfer. That transfer would also need use a higher fidelity model for perturbations. Nonetheless, this trajectory is a theoretical optimal for a transfer in the Earth-Moon CR3BP.

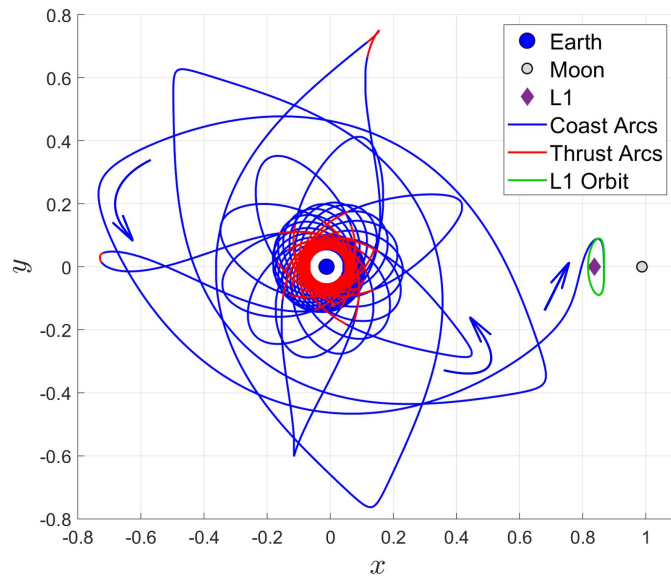


Figure 6.8: An optimal transfer from medium Earth orbit to an L1 Lyapunov orbit in the Earth-Moon CR3BP, plotted in the rotating frame

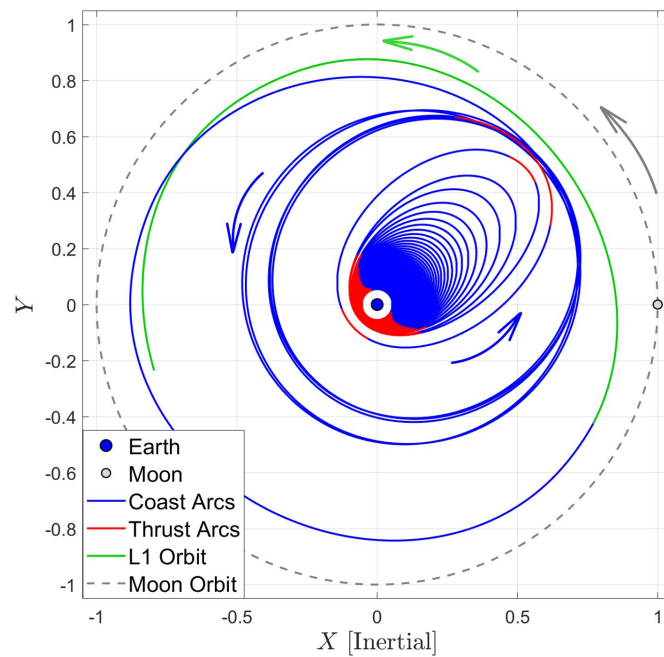


Figure 6.9: An optimal transfer from medium Earth orbit to an L1 Lyapunov orbit in the Earth-Moon CR3BP, plotted in the inertial frame

### 6.3 Optimal Transfer from Medium Lunar Orbit to L1 Lyapunov Orbit

The process from the previous section is applied to compute a transfer from a medium lunar orbit. To compute an optimal trajectory beginning from medium lunar orbit with a Jacobi constant of 4.00, an initial trajectory is computed beginning from a larger orbit with a smooth control profile and continuation methods are applied until the desired transfer is computed from a circular orbit with a radius of 4,559 km and a Jacobi constant of 4.00. The initial trajectory is a fully smoothed transfer from a circular lunar orbit with a Jacobi constant of 3.392. Starting from that trajectory, a continuation method shown conceptually in Figure 5.3 is used. The data from this method implemented for a MLO transfer is shown in Figure 6.10. Each circle in Figure 6.10 represents a computed transfer and Cases 1-6 are called out and plotted separately in Figure 6.11, where the color of the line represents the size of the control throttle magnitude. More information on the results from these cases is shown in Table 6.4. The patch point, or the point on an arc along the stable manifold that the transfer is targeting, is at  $x = 1 - \mu$ ,  $y = 0.063$ , and is visible on the plot for Cases 1-3 as the point at which the trajectory turns from purple to blue.

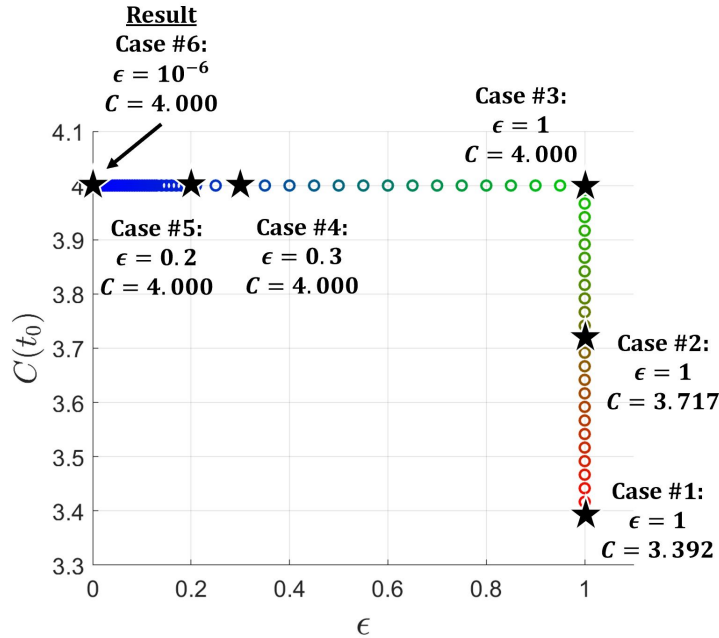


Figure 6.10: Trajectory data from the continuation method for computation of a MLO transfer

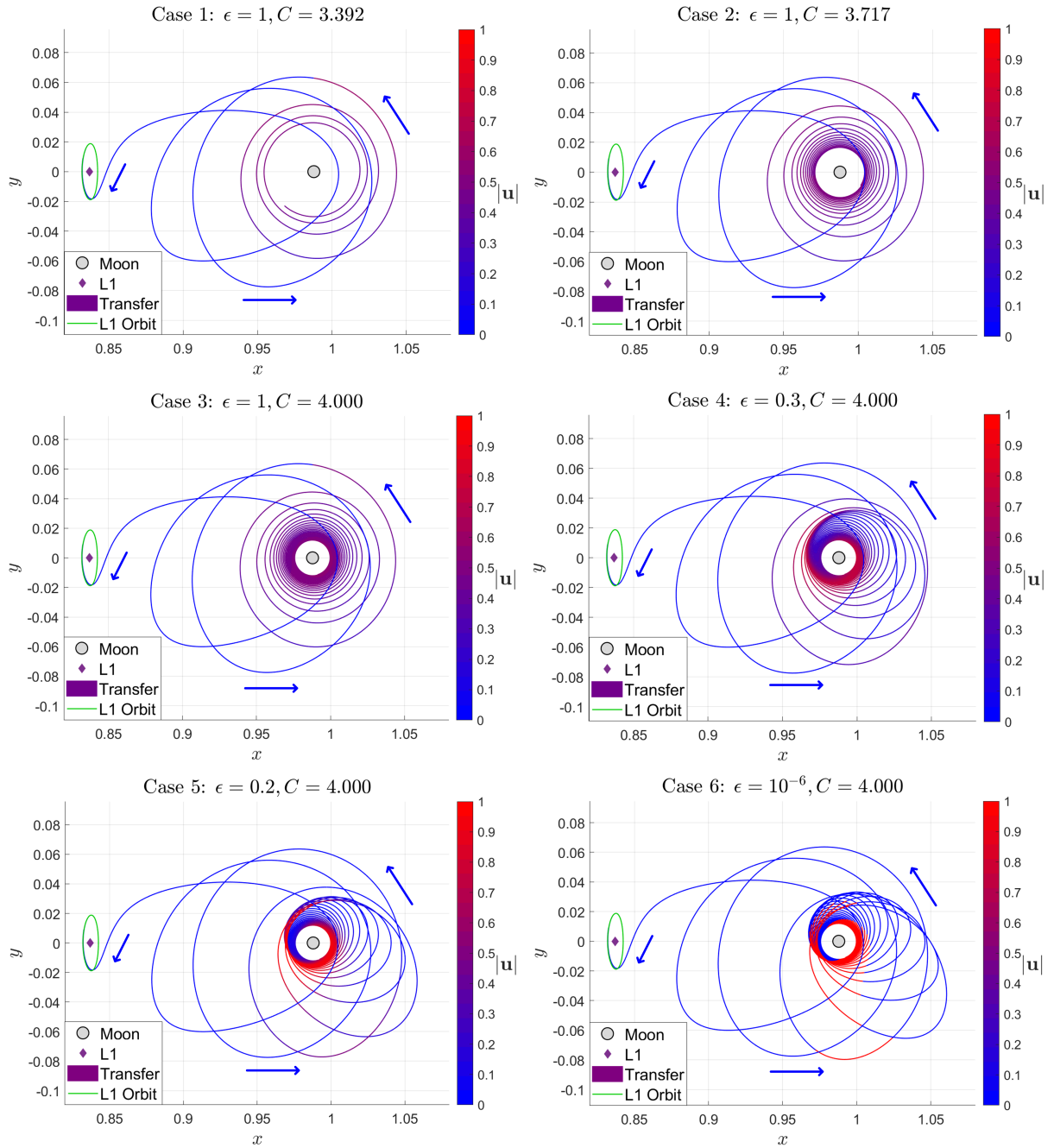


Figure 6.11: Selected cases (labeled in Figure 6.10) from the continuation methods employed to compute a desired MLO to L1 Lyapunov transfer

The smoothing affects the control magnitude, which can be compared as the smoothing factor  $\epsilon$  is lowered. The magnitude of the control vector and the switching function are shown in Figure 6.12 for intermediate transfers computed during the continuation process of lowering  $\epsilon$ .

Table 6.4: Resulting final mass and transfer time for each selected case from the continuation method employed to compute a desired MLO to L1 Lyapunov transfer

Case	$\epsilon$	$C(t_0)$	$t_f$ (days)	$m(t_f)$
<b>1</b>	1	3.392	8.4	0.946
<b>2</b>	1	3.717	17.2	0.893
<b>3</b>	1	4.000	22.7	0.858
<b>4</b>	0.3	4.000	24.8	0.863
<b>5</b>	0.2	4.000	25.9	0.872
<b>6</b>	0.000001	4.000	26.6	0.879

for  $C(t_0) = 4.00$ . Figure 6.13 shows the same control zoomed for just the first 1.5 time units for clarity. The control starts smooth at  $\epsilon = 1$ , but approaches a bang-bang control as the smoothing factor is lowered. Towards the end of the transfer, the switching function stays in the vicinity of zero for extended amounts of time, making control with small  $\epsilon$  values smooth. Yet for the final value, chosen as  $10^{-6}$ , the control is either in “on” or “off” mode; this is approximately the optimal bang-bang control. These same observations were also made for the MEO case.

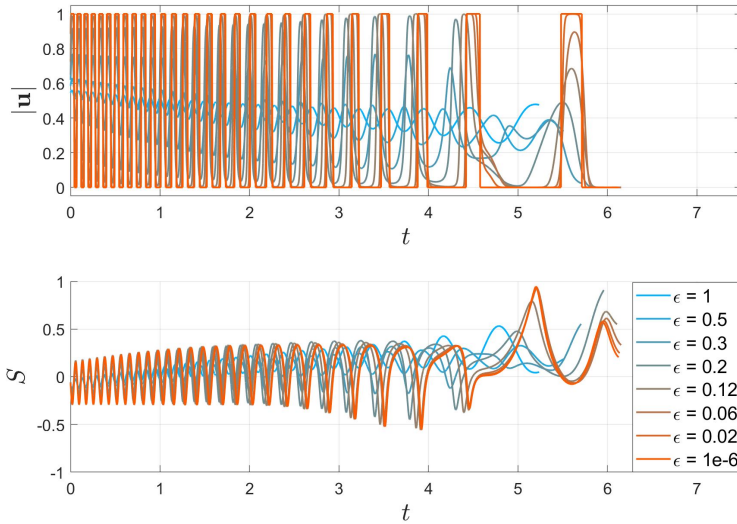


Figure 6.12: Control smoothing in computation of a MLO to L1 Lyapunov orbit transfer

The transfer is a local optimal transfer that uses maneuvers to lower the Jacobi constant and inject into the  $L_1$  Lyapunov orbit. The mass and Jacobi control are shown over time in Figure

6.14 below for each of the smoothed cases. This figure shows that the smoothed cases used more propellant, and the bang-bang case resulted in the greatest final mass. The mass appears to get lower in increments, and these burns cause the Jacobi constant to get lower accordingly. This shows that the burns are being applied strategically to reach the target Jacobi constant.

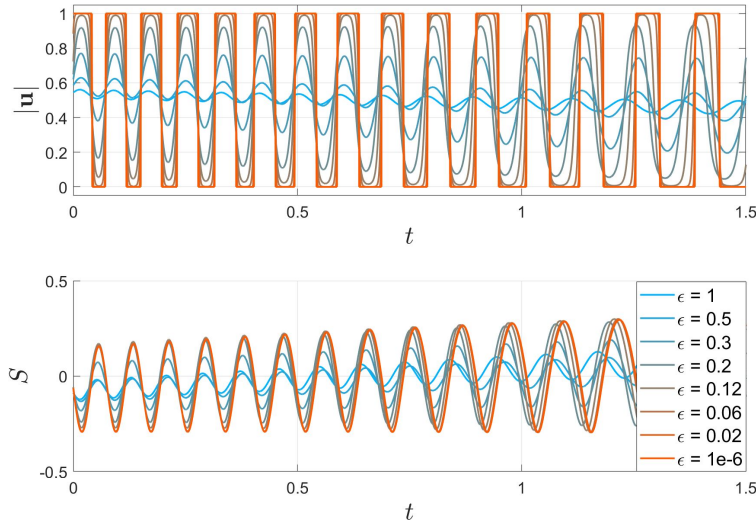


Figure 6.13: Control smoothing in computation of a MLO to L1 Lyapunov orbit transfer, zoomed to show the first 1.5 time units

The final control again has a pattern of cyclical “on” and “off” modes for the majority of the transfer. To investigate this phenomenon, the eccentricity and distance relative to the Moon is calculated over the entire transfer. This is plotted in Figure 6.15, which shows that close to Moon, thrust is centered around periapsis to raise the apoapsis of each spiral arc. This again shows that the the Jacobi constant is most effectively changed near periapsis. Similar to the MEO case, the control deviates from this pattern towards the end of the transfer with a thrust segment occurring near apoapsis. This occurs at about  $t = 5.5$ . Notice from Figure 6.14 and 6.15 that this coincides with a large drop in eccentricity and final mass, but a very small change in Jacobi constant. What is different in the Moon centered cases is that there is a significant drop in eccentricity during the final coast arcs. The Earth provides a large perturbing force to the Moon’s two-body problem; the trajectory capitalizes on this natural behavior to achieve the eccentricity of the desired target.

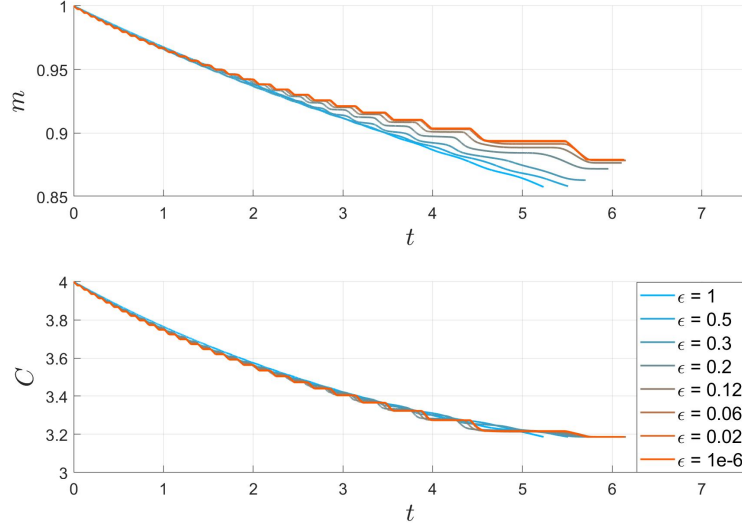


Figure 6.14: Mass and Jacobi constant measured over time for MLO transfers with a different value of  $\epsilon$

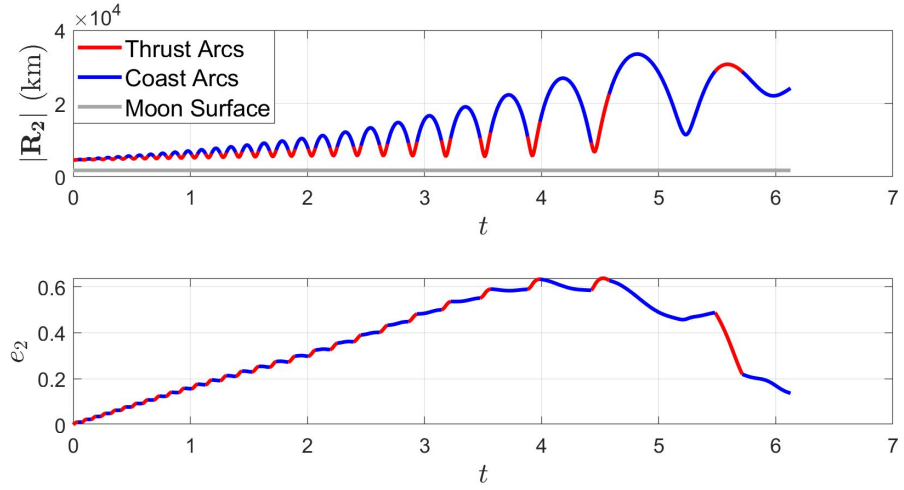
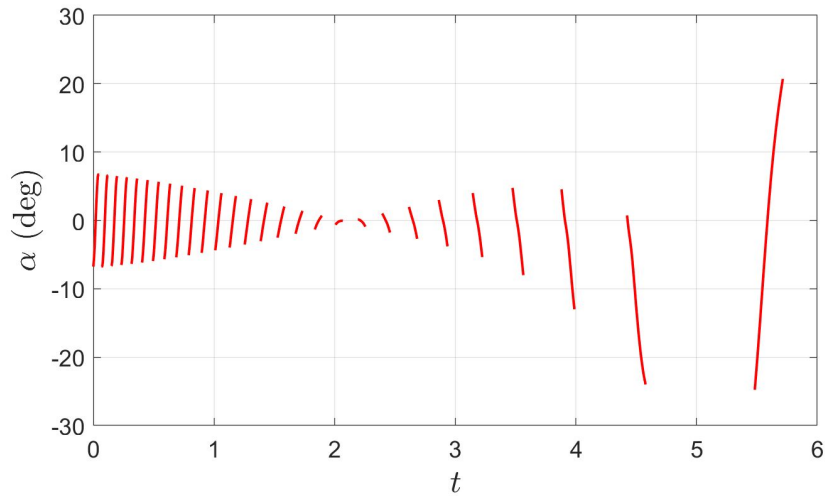


Figure 6.15: Eccentricity and distance relative to the Moon for an optimal MLO to L1 Lyapunov orbit transfer

Again for this case, the transfer essentially has two phases: the first phase to lower the Jacobi constant, and the second phase to correct onto the stable manifold of the desired L1 orbit.

Another principle from Chapter 5 states that the thrust is most effective if it is applied in the velocity direction. The angle  $\alpha$  is calculated for each thrust segment of the final transfer and plotted

in Figure 6.16 to investigate this principle. Notice that for the majority of the thrust segments, the value of  $\alpha$  is near zero. This means that the thrust is applied almost exactly in the velocity direction. The result of primer vector theory matched the results of investigating Eq. 5.4. Figure 6.16 also shows that the primer vector is almost exactly in the opposite direction of the velocity for each thrust segment. The final thrust segments begin to deviate from this pattern as the trajectory enters the aforementioned second phase.



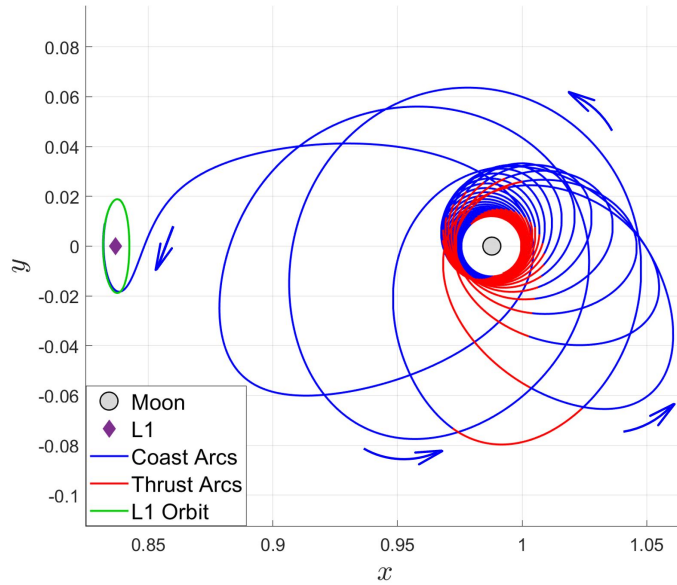


Figure 6.17: An optimal transfer from medium lunar orbit to an L1 Lyapunov orbit in the Earth-Moon CR3BP, plotted in the rotating frame

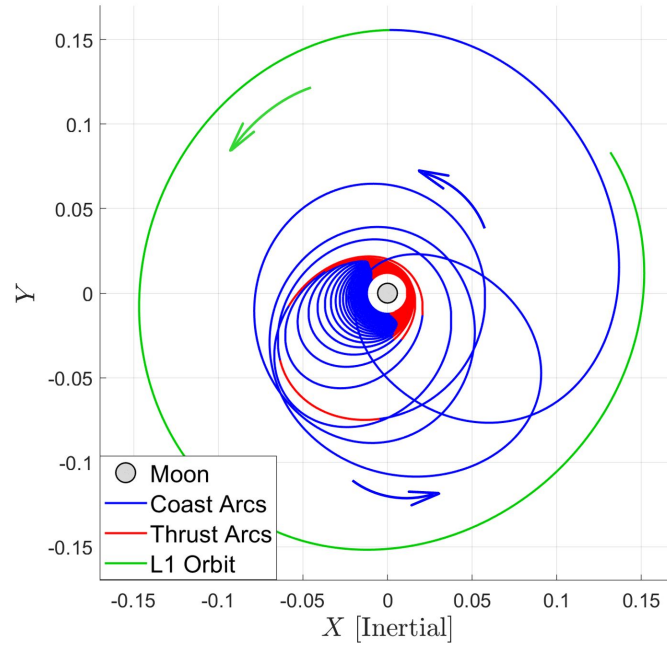


Figure 6.18: An optimal transfer from medium lunar orbit to an L1 Lyapunov orbit in the Earth-Moon CR3BP, plotted in the inertial frame

## 6.4 Optimal Transfer from Low Lunar Orbit to L1 Lyapunov Orbit

To compute a transfer that begins from LLO, continuation can be applied to the result from the MLO case. This continuation expands upon the previous continuation for the lunar case shown in Figure 6.10. The smoothing factor stays at  $10^{-6}$ , but the Jacobi constant at time  $t = 0$  is iteratively lowered via a boundary constraint. This is shown in Figure 6.19. The value of  $C(t_0)$  is iteratively lowered, but the sensitive nature of the region near the primary occasionally causes the correction method to fail because the initial guess is not sufficient. If an iteration fails to converge, the step size of change in  $C(t_0)$  is reduced and another iteration is attempted. This step size eventually goes to zero, and the specific method being applied to the problem has reached its limits and is stopped. This occurs at about  $C(t_0) = 4.3$ , which is not close enough to the Jacobi constant required for a LLO,  $C_{LLO} = 5.49$ . This is the limiting case of transfers from low circular orbits about the Moon that can be computed using the implementation.

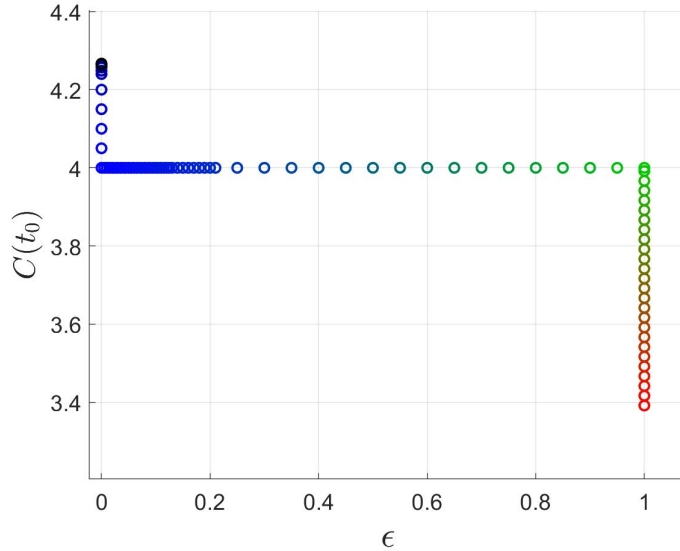


Figure 6.19: Further continuation for an MLO to L1 Lyapunov orbit transfer. The previous MLO continuation case is shown in Figure 6.10

The optimization method allows for the trajectory to be propagated backwards and retain optimality. Primer vector theory allows for the control to be determined by adjoints and state

variables, and the result is optimal if these variables are continuous and the end state has  $p_m = 0$ . If this end state is propagated backwards in time, it creates a local optimal transfer from whichever point it reaches to the desired end state. The resulting transfer geometry is not constrained or computed using a corrections method, but rather integrated backward until the desired Jacobi constant is reached.

This backwards propagation method is applied to the final state from the limiting case, shown in Figure 6.19 at about  $C(t_0) = 4.3$ , until the  $C_{LLO}$  is reached. The trajectory has an eccentricity of zero at the transfer time of the limiting case, but propagates further backwards. The eccentricity and radius to the center of the Moon is displayed in Figure 6.20, and zoomed to the first two time units for clarity in Figure 6.21. The transfer begins with an eccentricity of 0.0228 relative to the Moon and a semi-major axis of 1,860 km. Using the two-body problem to calculate the altitude bounds, this orbit would have a minimum altitude of 80 km, so it would not impact the Moon. Other perturbations must be taken into account at such low altitude to obtain a better estimate, but this is a reasonable starting point to compute an optimal trajectory from a circular LLO if higher fidelity is taken into account.

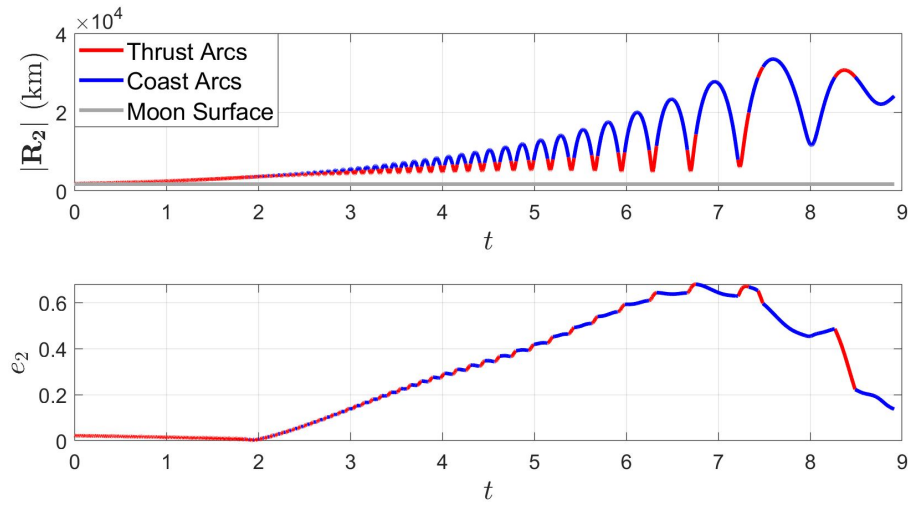


Figure 6.20: Eccentricity and distance relative to the Moon for an optimal LLO to L1 Lyapunov orbit transfer

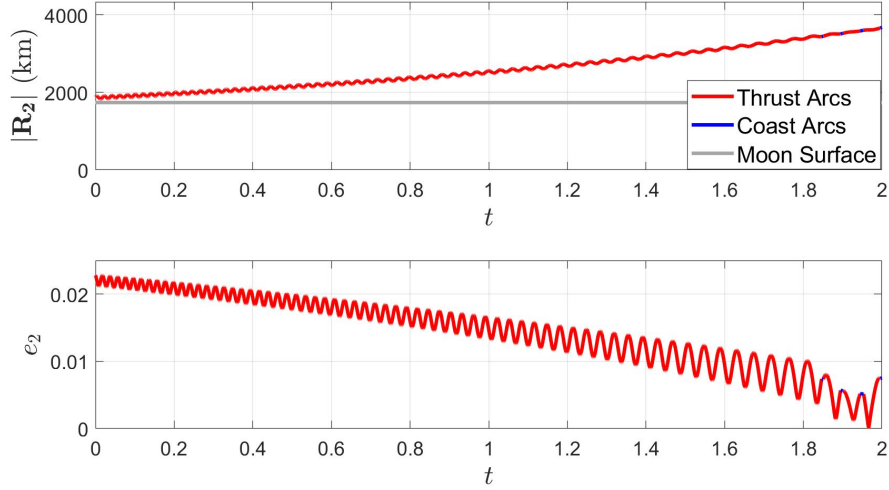


Figure 6.21: Eccentricity and distance relative to the Moon for an optimal LLO to L1 Lyapunov orbit transfer

While the computed pseudo-LLO transfer satisfies the Jacobi constant and optimality constraints, the backwards propagation causes the initial mass to be larger than the intended spacecraft mass. The mass and Jacobi constant are plotted in Figure 6.22. The initial nondimensional mass is 1.1241 rather than 1, corresponding to an initial spacecraft mass of 168.2 kg rather than 150 kg. While this is not intended, it can be accounted for and updated accordingly. If the problem was changed from the beginning to intend for an initial mass of about 130 kg, perhaps using the same methodology would result in a transfer that has an initial mass of 150 kg.

Notice from Figure 6.20 that thrust is applied continuously for nearly the first two nondimensional time units. Eventually the pattern of thrust resembles that of the previous examples in which thrust is only applied near periapsis. To investigate this and observe the thrust direction, the angle  $\alpha$  is plotted for the transfer in Figure 6.23. The magnitude of  $\alpha$  stays below 6 degrees for the first thrust arc, which means that thrust in the velocity direction is applied over that entire first phase. The first coast arc of the transfer occurs at  $t = 1.85$ , at which point  $R_2 = 3439$  km,  $e_2 = 0.0074$  and  $C = 4.32$ . After this critical point, the coast arcs begin to occupy larger and larger portions of each spiral.

The final optimal transfer from approximately LLO to an L1 Lyapunov orbit is displayed in

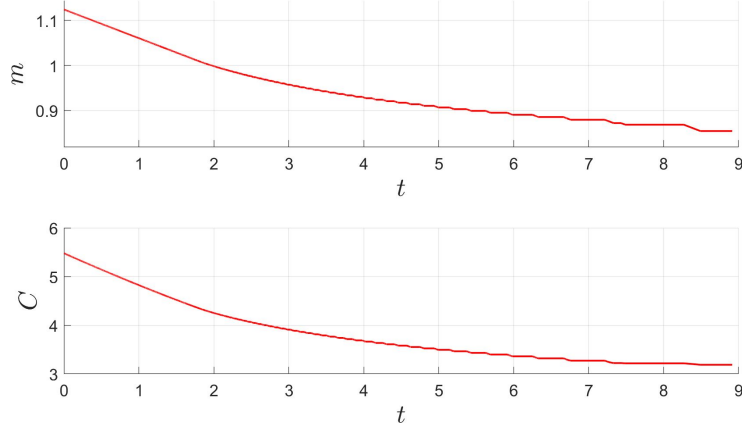


Figure 6.22: Mass and Jacobi constant measured over time for a transfer from LLO to an L1 Lyapunov orbit

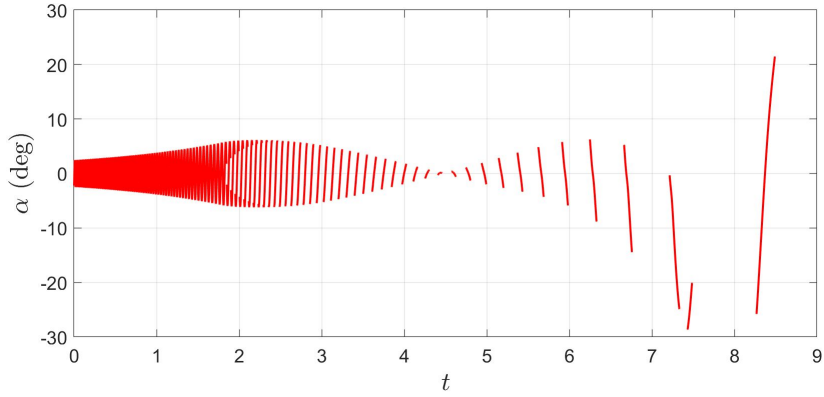


Figure 6.23: The angle between thrust and velocity for each thrust arc in an optimal LLO to L1 Lyapunov transfer

Figures 6.24 and 6.25, plotted respectively in the rotating and inertial frame. A mission could use this transfer if a mission required a small spacecraft in LLO to transfer to and L1 Lyapunov orbit; for example, the spacecraft could relay moon rock samples from a collector spacecraft in LLO to an Earth return spacecraft in LLO. While not as precise, the backwards propagation method generated an optimal trajectory that can be input into higher fidelity models that account for perturbations and constraints to output a feasible transfer.

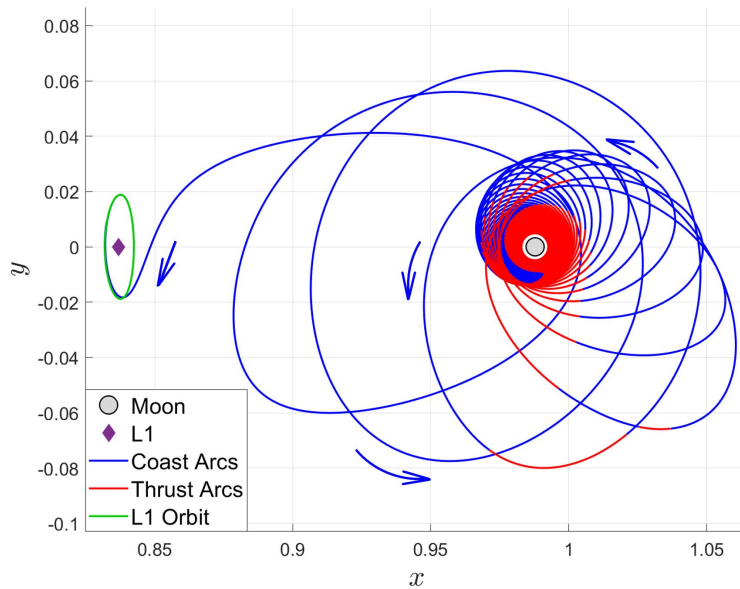


Figure 6.24: An optimal transfer from an approximately circular low lunar orbit to an L1 Lyapunov orbit in the Earth-Moon CR3BP, plotted in the rotating frame

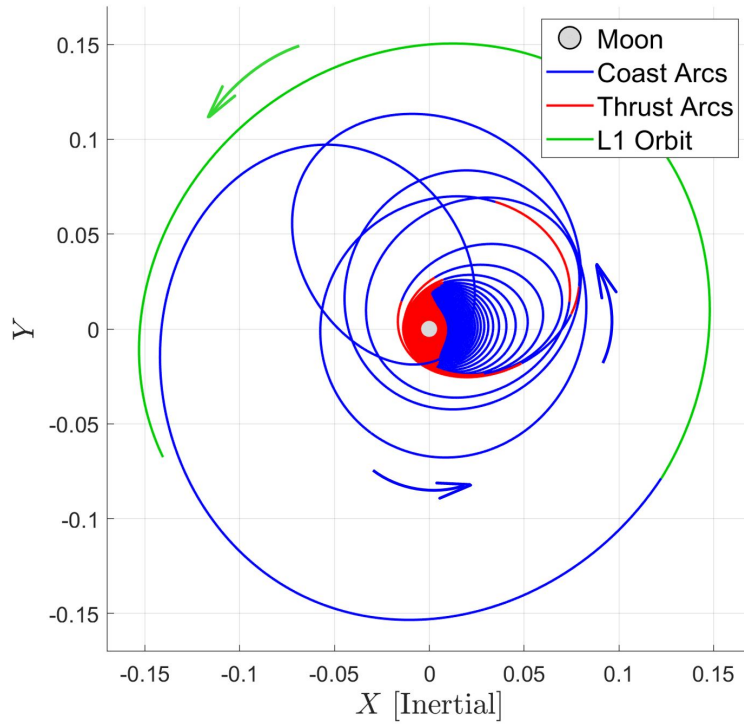


Figure 6.25: An optimal transfer from an approximately circular low lunar orbit to an L1 Lyapunov orbit in the Earth-Moon CR3BP, plotted in the inertial frame

## 6.5 Interpretation of Results

The results of applying primer vector theory to spiral out trajectories can reveal underlying principles of optimal transfers. The initial phase of the trajectories featured successive apoapsis raising maneuvers. Each thrust segment in this phase applied thrust approximately in the velocity direction and occurred near periapsis; this behavior is expected based on analysis of how thrust affects the Jacobi constant. These thrust segments also increased the eccentricity of the trajectory, which resulted in faster periapsis velocities and therefore increased the efficiency of the following maneuvers based on Eq. 5.4. The results of primer vector theory match the results of the analysis: the most effective way to change the Jacobi constant of a spacecraft is to apply thrust in the velocity direction at the points in the trajectory where the velocity is large. An interesting feature of the results is that the thrust segments near the end of the transfer broke the pattern of the first phase, producing periapsis raising maneuvers rather than apoapsis raising maneuvers. The second phase did not have a large effect on the Jacobi constant, but rather used thrust to correct to the desired end state.

## **Chapter 7**

### **Conclusion**

#### **7.1 Summary**

This thesis applied primer vector theory to compute fuel optimal transfers in the Earth-Moon CR3BP using parameters of small satellites with low-thrust propulsion system. This can be used to compute trajectories to support cislunar travel for SmallSats, which was the motivation behind this thesis. The growing interest in cislunar space requires trajectory designers to compute transfers in the Earth-Moon system, and effective maneuvering can have a very positive effect on the mission. This thesis outlined a method of computing optimal low-thrust transfers and can be used to support cislunar trajectory design.

Chapter 2 focused on the circular restricted three-body problem. The CR3BP is introduced to be used as a dynamical model for the Earth-Moon system. The equations of motion in the rotating frame are analyzed using parameters and structures such as the Jacobi constant, equilibrium points, periodic orbits, and manifolds. Methods of relating the Earth-Moon CR3BP to the Earth or Moon inertial two-body problem are derived to support the problem at hand. Finally, the equations of motion are augmented with continuous thrust.

The next section reviews methods of numerically computing trajectories. This is especially useful for the CR3BP because of the lack of an analytical solution. Shooting methods were explained and used in further sections to compute periodic orbits and transfers. Numerical continuation is reviewed, as continuation is used extensively to generate results. Poincaré maps are also discussed and used in Chapter 6 to patch two trajectories together. These numerical methods were very

important to generate the results in this thesis.

A method of optimization and related method of constructing a good initial guess were reviewed as those are necessary to generate optimal trajectories. Primer vector theory is derived and used as the method of optimization to generate optimal transfers in the CR3BP. The method of constructing initial guesses is outlined and uses analytical expressions to generate an educated guess. The computation process uses a Poincaré map, a multiple shooting method, and numerical continuation. Chapters 2, 3, 4, 5, can be used to compute optimal transfers in the CR3BP.

Chapter 6 selects two cases to study in particular: a spiral out transfer from lower Earth orbit to an L1 Lyapunov orbit and a spiral out transfer from lower lunar orbit to an L1 Lyapunov orbit. This revealed a pattern that is explained using analysis of the Jacobi constant. The sensitivities of the dynamics and computation near the primaries was explored and the limitations of the implementation were acknowledged. The results that were generated are fuel optimal spiral out transfers in the Earth-Moon CR3BP and can be used to design spacecraft trajectories in cislunar space.

## 7.2 Future Work

The methods discussed in this thesis were used to generate optimal trajectories, but they have limitations and can be expanded upon in a way that was beyond the intended scope. Some potential projects of interest are listed below:

- A large obstacle in this thesis was the numerical sensitivities near the primary bodies, and this warrants a deeper investigation. Coordinate transformations can be used to confront these sensitivities, so a study could be done on how these coordinate transformations influence/change the application of primer vector theory. The deployment of other numerical methods to handle the sensitivities could be studied as well. The sensitivities are essentially due to scaling, so a corrections process that uses relative constraints instead of absolute constraints could be explored. Other ways of handling the scaling issue that address the

nondimensionalization method could also potentially be a subject of study.

- The results in this study are locally optimal, but another locally optimal solution may exist that is preferable. A local optimal is commonly treated as a candidate for a global optimal, and it is common to compare different candidates and select the most desirable transfer. Different initial guesses could be used to compute locally optimal solutions with different geometries, and the results of comparing the different geometries may lead to interesting conclusions.
- Only one set of spacecraft and propulsion parameters were used for results. A trade study on how using different ranges of parameters affects the performance would be interesting and useful. The initial mass, the maximum thrust, or the specific impulse could be varied and the results could be compared.
- Mirror theorem could potentially be applied to use an optimal trajectory as a good initial guess for an optimal trajectory in the opposite direction. Mirror theorem in the CR3BP states that a trajectory can be reflected over the  $xz$  plane and propagated backwards in time to produce another valid trajectory. In other words, the equations of motion hold the same form if  $y$  is set to  $-y$  and  $t$  is set to  $-t$ . This clearly doesn't apply directly to mass in trajectories with continuous thrust, as backwards propagation will result in mass increasing over time. Nonetheless, the mirror theorem could be utilized to create a good initial guess if a method was developed to account for the mass. An investigation could be done on how mirror theorem relates to the adjoints involved in primer vector theory as well. An optimal spiral out trajectory from GEO to  $L_1$ , for instance, could be used to efficiently compute an optimal spiral in trajectory from  $L_1$  to GEO.
- The optimal trajectories computed in this thesis are time-fixed optimal, meaning that they are only optimal for the specific time of flight of the transfer. Additional constraints on the Hamiltonian can be enforced to make these trajectories time-free optimal, or optimal

for any transfer time; this is discussed in Chapter 4. A continuation method could be employed to use the results for the time-fixed case as a starting point to generate results for the time-free case.

## Bibliography

- [1] Natasha Bosanac. Leveraging Natural Dynamical Structures to Explore Multi-body Systems. PhD thesis, Purdue University, 2016.
- [2] B. Bradie. A Friendly Introduction to Numerical Analysis. Pearson Education, Inc, 2006.
- [3] Arthur E. Bryson and Yu-Chi Ho. Applied Optimal Control. Hemisphere Publishing Corporation, 1975.
- [4] Bruce A Conway. Spacecraft Trajectory Optimization. Cambridge University Press, 2014.
- [5] Kathryn E. Davis. Locally Optimal Transfer Trajectories Between Libration Point Orbits Using Invariant Manifolds. PhD thesis, University of Colorado, 2009.
- [6] Georg Herdrich 2 Dillon O'Reilly and Darren F. Kavanagh. Electric propulsion methods for small satellites: A review. Aerospace, 2021.
- [7] Michael Dropmann, Manfred Ehresmann, Adam Pagan, Francesco Romano, Quang Hoa Le, , Christoph Montag, and Georg Herdrich. Low power arcjet application for end of life satellite servicing. In 7th European Conference on Space Debris. ESA/ESOC, 2017.
- [8] Ian Elliott, Christopher Sullivan Jr., Natasha Bosanac, Jeffrey R. Stuart, and Farah Alibay. Designing low-thrust trajectories for a smallsat mission to sun-earth l5. Journal of Guidance, Control, and Dynamics, 43(10), 2020.
- [9] Leonhard Euler. De motu rectilineo trium corporum se mutuo attrahentium. Novi Commentarii academiae scientiarum Petropolitanae, 11:144–151, 1765.
- [10] Robert Farquhar. Station-keeping in the vicinity of collinear libration points with an application to a lunar communications problem. AAS Science and Technology Series: Space Flight Mechanics Specialist Symposium, pages 519—535, 1966.
- [11] Matthew Gerberich and Steven R. Oleson. Estimation model of spacecraft parameters and cost based on a statistical analysis of compass system designs. AIAA SPACE 2013 Conference and Exposition, 2013.
- [12] GeoGebra GmbH. Geogebra, 2013. <http://www.geogebra.org>.
- [13] Martin Gutzwiller. Moon-earth-sun: The oldest three-body problem. Reviews of Modern Physics, 70:589–639, 1998.

- [14] Rodney L. Anderson Jeffrey S. Parker. Low-Energy Lunar Trajectory Design. Wiley, 2014.
- [15] NASA JPL. Jpl three-body periodic orbit catalog. [https://ssd.jpl.nasa.gov/tools/periodic\\_orbits.html](https://ssd.jpl.nasa.gov/tools/periodic_orbits.html).
- [16] Joseph-Louis Lagrange. Tome 6, Chapitre II: Essai sur le problème des trois corps. Gauthier-Villars, 1772.
- [17] D.F. Lawden. Optimal Trajectories for Space Navigation. Butterworths, 1963.
- [18] NASA. About cubesat launch initiative. <https://www.nasa.gov/content/about-cubesat-launch-initiative>.
- [19] NASA. Chandrayaan 2, 2019. <https://nssdc.gsfc.nasa.gov/nmc/spacecraft/display.action?id=2019-042A>.
- [20] NASA. Gateway destination orbit model: A continuous 15 year nrho reference trajectory, 2019.
- [21] NASA. Chang'e 5, 2020. <https://nssdc.gsfc.nasa.gov/nmc/spacecraft/display.action?id=2020-087A>.
- [22] NASA. Artemis i, 2022. <https://www.nasa.gov/specials/artemis-i/>.
- [23] NASA. Artemis ii crew, 2023. <https://www.nasa.gov/specials/artemis-ii/>.
- [24] NASA. Artemis iii: Nasa's first human mission to the lunar south pole, 2023. <https://www.nasa.gov/feature/artemis-iii>.
- [25] Isaac Newton. Philosophiae naturalis principia mathematica. London, 1687.
- [26] Jules Henri Poincaré. Les Méthodes Nouvelles de la Mécanique Céleste, volume 1-3. Gauthier-Villars et fils, 1899.
- [27] Shane D Ross, Wang Sang Koon, Martin Wen-Yu Lo, and Jerrold E. Marsden. Dynamical Systems, the Three Body Problem and Space Mission Design. Springer-Verlag New York Incorpoarted, 2006.
- [28] A. Roy and M. Ovenden. On the occurrence of commensurable mean motions in the solar system: The mirror theorem.
- [29] Hanspeter Schaub and John Jenkins. Analytical Mechanics of Space Systems. American Institute of Aeronautics and Astronautics, 4 edition, 2018.
- [30] Daniel J. Scheeres. Orbital Motion in Strongly Perturbed Environments: Applications to Asteroid, Comet and Planetary Satellite Orbiters. Springer Praxis Books, 2012.
- [31] Yanis Sidhoum. On the performance of different smoothing methods for indirect low-thrust trajectory optimization. In Space Flight Mechanics Meeting, 33. AAS/AIAA, 2023.
- [32] Advanced Space. Capstone — advanced space, 2023. <https://advancedspace.com/missions/capstone/>.
- [33] SpaceX. Launches, 2023. <https://www.spacex.com/launches/>.

- [34] Oskar Von Stryk and Roland Zdenek Bulirsch. Direct and indirect methods for trajectory optimization. *Annals of Operations Research*, 1992.
- [35] Christopher J. Sullivan, Jeffrey Stuart, , Rodney L. Anderson, and Natasha Bosanac. Designing low-thrust transfers to high-inclination science orbits via hybrid optimization. *Journal of Spacecraft and Rockets*, 58(5), 2021.
- [36] Victor G. Szebehely. *Theory of Orbits: The Restricted Problem of Three Bodies*. Academic Press, 1967.
- [37] David A. Vallado. *Fundamentals of Astrodynamics and Applications*. Microcosm Press, 4th edition, 2013.
- [38] Chen Zhang and Yu-Shan Zhao. Low-thrust minimum-fuel optimization in the circular restricted three-body problem. *Journal of Guidance, Control, and Dynamics*, 38:1501—1510, 2015.